

Coupling thermodynamic mineralogical models and mantle
convection.

Antonio Sebastiano Piazzoni

October 22, 2008

*Dissertation der Fakultät für Geowissenschaften der
Ludwig-Maximilians-Universität München*

Erstgutachter: *Prof. Hans-Peter Bunge*
Zweitgutachter: *Dr. Gerd Steinle-Neumann*

Tag der mündlichen Prüfung: 05.12.2007

Contents

1	Introduction	10
2	A mineralogical model for density and elasticity of the Earth's mantle	18
2.1	Introduction	18
2.2	Previous Work	21
2.3	Methodology	22
2.3.1	Equation of state and physical properties	22
2.3.2	Thermodynamic relationships	26
2.4	Gibbs free energy minimization	28
2.5	Characteristics of the database	33
2.6	Web interface	35
2.7	Mantle structure	40
2.8	Conclusions and limitations	47
3	Thermal and Elastic Structure in Multiphase Mantle Convection Models	59
3.1	Introduction	59
3.2	The model	62
3.2.1	Thermodynamically Self-Consistent Mantle Mineralogy Model	62
3.2.2	Mantle Convection Model	62
3.3	Results	64
3.3.1	The thermal structure	64
3.3.2	The elastic structure	68
3.4	Conclusions	73
4	Appendix: Transition zone thickness	81

List of Figures

- 1 Fitting of P-V-T data for equation of state parameters for magnesium perovskite (left panels) and forsterite (right panels). The upper panels (a and b) show isothermal equations of state at 298, 1298 and 2298 K (solid lines) in comparison to experimental data (color coded for temperature). In the middle panels (c and d) I show the misfit between experimental data and my model (black points) and that of *Stixrude and Lithgow-Bertelloni*, [2005] as a function of temperature. The lower panels (e and f) show the difference between the two models. Experimental data for perovskite are from *Funamori et al.* [1996], *Fiquet et al.* [1998; 2000], *Saxena et al.* [1999] and *Utsumi et al.* [1999]. Data for forsterite are from *Hazen* [1976], *Kudoh and Takeuchi* [1985], *Will et al.* [1986], *Meng et al.* [1993], *Bouhifd et al.* [1996] and *Downs et al.* [1996]. 25
- 2 Illustration of the simplex minimization routine for the system MgO-FeO-SiO₂. Label q indicates the bulk composition in the base of the oxide system. Geometrically, the quantity to be minimized is the distance g between q and its projection on the plane that passes through the three metastable phases. 29
- 3 Phase transformation for the (Mg,Fe)₂SiO₄ system. The panel (a) shows the pressure and temperature dependence of the phase transitions for Mg₂SiO₄: Solid lines indicate my model, the dashed (green) line is from *Fei et al.* [2004] and the dotted-dashed lines (red) show three permissible Calpeyron slopes from *Katsura et al.* [2003]. The panel (b) shows phase transitions and coexistence areas as a function of pressure for the (Mg,Fe)₂SiO₄ system at constant temperature (1673 K). Red symbols show the experiments of *Frost* [2003] for stable phases near the transition. Open circles stand for α , solid circles for the β phase and open squares for γ spinel. The vertical error indicates the pressure uncertainty from *Frost* [2003]. 36
- 4 Chemical effects on the adiabatic bulk modulus (left column) and molar volume/density (right column) of pv at 298K and 28 GPa. The upper panels show my calculation (black solid line) for the binary solid solution Mg- pv – Al- pv , up to an Al₂O₃ content of 15%. The lower panels for the Mg- pv and Fe- pv binary solid solution. The molar volume is converted to density (green solid line in the right column). All results are compared with experiments that have been interpolated or extrapolated to 28 GPa and 298 K: circles (blue) [*Walter et al.*, 2004]; triangles down (red) [*Daniel et al.*, 2004]; squares (yellow) [*Yagi et al.*, 2004]; diamonds (turquoise) [*Andrault et al.*, 2001]; triangles up (violet) [*Mao et al.*, 1991]. Error-bars are taken from the experiments and appropriately propagated. Errors in *Mao et al.* [1991] were not reported and are added consistently with other experiments 37

5	Iron partitioning in the $(\text{Mg,Fe})_2\text{SiO}_4$ system (α , β and γ) at transition zone pressures and 1800 K. Dotted curves show my model for two FeO contents (6% and 10%) in a pyrolite based bulk composition. The solid line is from experiments for dry peridotite (10% FeO) [<i>Frost, 2003</i>]. The calculation takes into account all the other stable phases of a pyrolite composition, i.e. <i>gt</i> and <i>cpz</i> . Dashed lines show the phase transition pressures of the phase transitions in the $(\text{Mg,Fe})_2\text{SiO}_4$ system as a function of Fe-content.	38
6	Stable phases and their proportions at a constant temperature of 1800 K. The upper panel shows the diagram for pyrolite bulk composition. The lower panel is computed at the same conditions as above but for piclogite composition. Abbreviations for mineral phases are introduced in Table 2. The diagram is not smoothed in order to illustrate numerical fluctuations in the minimization routine and the effect of discontinuities of the physical properties (as iron partitioning) on the phase abundances.	39
7	Adiabatic temperature profiles from the mantle mineralogical model. (a) shows lines of constant entropy as a function of pressure for pyrolitic composition. The adiabats are spaced at fixed difference of entropy, and cover a wide range of temperatures (800-3300 K). (b) is a blow-up of (a), focusing on the pressure range where the phase transitions occur and where jumps in temperature compensate for entropy changes due to exothermic and endothermic transitions. The three adiabats shown have a footing temperature of 1350 K (dashed), 1500 K (solid), and 1650 K (dotted). (c) shows the differences between pyrolite and piclogite models from the surface to the top of the lower mantle for three adiabats with the same footing temperatures as in panel (b). Differences are on the order of 10-15 K and are most pronounced in the transition zone.	42
8	Physical properties of the stable phases in a pyrolitic mantle for isotherms of 1000 K (blue), 2000 K (yellow) and 3000 K (red) for pressures up to 70 GPa (mid-lower mantle). (a) Molar volume of the stable phases as a function of pressure. (b) Adiabatic bulk modulus of the stable phases. The stoichiometry of some of the phases has been rescaled for better comparison among different phases (e.g. pyrope <i>gt</i> volume is calculated on the stoichiometry $\text{Mg}_{3/4}\text{Al}_{1/2}\text{Si}_{3/4}\text{O}_3$), consistent with Table 2.	43
9	Comparison of physical properties from the mineralogical model for pyrolite and piclogite bulk compositions along an adiabat (footing temperature of 1500 K) with seismic reference models (PREM and AK135M). Panels (a)-(f) show the density, bulk and shear modulus, p-, s-wave and bulk sound velocities, respectively. The comparison is shown on a pressure scale, the natural variable in the Gibbs free energy minimization; the pressure values for the seismological models are based on the density structure of the seismological models themselves.	45

10	Molar percentage of the stable phases for a pyrolitic mantle at different temperatures (1700-2300K) over the pressure range of the transition zone. At low temperature (panels (c) and (d)) <i>pv</i> , <i>mw</i> and <i>Ca-pv</i> form over a narrow depth interval from <i>gt</i> and γ via the post-spinel transition (with negative Clapeyron slope). I note that my database does not include ~ 10 vol% of <i>il</i> (denser than <i>gt</i>) that is expected to be present at low temperatures [Hirose, 2002]. At high temperatures (panels (a) and (b)) <i>gt</i> is stable up to lower mantle pressures, transforming smoothly into <i>pv</i> (with positive Clapeyron slope). The pressure at which <i>gt</i> is completely transformed into <i>pv</i> corresponds at high temperature to about 720km. The post-spinel phase transition occurs at 23-24 GPa (650-670km).	46
11	Parameters of the convection models (see text for details).	63
12	Contourplots of temperature for the convection models. The color indicates temperature (blue is 298 K, red is 3500K, the palette is linear). The panels show (from above to below) the "BOTTOM, ISOVISCIOUS", the "BOTTOM, LAYERED VISC.", the "MIX, ISOVISCIOUS" and the "MIX, LAYERED VISC." models.	64
13	Radial average temperature for the "BOTTOM" (panel (a)), for the "MIX" (panel (b)) and "INTERNAL" (panel (c)) models. Solid lines show the isoviscous calculations, dashed ones indicate layered viscosity. Note that in correspondence with the "660km" there are sharp increases of temperature, created by the flow in order to compensate for the entropy change of the phase transitions (see text). Such discontinuities increase with temperature increasing; thus they are more pronounced on hotter profiles and barely visible for the "INTERNAL" cases.	65
14	(a) Contourplot of density from my mineralogical model (section 2). The three overlapped lines represent the maximum, mean and minimum temperature at each depth from snapshots of the "BOTTOM, ISOVISCIOUS" model (solid line) and the "BOTTOM, LAYERED VISC." model (dashed line). (b) Lateral differences of density $\Delta\rho$ between the mean and the maximum and the minimum temperatures, respectively. Negative $\Delta\rho$ represent the rising buoyancy of plumes due to their excess temperature. Positive $\Delta\rho$ indicate the downward buoyancy of the cold material. The solid line is for "BOTTOM, ISOVISCIOUS", the dashed one for "BOTTOM, LAYERED VISC.". Panels (c) and (d) correspond to panels (a) and (b), respectively, for the "MIX" case.	67

15	(a) Curves of constant entropy from the mineralogical model of [Piazzoni et al., 2007] for footing (zero-pressure) temperatures of 750, 1250, 1750, 2250 K. The slope of the adiabat increases with footing temperature and generally decreases with depth. Temperature jumps corresponding to the discontinuities in entropy of the phase reactions are less pronounced in colder profiles. (b) Total adiabatic temperature variation from surface to CMB plotted against footing temperature. There is a sharp increase in adiabatic excess temperature with increasing footing temperature. Also shown are the footing temperatures corresponding to mean, minimum and maximum radial temperatures in the convection model (see text). Note that hot thermal upwellings (plumes) undergo strong adiabatic cooling relative to surrounding mantle, so that their excess temperature decreases systematically in the mantle from the bottom to the top.	69
16	Contourplots of shear wave velocity (V_S) for the convection models presented above. The panels show (from above to below) the "BOTTOM, ISO-VISCOUS", the "BOTTOM, LAYERED VISC.", the "MIX, ISOVISCIOUS" and the "MIX, LAYERED VISC." models. The linear palette ranges from -2 % (red) to +2 % (blue).	70
17	Contour plot (black=fast, white=slow) of bulk sound velocity (V_Φ) and shear wave velocity (V_S) over the mantle temperature and pressure range for a pyrolite bulk composition as provided by my mineralogy model (see text). V_Φ generally increases with depth and decreases with temperature, The solid and dot-dashed curves are Brown and Shankland [Brown and Shankland, 1981] and Stacey [Stacey, 1995] geotherms. I clip the figure at temperatures larger than the dry solidus [Zerr et al., 1998], where melting invalidates the considerations underlying the physical properties of the mineral assemblage.	72
18	Root Mean Square (R.M.S.) of shear wave anomalies for the "BOTTOM" models (black lines) and for the "MIX" cases (blu lines). Solid lines indicate "ISOVISCIOUS" models, dashed lines represent "LAYERED VISC." models. I have performed the root mean square calculation at full resolution of about 20 km (panel (a)) and also averaged over a scale of about 200 km (panel (b)). Red symbols show seismic tomography models: triangles for S20RTS [Ritsema et al., 1999], crosses for PRI-S05 [Montelli et al., 2006], diamonds for RMSL-S06 [Reif et al., 2006], plus for TX2007 [Simmons et al., 2007] and circles for SB10L18 [Masters et al., 2000].	73
19	Depth variations of the 410 km and 660 km seismic discontinuities for the four convection models. In order to isolate temperature effects on transition zone thickness, the post-spinel transition has been modeled here with a constant Clapeyron slope of -2 MPa/K. Negative variations of the "410 km" appear less pronounced then positive variations for slab-like temperatures.	83

- 20 Sketch of temperature effects on the topography for the "410km and the "660km". The labels (s), (a) and (p) indicate slab, average and plume temperature, respectively. The symbols "X" point to the average thickness, that does not correspond necessary to the thickness of the average temperature (a). For this diagram, the relative differences of temperature between cold and hot structures are taken from the model "BOTTOM, ISOVISCIOUS". Due to a reduction of the excess temperature of plumes above the "660km", the "410km" varies less than the "660km" on plume-like temperature. A similar effect occurs at low temperature, where the temperature differences are generally smaller than on the "660km". So, the variations of the "410km" are reduced in respect to what is expected from mineralogy (see text). . . . 84

List of Tables

1	Chemical bulk compositions of the global mantle in molar percent. Pyrolite is after <i>Irifune</i> [1987], piclogite from <i>Duffy and Anderson</i> [1989]. Xenolith is from <i>Wänke et al.</i> [1984], the “modified” chondritic model from <i>Allègre et al.</i> [1995].	20
2	Model of the solid solutions and their end-members. Each line gives the name of the end-member, its chemical formula, the name of the solid solutions it belongs to, an abbreviation that is used all-through the text and the ideal activity in the solid solution. The column “Activity“ defines the activity of the end-member as a non-linear function of the mole fractions of individual end-members.	31
3	Database of the equation of state parameters and calorimetric data. The physical quantities are defined in the text. The letters in the first column indicate the mineral phases as in Table 2.	32

1 Introduction

The mantle is the largest portion of the Earth’s interior, extending from the crust to the fluid core at 2890 km depth. Direct knowledge of it is limited, however, as samples of the mantle are scarce. We have occurrence of upper mantle mineralogy in mantle xenoliths, i.e. mantle rocks that are rapidly carried to the surface in volcanic eruptions [Nixon, 1987] and in ophiolite complexes where the mantle wedge below former transition zones is exposed [Moores, 2003]. Inclusions in diamonds show some of the few minerals that we have from the transition zone of the mantle [Stachel, 2001] and only there majoritic garnet, for example, can be found [Sautter et al., 1991]. These samples provide important inferences about composition and chemical conditions in the mantle (e.g. oxygen fugacity, [McCammon, 2005]). In addition, at mid ocean ridges basalt is extracted from the mantle, leaving behind a depleted layer of harzburgite [Matthes, 2005]. Using petrologic relations, a model of upper mantle composition can be inferred, the pyrolite model [Ringwood, 1975; Irifune, 1987]. Despite these important constraints from petrology, the bulk of the mantle, and in particular the lower mantle, are only accessible through remote sensing, using electro-magnetic (magnetotellurics) or elastic waves (seismology) or gravity data.

Seismological measurements on the Earth’s interior provide some of the most valuable information on mantle structure. In particular, seismic tomography has revealed a range of heterogeneities in the mantle [Grand et al., 1997; van der Hilst et al., 1997; Bijwaard et al., 1998; Masters et al., 2000; Mégnin and Romanowicz, 2000] and has resolved seismically fast, slab-like structures extending deep into the lower mantle [Grand et al., 1997; van der Hilst et al., 1997; Bijwaard et al., 1998]. At the same time, joint models of bulk sound and shear wave velocities [Kennett et al., 1998; Masters et al., 2000], models of probabilistic mantle heterogeneity [Resovsky and Trampert, 2002], and studies of finite frequency effects [Montelli et al., 2004] show considerable complexity for the mantle structure. In particular maps of bulk sound (V_{Φ}) and shear wave (V_S) velocities do not identify a unique picture of mantle heterogeneities: V_{Φ} variations diminish at lower depths compared to V_S variations. Furthermore, studies based on seismic precursors have increased the precision in mapping the depth variation of seismic discontinuities that correspond to phase transitions, e.g. the 410 km and the 660 km depth discontinuities [Shearer and Flanagan, 1999; Shearer, 2000; Deuss et al., 2006].

Seismology thus reveals information on thermal and chemical conditions for the macrocosm deep Earth that need to be interpreted in terms of material properties in the microcosm mantle minerals and/or the dynamic state of the Earth’s interior. For example, to this date we do not have a sample of MgSiO_3 perovskite (Mg-*pv*) from the mantle. The inference that Mg-*pv* is the major phase of the Earth’s lower mantle comes from three sources: (1) a cosmo-/geochemical model of composition of the Earth [McDonough and Sun, 1995], (2) the study of phase transitions at high pressure and temperature [Yagi et

al., 1978] and (3) a comparison of its P-V-T equation-of-state with the compressibility of the lower mantle [Stixrude *et al.*, 1992].

Progress in mineral physics at high pressure has now advanced to a point where petrologic studies can be performed at lower mantle conditions [e.g. Walter *et al.*, 2004]. It is now possible to build a self-consistent mantle mineral models of (dry) phases in the Earth's mantle [Fabrichnaya, 1999; Matas, 1999; Stixrude and Lithgow-Bertelloni, 2005; Piazzoni *et al.*, 2007], based exclusively on phase relations, compressional and thermochemical measurements. Simultaneous advances in elastic measurements of minerals at high pressure using Brillouin spectroscopy [Sinogeikin *et al.*, 2004], ultrasonic measurements in the multi-anvil press [Li and Zhang, 2005] and diamond anvil cell [Kantor *et al.*, 2004], and ab-initio modeling [Oganov *et al.*, 2001] yield, for the first time, a comprehensive model of shear wave elastic properties at mantle conditions [Stixrude and Lithgow-Bertelloni, 2005]. These two developments provide important constraints for the interpretation of seismic measurements in terms of physical properties of constituting mineralogy.

Geodynamic models that simulate convection at high resolution provide an alternative route to explore the thermal and chemical state of the mantle. Whole mantle geodynamics has focused on the geotherm of the Earth [Bunge *et al.*, 2001], plume flux [Labrosse, 2002; Bunge, 2005; Mittelstaedt and Tackley, 2006; Zhong, 2006] and the evolution of convection having different chemical components [Tackley, 2002; Samuel *et al.*, 2005; Tackley *et al.*, 2005]. However, convection models have traditionally applied a much simplified representation of mantle mineralogy. Some models restrict themselves to the Bousinesq approximation [McKenzie *et al.*, 1974; Christensen and Yuen, 1985; Bunge and Richards, 1996; McNamara and Zhong, 2005], in which all parameters are held constant and where density changes enter only through the buoyancy term of the Navier-Stokes equation, giving rise to gravitational forces. Other models have adopted a depth-dependent formalism through the use of the anelastic liquid approximation [Jarvis and McKenzie, 1980; Glatzmaier, 1988, Bunge *et al.*, 1997]: The fluid under this assumption sustains compression or expansion due to changes in pressure as it sinks or rises, but thermal effects are ignored. In addition to mantle structure, the mantle phase transitions interact with upwelling and downwelling thermal structures in a complex way that cannot be easily modeled by parameterized buoyancy forces, e.g. based only on the post-spinel transition in the Mg_2SiO_4 part of mantle mineralogy. The phase transitions leading to the 410 km and 660 km discontinuities are highly simplified in geodynamic models: they are commonly modeled as two sharp boundaries where anomalous buoyancy forces reproduce the dynamic effects of the phase transitions [Christensen and Yuen, 1985; Tackley *et al.*, 1993; Bunge *et al.*, 1997]. Such sharp transitions do not adequately describe the complexity of the phase transitions [e.g. Hirose, 2002; Frost, 2003].

Traditionally the mineralogical interpretation of tomography suffers from the tradeoff

between temperature and composition. However this limitation can be overcome by evaluating the compositional effects of a mineralogical model within geodynamic models. Here I advance the integration of mineral thermodynamics into convection modeling. I have compiled a thermodynamic model of mantle mineralogy in the five component CFMAS system (CaO-FeO-MgO-Al₂O₃-SiO₂), including mineral phases that occur close to typical chemical models of the mantle and reasonable mantle temperatures. In this system I have performed a system Gibbs free energy minimization, including pure end-member phases and a non-ideal formulation for solid solutions. Solid solutions were subdivided into discrete pseudocompounds and treated as stoichiometric phases during computation of chemical equilibrium by the simplex method. I have complemented the thermodynamic model with a model of shear wave properties [*Stixrude and Lithgow-Bertelloni, 2005*] to obtain a full description of aggregate elastic properties (density, bulk and shear moduli) that provide a useful basis for the consideration of seismic and geodynamic models of the Earth's mantle.

By using this new thermodynamic database for the mantle I have coupled the resulting density dynamically (through the buoyancy term) with mantle convection models. I have linked the database with a high-resolution 2-D convection code (2DTERRA), dynamically coupling the thermodynamic model (density) with the conservation equations of mantle flow. The coupled model is run for different parameterisations of viscosity, initial temperature conditions, and varying internal vs. external heating. A common feature of all the models is that the convecting flow creates a characteristic discontinuity of temperature around 660 km depth in order to compensate for the entropy change due to the phase transitions. I have studied the importance and the possible consequences of such a thermal regime on the excess temperature of plumes and on the transition zone thickness. The thermodynamic mantle mineralogy model provides the conversion of the temperature field into seismic velocities so that predictions from mantle convection can be compared to seismic observations in terms of radial profiles or lateral variations. This approach allows us to predict a number of seismic observables from the convection model, all of which agree remarkably well with observations from seismic tomography.

This thesis is organized as follows:

In **section 2** I present a detailed description of the mineralogical model and an assessment of its validity, comparing it to experimental data. The thermodynamic model considers five oxide components (CFMAS), including mineral phases that occur close to typical chemical models of the mantle. In this system I have performed a system Gibbs free energy minimization via the simplex method on the pure end-member phases and their solid solutions. This method allows for the self-consistent calculation of phase equilibria, physical, thermodynamic and chemical properties of the stable phases as well as the element partitioning at pressure and temperature of interest. This section concludes by exploring results from my model in terms of the thermal and physical state of the mantle. We

find good agreement between the elasticity of our model and 1D seismic reference profiles, and are able to construct mineralogically self-consistent adiabatic profiles that provide the basis for a discussion on the thermal state of the mantle. In particular we find that hot adiabats are steeper than cold ones, and quantify the excess temperature along various adiabats. This part of my thesis has been accepted for publication as: Piazzoni, A.S., G. Steinle-Neumann, H.-P. Bunge and D. Dolejš, 2007, *A mineralogical model for density and elasticity of the Earth's mantle*, in press, *Geochem. Geophys. Geosyst.*

In **section 3** I provide a detailed description of the convection models coupled with mineral physics. I explore the importance and the possible consequences of the thermal regime of geodynamic models on plume and slab excess temperature, using different models for the viscosity structure and heating regimes in the mantle. The thermodynamic model of mantle mineralogy provides the conversion of the temperature field into seismic velocities so that the predictions of mantle convection can be compared to seismic observations in terms of lateral variations and radial profiles.

Section 4 (appendix) focuses on the transition zone for the coupled models presented in section 3. By studying topography variations of the seismic discontinuities as a consequence of the resulting temperature field, I obtain a striking agreement with recent seismic observations on transition zone thickness. The most relevant depth-changes occur on the 660 km and not on the 410 km discontinuities, even if their Clapeyron slopes would suggest the opposite, and obtain clear anti-correlation of topographies on the discontinuities only around subduction areas. Around upwellings the topographies are usually un-correlated.

References

- [1] Bijwaard, H., W. Spakman and E.R. Engdahl, Closing the gap between regional and global travel time tomography, *J. Geophys. Res.*, *103*, 30,055-30,078, 1998.
- [2] Bunge H.-P. and M.A. Richards, The origin of large scale structure in mantle convection: Effects of plate motions and viscosity stratification, *Geophys. Res. Lett.*, *23*, 2987-2990, 1996.
- [3] Bunge, H.-P., M.A. Richards and J.R. Baumgardner, A sensitivity study of three-dimensional spherical mantle convection at 10^8 Rayleigh number: Effects of depth-dependent viscosity, heating mode, and an endothermic phase change, *J. Geophys. Res.*, *102*, 11,991-12,007, 1997.
- [4] Bunge, H.-P., Y. Ricard and J. Matas, Non-adiabaticity in mantle convection, *Geophys. Res. Lett.*, *28*, 879-882, 2001.

- [5] Bunge, H.-P., Low plume excess temperature and high core heat flux inferred from non-adiabatic geotherms in internally heated mantle circulation models, *Phys. Earth Planet. Interiors*, *153*, 3-10, 2005.
- [6] Christensen, U.R. and D.A. Yuen, Layered convection induced by phase-transitions, *J. Geophys. Res.*, *90*, 291-300, 1985.
- [7] Deuss, A., A.T. Simon, K.C Redfern and J.H. Woodhouse, The Nature of the 660-Kilometer Discontinuity in Earth's Mantle from Global Seismic Observations of PP Precursors, *Science*, *311*, 198-201, 2006.
- [8] Fabrichnaya, O.B., The phase relations in the FeO-MgO-Al₂O₃-SiO₂ system: assessment of thermodynamic properties and phase equilibria at pressures up to 30 GPa, *Calphad*, *23*, 19-67, 1999.
- [9] Frost, D.J., The structure and sharpness of (Mg,Fe)₂SiO₄ phase transformations in the transition zone, *Earth Planet. Sci. Lett.*, *216*, 313-328, 2003.
- [10] Glatzmaier, G.A., Numerical simulations of mantle convection: time-dependent, threedimensional, compressible, spherical shell, *Geophys. Astrophys. Fluid Dyn.*, *43*, 223-264, 1988.
- [11] Grand, S.P., R. D. Van der Hilst and S. Widiyantoro, High resolution global tomography: A snapshot of convection in the Earth, *Geol. Soc. Am. Today*, *7*, 1-7, 1997.
- [12] Hirose, K., Phase transitions in pyrolitic mantle around 670-km depth: Implications for upwelling of plumes from the lower mantle, *J. Geophys. Res.*, *107*, B4, 2078, doi:10.1029/2001JB000597, 2002.
- [13] Irifune, T., An experimental investigation of the pyroxene-garnet transformation in a pyrolite composition and its bearing on the constitution of the mantle, *Earth. Planet. Sci. Lett.*, *45*, 324-336, 1987.
- [14] Jarvis, G.T. and D. McKenzie, Convection in a compressible fluid with infinite Prandtl number, *J. Fluid Mech.*, *96*, 515-83, 1980.
- [15] Kantor, A.P., S. Jacobsen, I.Y. Kantor, L. Dubrovinsky, C.A. McCammon, H.J., Reichmann and I.N. Goncharenko, Pressure-Induced Magnetization in FeO: Evidence from Elasticity and Mossbauer Spectroscopy, *Phys. Rev. Lett.*, *93*, 215502, 2004.
- [16] Kennett, B.L.N., S. Widiyantoro and R.D. van der Hilst, Joint seismic tomography for bulk sound and shear wave speed in the Earth's mantle, *J. Geophys. Res.*, *103*, 12,469-12,494, 1998.

- [17] Labrosse, S., Hotspots, mantle plumes and core heat loss, *Earth Planet. Sci. Lett.*, *199*, 147-156, 2002.
- [18] Li B.S. and J.Z. Zhang, Pressure and temperature dependence of elastic wave velocity of MgSiO₃ perovskite and the composition of the lower, *Phys. Earth Planet. Interiors*, *151*, 143-154, 2005.
- [19] Matas, J., Modélisation thermochimique des propriétés de solides a hautes pressions et hautes températures. Application géophysique. *PhD thesis, École Normale Supérieure*, Lyon, 1999.
- [20] Matthes, M.O.S., Mineralogie, *Springer-Verlag, Berlin*, 2005.
- [21] Masters G., G. Laske, H. Bolton and A. Dziewonski, The relative behavior of shear velocity, bulk sound speed, and compressional velocity in the mantle: Implications for chemical and thermal structure, in: S. Karato, A.M. Forte, R.C. Liebermann, G. Masters and L. Stixrude (eds.) *Earth's Deep Interior*, AGU Monograph 117, AGU, Washington D.C, 2000.
- [22] McCammon, C., The Paradox of Mantle Redox, *Science*, *308*, 807-808, 2005.
- [23] McDonough, W.F and Sun, S.-S., Composition of the Earth, *Chemical Geology*, *120*, 223-253, 1995.
- [24] McKenzie, D., J. Roberts and N.O. Weiss, Convection in the Earth's mantle: towards a numerical simulation, *J. Fluid Mech.*, *62*, 465-538, 1974.
- [25] McNamara, A.K. and S.J. Zhong, Thermochemical structures beneath Africa and the Pacific Ocean, *Nature*, *437*, 1136-1139, 2005.
- [26] Mégnin, C. and B. Romanowicz, The 3D shear velocity structure of the mantle from the inversion of body, surface and higher mode waveforms, *Geophys. J. Inter.*, *143*, 709-728, 2000.
- [27] Mittelstaedt, E. and P.J. Tackley, Plume heat flow is much lower than CMB heat flow, *Earth. Planet. Sci. Lett.*, *241*, 202-210, 2006.
- [28] Montelli, R., G. Nolet, F.A. Dahlen, G. Masters, E.R. Engdahl and S.-H. Hung, Finite-frequency tomography reveals a variety of plumes in the mantle, *Science*, *303*, 338-343, 2004.
- [29] Moores, E.M., A personal history of the ophiolite concept, in Ophiolite Concept and the Evolution of Geologic Thought, ed. Dilek and Newcomb, *Geological Society of America*, *373*, 17-29, 2003.
- [30] Nixon, P. H, Mantle Xenoliths, ed. *John Wiley, New York*, 267-280, 1987.

- [31] Oganov A.R., Brodholt J.P., Price G.D., The elastic constants of MgSiO₃ perovskite at pressures and temperatures of the Earth's mantle, *Nature*, *411*, 934-937, 2001.
- [32] Piazzoni, A.S., G. Steinle-Neumann, H.-P. Bunge and D. Dolejš, A mineralogical model for density and elasticity of the Earth's mantle, in press, *Geochem. Geophys. Geosyst*, 2007
- [33] Resovsky, J. and J. Trampert, Reliable mantle density error bars: An application of the neighbourhood algorithm to normal mode and surface wave data, *Geophys. J. Int.*, *150*, 665-672, 2002.
- [34] Ringwood, A.E., Composition and Petrology of the Earth's Mantle, *McGraw-Hill, New York*, 1975.
- [35] Samuel, H., C.G. Farnetani and D. Andrault, Heterogeneous lowermost mantle: compositional constraints and seismological observables, in *Earth's Deep Mantle: Structure, composition and evolution of Earth's mantle*, edited by R.D. van der Hilst, J.D. Bass, J. Matas and J. Trampert, *Geophys. Monogr. Ser.*, AGU, Washington, D.C., pp. 103-108, 2005.
- [36] Sautter, V., S. E. Haggerty and S. Field, Ultradeep (*>*300 Kilometers) Ultramafic Xenoliths: Petrological Evidence from the Transition Zone, *Science*, *252*, 827-830, 1991.
- [37] Shearer, P.M. and M.P. Flanagan, Seismic velocity and density jumps across the 410- and 660-kilometer discontinuities, *Science*, *285*, 1545-1548, 1999.
- [38] Shearer, P.M., Upper mantle seismic discontinuities, in *Earth's Deep Interior: Mineral Physics and Tomography from the Atomic to the Global Scale*, AGU Geophysical Monograph 117, 115-131, 2000.
- [39] Sinogeikin, S.V., J.Z. Zhang and J.D. Bass, Elasticity of single crystal and polycrystalline MgSiO₃ perovskite by Brillouin spectroscopy, *Geophys. Res. Lett.*, *31*, L06620, doi:10.1029/2004GL019559, 2004.
- [40] Stachel, T., Diamonds from the asthenosphere and the transition zone. *European Journal of Mineralogy*, *13*, 883-892, 2001.
- [41] Stixrude, L., R.J. Hemley, Y. Fei and H. K. Mao, Thermoelasticity of silicate perovskite and magnesiowustite and stratification of the Earth's mantle, *Science*, *257*, 1099-1101, 1992.
- [42] Stixrude, L. and C. Lithgow-Bertelloni, Thermodynamics of mantle minerals: 1. Physical properties, *Geophys J. Int.*, *162*, 610-632, 2005.

- [43] Tackley, P.J., D.J. Stevenson, G.A. Glatzmaier and G. Schubert GLATZMAIER GA, Effects of an endothermic phase-transition at 670 km depth in a spherical model of convection in the Earth's mantle, *Nature*, *361*, 699-704, 1993.
- [44] Tackley, P.J., Strong heterogeneity caused by deep mantle layering, *Geochem. Geophys. Geosystems*, *3*, 4, 1024, doi:10.1029/2001GC000167, 2002.
- [45] Tackley, P.J., S. Xie, T. Nakagawa and J.W. Hernlund, Numerical and laboratory studies of mantle convection: Philosophy, accomplishments and thermo-chemical structure and evolution, in *Earth's Deep Mantle: Structure, Composition, and Evolution*, edited by R.D. van der Hilst, J.D. Bass, J. Matas and J. Trampert, *Geophys. Monogr. Ser.*, AGU, Washington, D.C, pp. 83-99, 2005.
- [46] van der Hilst, R., S. Widiyantoro and E.R. Engdahl, Evidence for deep mantle circulation from global tomography, *Nature*, *386*, 578-584, 1997.
- [47] Walter, M., A. Kubo, T. Yoshino, J. Brodholt, K. Koga and Y. Ohishi, Phase relations and equation-of-state of aluminous Mg-silicate perovskite and implications for Earth's lower mantle, *Earth Planet. Sci. Lett.*, *222*, 501- 516, 2004.
- [48] Yagi, T., H.K. Mao and P.M. Bell, Structure and crystal-chemistry of perovskite-type MgSiO_3 , *Phys. Chem. Min.*, *3*, 97-110, 1978.
- [49] Zhong, S., Constraints on thermochemical convection of the mantle from plume heat flux, plume excess temperature and upper mantle temperature, *J. Geophys. Res.*, *111*, B04409, doi: 10.1029/2005JB003972, 2006.

2 A mineralogical model for density and elasticity of the Earth's mantle

Here I present a thermodynamic model of high pressure mineralogy that allows the evaluation of phase stability and physical properties for the Earth's mantle. The thermodynamic model is built from previous assessments and experiments in the five component CFMAS system (CaO-FeO-MgO-Al₂O₃-SiO₂), including mineral phases that occur close to typical chemical models of the mantle and reasonable mantle temperatures. In this system I have performed a system Gibbs free energy minimization, including pure end-member phases and a non-ideal formulation for solid solutions. Solid solutions were subdivided into discrete pseudocompounds and treated as stoichiometric phases during computation of chemical equilibrium by the simplex method. I have complemented the thermodynamic model with a model of shear wave properties to obtain a full description of aggregate elastic properties (density, bulk and shear moduli) that provide a useful basis for the consideration of seismic and geodynamic models of the Earth's mantle. The thermodynamic model described here is made available for research and training purposes through a web-interface (www.earthmodels.org). I examine its validity in light of experiments from mineral physics, and briefly discuss inferences for mantle structure.

2.1 Introduction

Geophysical studies of the deep Earth have advanced to the point where they now provide considerable insight into the physical state of my planet. This is seen most directly from seismic tomography [*Grand et al.*, 1997; *van der Hilst et al.*, 1997; *Bijwaard et al.*, 1998; *Masters et al.*, 2000; *Mégnin and Romanowicz*, 2000], which has brought a wide range of mantle heterogeneity into focus, reaching a state where these models are useful in guiding tectonic interpretations [*van der Voo et al.*, 1999; *Miller et al.*, 2006]. It is also evident from comparing seismic images with mantle circulation models [*Bunge et al.*, 1998; *McNamara and Zhong*, 2005; *Davies and Bunge*, 2006], i.e. models that assimilate records of past plate motion to approximate the pattern of Mesozoic and Cenozoic mantle flow.

At the same time, seismic tomography shows substantial complexity throughout the mantle as brought out by simultaneous mapping of bulk sound and shear wave velocities [*Kennett et al.*, 1998], models of probabilistic mantle heterogeneity [*Resovsky and Trampert*, 2002], or studies of finite frequency effects [*Montelli et al.*, 2004]. Seismology thus reveals thermal and chemical conditions in the deep Earth which are not easily understood in terms of mantle flow that is predominantly internally heated and chemically uniform. The realisation has prompted detailed geodynamic investigations of mantle temperature [*Bunge et al.*, 2001], plume flux [*Labrosse*, 2002; *Bunge*, 2005; *Mittelstaedt and Tackley*, 2006; *Zhong*, 2006], and the thermal state of convection having different chemical components [*Tackley*, 2002; *Samuel et al.*, 2005; *Tackley et al.*, 2005]; all such geodynamics studies must be compared to the seismic properties mapped by tomography.

Geodynamic models investigate variations in temperature (T), but the changes in physical properties revealed by seismological investigations can have their cause in either T or compositional effects (x). The trade-offs between thermal and chemical effects do not allow an unequivocal identification of the cause of heterogeneities in both the upper [Cammarrano *et al.*, 2003] and the lower mantle [Mattern *et al.*, 2005]. The solution to this problem can alternatively be attempted in a forward model, implementing more detailed mineralogical models or as an inverse problem, assuming additional constraints to the seismological observations, as gravity or geoid data [Ishii and Tromp, 1999; Deschamps *et al.*, 2002; Khan *et al.*, 2007], or electrical conductivity data [Khan *et al.*, 2006].

Progress in extent and precision of experiments in high pressure (P) mineralogy and petrology now makes it possible to build a thermodynamical model of mantle mineralogy based only on physical measurements (i.e. equation of state by X-ray diffraction, phase equilibria, calorimetric data) of material properties. Therefore, every P,T,x condition of the mantle can in principle be converted to a stable phase assembly and to physical properties such as density, bulk and shear moduli directly from equations of state. Here I present such a thermodynamic model of mantle mineralogy that is based on system Gibbs free energy minimization, coupled with a model of shear moduli [Stixrude and Lithgow-Bertelloni, 2005] and investigate consequences of the model on radial profiles of mantle properties. I consider the CaO, FeO, MgO, Al₂O₃, SiO₂ (CFMAS) components of the mantle and a comprehensive list of phases that describe a global mantle model, and fully consider chemical partitioning between the phases. The CFMAS system covers more than 99% of chemical models of the mantle, for example pyrolite [Ringwood, 1975; Irifune, 1987], and is able to accurately describe a wide range of petrological mantle models, e.g. piclogite [Duffy and Anderson, 1989], xenolith, [Wänke *et al.*, 1984] or a modified chondritic composition [Allègre *et al.*, 1995] (Table 1). Among these mantle models pyrolite and piclogite are chemically most distinct, with pyrolite being the source of mid ocean ridge basalt and residual peridotite. The piclogite model has been postulated in order to improve the fit of the seismic 1-D profiles at transition zone depth. Its origin has been proposed in the frame of a mantle evolution leading to a chemical differentiation that survives homogenization by mantle mixing [Bass and Anderson, 1984; Anderson and Bass, 1986; Duffy and Anderson, 1989]. Piclogite is much richer in both CaO and SiO₂ compared to pyrolite, while it is strongly depleted in FeO (Table 1). In order to assess the possible range of chemical and physical properties of the mantle I will in the following explore these two chemical models.

Convection models have traditionally applied a much simplified representation of mantle mineralogy. Some models restrict themselves to the Boussinesq approximation [McKenzie *et al.*, 1974; Christensen and Yuen, 1985; Bunge and Richards, 1996; McNamara and Zhong, 2005], in which all parameters are held constant and where density changes enter only through the buoyancy term of the Navier-Stokes equation, giving rise to gravitational forces. Other models have adopted a depth-dependent formalism through the use of the anelastic liquid approximation [Jarvis and McKenzie, 1980; Glatzmaier, 1988, Bunge *et al.*,

Table 1: Chemical bulk compositions of the global mantle in molar percent. Pyrolite is after *Irifune* [1987], piclogite from *Duffy and Anderson* [1989]. Xenolith is from *Wänke et al.* [1984], the “modified” chondritic model from *Allègre et al.* [1995].

Model	MgO	FeO	CaO	Al ₂ O ₃	SiO ₂
pyrolite	49.33	6.27	3.3	2.22	38.3
piclogite	42.32	5.29	8.67	1.78	41.94
xenolith	52.90	7.76	4.260	0.99	34.09
chondritic	53.16	7.67	3.92	1.00	34.25

1997]: The fluid under this assumption sustains compression or expansion due to changes in pressure as it sinks or rises, but thermal effects are ignored.

Similarly, the phase transitions leading to the 440 km and 660 km discontinuities are highly simplified in geodynamic models: they are commonly modeled as two sharp boundaries where anomalous buoyancy forces reproduce the dynamic effects of the phase transitions [*Christensen and Yuen*, 1985; *Tackley et al.*, 1993; *Bunge et al.*, 1997]. Such sharp transitions do not adequately describe the complexity of the phase transitions [e.g. *Hirose*, 2002; *Frost*, 2003] that have considerable effect on the dynamics of up- and downwelling flow in response to temperature and composition. For example, within high temperature upwellings perovskite (*pv*) transforms to majorite garnet (*gt*) first, before ringwoodite (γ) is formed from majorite and magnesiowüstite (*mw*) at lower pressure.

Moreover, in the context of the rapidly growing field of forward modeling of seismic wave propagation [e.g. *Igel et al.*, 1995; *Komatitsch and Tromp*, 2002a, 2002b], a model of density and elasticity in the mantle must be supplied as an input medium. Such an input model is commonly taken from tomography. A mineralogically self-consistent description of the physical properties in the mantle provides an alternative route to obtain absolute seismic velocities and travel times, independent of tomographic models [*Schuberth et al.*, 2005], and allows the comparison of simulated and observed seismograms for a range of dynamic hypotheses. For a detailed quantitative comparison anelastic corrections may need to be applied, as anelasticity causes both dissipation and dispersion of seismic waves [*Jackson et al.*, 2002; *Webb and Jackson*, 2003; *Matas and Bukowinski*, 2007].

In this section I present a model of mineral physics that can be used for such applications in geodynamics and seismology. After providing the context of the present work in the field of thermodynamics of mantle mineralogy I introduce my approach to the system Gibbs free energy minimization and the computation of physical properties. I will then show how my database performs compared to experimental data. I then introduce a web interface of my model that I provide for studies of mantle structure; this web-interface can be used for research, but it is also a valuable tool for teaching in structure and properties of the Earth’s deep interior. I conclude the section by briefly exploring results from my model in terms of the thermal and physical state of the mantle, compare to observational constraints, and

discuss limitations.

2.2 Previous Work

In order to understand Earth's mantle mineral assemblages and their physical properties studies in the fields of mineral physics, experimental petrology and thermochemistry have focused on two major efforts: (1) computation of the equilibrium mineral assemblages and (2) assessment of physical properties of the stable phases at mantle pressures and temperatures. These two aspects are now being combined into a coherent predictive model of mantle geodynamics.

Phase equilibria of ultramafic systems at high pressures have been computed in several subsystems: FeO-MgO-SiO₂ (FMS) [Saxena, 1996] and FeO-MgO-Al₂O₃-SiO₂ (FMAS) [Fabrichnaya, 1999]. The model of Fabrichnaya [1999] ensures by system Gibbs free energy minimisation the consistency of the database with both the measured phase transitions and the equation of state experiments. However, the presence of CaO and Al₂O₃ (> 5 wt% each) changes the stability of the solid solutions and the co-existence of different phases in the mantle. In addition, incorporation of CaO and Al₂O₃ into pyroxene and garnet solid solutions affects physical properties such as elastic properties [e.g. Andraut *et al.*, 2001; Frost and Langenhorst, 2002] that are of particular importance in seismology and geodynamics.

A number of studies have focused on physical properties in an attempt to understand the elastic and density structure of the mantle in terms of mineralogical data [e.g. Duffy and Anderson, 1989; Stixrude *et al.*, 1992; Vacher *et al.*, 1996; 1998]. More advanced physical models have integrated phase equilibria from an independent source and combined it with a model of physical properties. Such studies include those of Ita and Stixrude [1992] and Cammarano *et al.* [2003]. Ita and Stixrude [1992] advanced an accurate mineral physics model of volume and bulk modulus based on a Debye-Mie-Grüneisen approach for the thermal equation of state [see also Jackson and Rigden, 1996; Stixrude and Lithgow-Bertelloni, 2005]. Stixrude and Lithgow-Bertelloni [2005] have also incorporated an advanced treatment of the shear modulus for all the relevant phases of the mantle. It must be noted that until Stixrude and Lithgow-Bertelloni [2005], self-consistent thermodynamical models did not include shear properties that are essential to compute absolute values and partial derivatives of seismic velocities.

In recent years the integration of these two inseparable aspects has been approached by Matas [1999] and by Stixrude and Lithgow-Bertelloni [2005], although in the latter case the scheme to compute stable phase assemblages has not been published to date. Such databases take into account the physical properties from the equation of state, the thermodynamic quantities of all mantle phases and investigates their relative stabilities in a given chemical composition.

Here I have developed a computational scheme and compiled a database that evaluates phase stabilities and their physical properties in the CFMAS system. The assessment of

phase stability and phase compositions is based on a global Gibbs free energy minimization with discretized solid solutions, similar to the PERPLEX package [Connolly and Petrini, 2002; Connolly, 2005].

My approach is based on the simultaneous evaluation of calorimetric data (heat capacity, enthalpies where available) and experimental phase equilibria, combined with equation of state measurements. Therefore, it is designed to reproduce multicomponent mineral assemblages, their phase transitions and element partitioning. I can hence expect my model to perform well in computing width of phase transitions and effects of incorporating minor elements (e.g. Al in *pv*). I combine my thermodynamic database with the formulation of the shear modulus by *Stixrude and Lithgow-Bertelloni* [2005] to have a predictive tool to evaluate seismic structure in the mantle.

2.3 Methodology

My thermodynamic and physical model of the Earth’s mantle is based on the CFMAS system which closely represents the bulk silicate Earth. Other chemical components (e.g. Na₂O, K₂O) are present in abundances of less than 1% in typical mantle compositions and are neglected here, following previous work in the field [e.g. *Stixrude and Lithgow-Bertelloni*, 2005; *Ricard et al.*, 2005; *Mattern et al.*, 2005]. The thermodynamic dataset has been compiled on the basis of previous optimizations (more details below) of anhydrous mantle phases that provide reliable estimates of phase stability and physical properties and includes minerals that are expected to be stable at pressure and temperature conditions of the mantle (Table 2). Through the choice of the mineral phases considered (Table 2) I restrict the model to compositions close to that of standard mantle models (Table 1), a choice that precludes the use of the present database, for example, for the study of phase stabilities in basalt. The basalt composition is significantly richer in Al₂O₃ and FeO, and free phases of Al₂O₃ that could occur in basalts are not included in the mineralogical database, consistent with previous mantle mineralogy models [*Saxena*, 1996; *Cammarano et al.*, 2003; *Stixrude and Lithgow-Bertelloni*, 2005].

2.3.1 Equation of state and physical properties

The volume-pressure-temperature relationship of a solid phase is commonly treated by a pressure explicit formulation of the equation of state that combines isothermal compression (third order finite strain or Birch-Murnaghan equation of state [*Birch*, 1952]) with an expression for the thermal pressure P_{th} :

$$P(V, T) = 3K_0 f(1 + 2f)^{\frac{5}{2}}(1 + a_1 f) + P_{th},$$

where K_0 is the bulk modulus at zero pressure. The finite Eulerian strain f is given by

$$f = \frac{1}{2} \left(\left(\frac{V_0}{V} \right)^{2/3} - 1 \right) \quad (1)$$

where V_0 is the volume at zero pressure. In Eq. 1 the parameter a_1 includes the pressure derivative of the bulk modulus evaluated at zero pressure (K'_0):

$$a_1 = \frac{3}{2} (K'_0 - 4). \quad (2)$$

The thermal pressure is either introduced by a Mie-Debye-Grüneisen equation of state [e.g. *Jackson and Rigden, 1996*]

$$P_{th}(V, T) = \left(\frac{\gamma}{V} \right) (E_{th}(V, T) - E_{th}(V, 298K)), \quad (3)$$

$$E_{th}(V, T) = 9nRT \left(\frac{T}{\theta} \right)^3 \int_0^{\theta/T} \frac{t^3}{e^t - 1} dt, \quad (4)$$

or by a polynomial description of thermal expansion (α), typically containing fmy terms [*Saxena, 1996; Fabrichnaya, 1999; Mattern et al., 2005*]:

$$\alpha(T) = a + bT + \frac{c}{T} + \frac{d}{T^2}. \quad (5)$$

In the latter case P_{th} is computed according to

$$P_{th}(V, T) = \int_0^T (\alpha K_T)_V dT. \quad (6)$$

In Eq. 4 R is the universal gas constant, n the number of atoms in the formula unit, and θ the Debye temperature.

The Debye model is based on the approximation of a parabolic phonon density of state in a material, which allows the characterization of the thermal part, by the Debye temperature (θ) alone. However, this assumption is not always fulfilled in mantle minerals; for example, MgSiO_3 *pv* deviates rather strongly from this approximation [*Oganov et al., 2000*]. I have studied P-V-T fits with both models and found that there is very little difference in the misfit of data (Fig. 1), in particular relative to pressure and temperature uncertainties in experiments. I found that fitting θ is very sensitive to the choice of data in the fit, while I obtain robust results for the polynomial expansion of α . For many mineral phases P-V-T data at simultaneous high pressure and temperature are scarce; here, the physical foundation of the Debye model has a potential strenght in predicting equation of state properties, but I find very little difference for cases where I have compared the Debye model with a polynomial fit for α in the thermal equation of state. In computing the phase stability of minerals the equation of state plays only a minor role, and no significant deviations between phase stability diagrams can be observed between the two methods.

Due to the conceptual simplicity I have chosen a polynomial description of the thermal expansion here that allows us to use previous assessments of thermodynamic databases, e.g. by *Saxena* [1996], *Fabrichnaya* [1999] and *Matas* [1999]. The thermal expansion for all phases is summarized in Table 3.

The isothermal bulk modulus K_i^T of each phase is the reciprocal value of compressibility (in terms of volume V or Gibbs free energy G):

$$\frac{1}{K_i^T} = -\frac{1}{V} \frac{\partial V}{\partial P} \Big|_T = -\frac{1}{V} \frac{\partial^2 G}{\partial P^2} \Big|_T \quad (7)$$

Due to finite frequency of seismic wave the acoustic wave velocities in seismic reference models are related to the adiabatic bulk modulus (K_i^S). K_i^S is related to K_i^T by

$$K_i^S = K_i^T (1 + \alpha \gamma T) = \frac{C_p}{C_V} K_i^T \quad (8)$$

[*Poirier*, 2000], where C_V and C_p are the isochoric and isobaric heat capacity, respectively, and γ is the Grüneisen parameter. Heat capacities, γ and α are calculated by differentiating the Gibbs free energy:

$$C_p - C_V = \frac{V \alpha^2 T}{K_i^T} \quad (9)$$

$$C_p = -T \frac{\partial^2 G}{\partial T^2} \Big|_P \quad (10)$$

$$\alpha = \frac{1}{V} \frac{\partial^2 G}{\partial P \partial T} \quad (11)$$

$$\gamma = \frac{V}{C_V} \frac{dP}{dT} \Big|_V \quad (12)$$

Parameters such as density, bulk and shear moduli are calculated for these stable phases at pressure and temperature of interest. The physical properties of the aggregate can then be calculated from the physical property Ψ_i (for example, bulk or shear moduli) of n constituents of volume V_i and proportion x_i using the Reuss average under the assumption of uniform stress:

$$\Psi_R = \sum_{i=1}^n x_i V_i \Psi_i / V, \quad (13)$$

with $V = \sum_{i=1}^n x_i V_i$ or using the Voigt average under the assumption of uniform strain:

$$\Psi_V = V / \sum_{i=1}^n \frac{x_i V_i}{\Psi_i}. \quad (14)$$

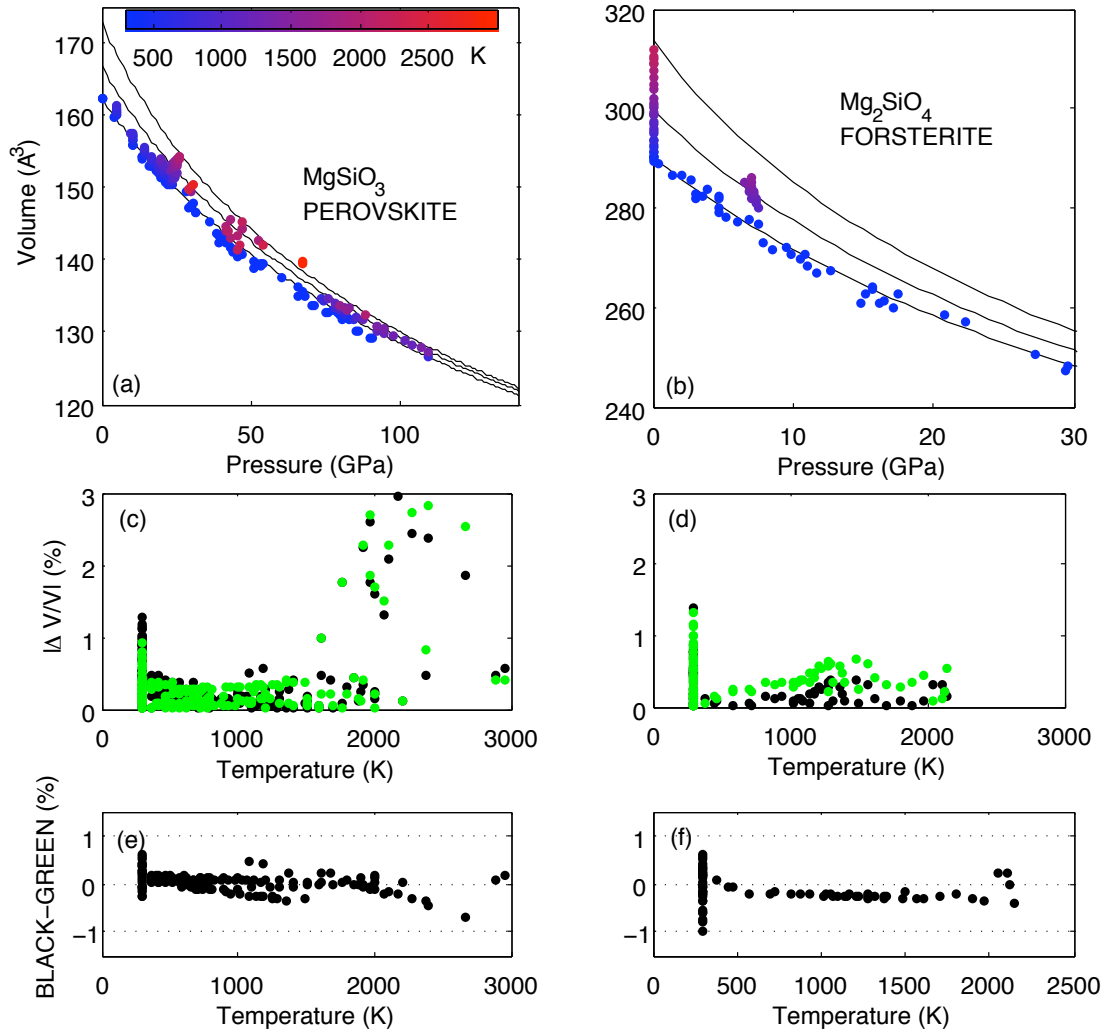


Figure 1: Fitting of P-V-T data for equation of state parameters for magnesium perovskite (left panels) and forsterite (right panels). The upper panels (a and b) show isothermal equations of state at 298, 1298 and 2298 K (solid lines) in comparison to experimental data (color coded for temperature). In the middle panels (c and d) I show the misfit between experimental data and my model (black points) and that of *Stixrude and Lithgow-Bertelloni*, [2005] as a function of temperature. The lower panels (e and f) show the difference between the two models. Experimental data for perovskite are from *Funamori et al.* [1996], *Fiquet et al.* [1998; 2000], *Saxena et al.* [1999] and *Utsumi et al.* [1999]. Data for forsterite are from *Hazen* [1976], *Kudoh and Takeuchi* [1985], *Will et al.* [1986], *Meng et al.* [1993], *Bouhifd et al.* [1996] and *Downs et al.* [1996].

These two schemes represent upper and lower limit of the aggregate properties, respectively. It is common to use their arithmetic mean (Voigt-Reuss-Hill scheme):

$$\Psi = (\Psi_R + \Psi_V)/2. \quad (15)$$

I adopt Eq. 15 here to calculate the physical properties of the aggregates. The difference between the Voigt and the Reuss averages is significant only in the upper mantle (where the maximum difference is 4%) and always smaller than 1% in the lower mantle.

2.3.2 Thermodynamic relationships

The solution of a multiphase equilibrium requires knowledge of the Gibbs free energy of each phase at P and T of interest. This is provided by thermochemical properties at 1 bar and an equation of state for volumetric properties (Table 3). These data are derived from previous thermodynamic assessments in the FMS and FMAS systems [Saxena, 1996; Fabrichnaya, 1999] and from the database of Matas [1999].

The apparent Gibbs free energy of a pure phase or a solution end-member, i , at temperature and pressure of interest, $\Delta_a G_{i(P,T)}$, is related to reference state properties (1 bar, 298.15 K) as follows:

$$\begin{aligned} \Delta_a G_{i(P,T)} &= \Delta_f H_{i(1,298)} + \int_{298}^T C_p^i(T) dT \\ &- T \left(S_{i(1,298)} + \int_{298}^T C_p^i(T)/T dT \right) \\ &+ \int_1^P V_i(P,T) dP, \end{aligned} \quad (16)$$

where $\Delta_f H_{i(1,298)}$ and $S_{i(1,298)}$ are enthalpy of formation from elements and entropy at 298.15 K and 1 bar, respectively. The heat capacity, $C_p^i(T)$ is a polynomial function of temperature (Table 3). For computational convenience, the volume integral in Eq. 16 is evaluated from a pressure-explicit equation of state (Eq. 1) using the following transformation:

$$\int_1^P V_i(P,T) dP = \int_{V_i(P,T)}^{V_i(1,T)} P_i(V_i,T) dV + (P-1)V_i(P,T). \quad (17)$$

The Gibbs free energy of a solid solution, $\Delta_a G_{ss(P,T)}$, incorporates additional contributions from configurational entropy and non-ideal enthalpy interactions. It is defined as

$$\Delta_a G_{ss(P,T)} = \sum_i n_i G_{i(P,T)} - TS_C + G_E. \quad (18)$$

S_C and G_E are configurational entropy and excess Gibbs free energy of mixing, respectively. Configurational entropy is related to the number of distinct mixing sites, site occupancy and mixing multiplicity. In terms of end-members concentrations n_i and chemical activity a_i ,

$$S_C = -R \sum_i (n_i \ln a_i) \quad (19)$$

In algorithmic implementation, element occupancies of individual crystallochemical sites are expressed in terms of end-member mole fractions. For example, the pv solid solution, $(\text{Mg,Fe,Al})(\text{Al,Si})\text{O}_3$, with one dodecahedral site, M, and one octahedral site, T, contains three linearly independent end-members: Mg- pv (MgSiO_3), Fe- pv (FeSiO_3) and Al- pv ($\text{Mg}_{.75}\text{Al}_{.5}\text{Si}_{.75}\text{O}_3$). Site fractions for individual elements are as follows:

$$y_{Mg}^M = \frac{n_{Mg-pv} + \frac{3}{4}n_{Al-pv}}{\sum_i n_i}, \quad (20)$$

$$y_{Si}^T = \frac{n_{Mg-pv} + n_{Fe-pv} + \frac{3}{4}n_{Al-pv}}{\sum_i n_i}, \quad (21)$$

where y_i^j is the mole fraction of element i in the j -th site.

Thus, in terms of phase fractions, the ideal activity of magnesium perovskite is

$$a_{Mg-pv} = (x_{Mg-pv} + 3/4x_{Al-pv})(x_{Mg-pv} + x_{Fe-pv} + 3/4x_{Al-pv}). \quad (22)$$

The ideal activity coefficients of all solid solution end-members as a function of the species concentrations are listed in Table 2.

The excess Gibbs free energy of mixing is described by the compound energy formalism [Sundman and Aagren, 1981; Hillert et al., 1988; Barry et al., 1992] with symmetric interaction parameters:

$$G_E = \sum_i^s \sum_j^m \sum_{k \neq j}^m (y_j^i y_k^i) \sum_q L_{jkq} (y_k^i - y_j^i)^q, \quad (23)$$

where L_{jkq} is the interaction parameter of the q -th order in the Redlich-Kister polynomial expansion. The summations include s crystallochemical sites and combine m elements in each site into pair interactions (j, k). Substitution of Eqs. 19 and 23 into 18 provides a complete description for the apparent Gibbs free energy of a solid solution at the pressure and temperature of interest.

2.4 Gibbs free energy minimization

Stable assemblage and phase composition at pressure, temperature and bulk composition of interest can be calculated by the equilibrium-constant method or by Gibbs free energy minimization (for a review see e.g. *Albarède [1995]* or *Anderson [2005]*). The equilibrium constant method employs the solution of a set of linear mass-balance constraints and non-linear mass-action equilibria [*Powell et al., 1998; Reed, 1998*]. This technique provides phase proportions and solution compositions, but it can not evaluate the phase stability. Therefore, it is not possible to eliminate unstable phases and/or include new potentially stable phases. This limitation hinders its use in this study because the stable phase assemblage at elevated pressure and temperature is not known a priori.

On the other hand, the Gibbs free energy minimization includes simultaneous evaluation of phase stability and computation of phase compositions and proportions [e.g. *de Capitani and Brown, 1987*]. In this study, I use a modification of the Gibbs free energy minimization [*Connolly and Kerrick, 1987; Connolly and Petrini, 2002; Connolly, 2005*]. The computation requires solving a set of linear mass-balance and evaluating phase stability. The solution procedure can be converted to a linear-programming task by dividing solid solutions into individual, stoichiometric pseudocompounds [*Connolly, 1990; Connolly and Petrini, 2002*]. The equilibrium assemblage is then found by the simplex algorithm [*Connolly and Kerrick, 1987; Albarède, 1995; Connolly, 2005*] that guarantees convergence to the global minimum of the Gibbs free energy hypersurface (Fig. 2). This approach is particularly suitable for systems with a small number of independent components but large number of phases whose stability must be evaluated.

At arbitrary P and T the system has the bulk composition \mathbf{q} , which is a vector of mole fractions of s oxides (here five: SiO₂, Al₂O₃, FeO, MgO and CaO). The database contains a total of p phases and solution pseudocompounds. The Gibbs free energy and oxide composition in the CFMAS space of each phase (or pseudocompound) are stored in vector \mathbf{g} and matrix \mathbf{B} , respectively (Fig. 2).

The function to be minimised is the total Gibbs free energy of the system, G :

$$G = \sum_{i=1}^s n_i g_i = \mathbf{n}^T \mathbf{g} \tag{24}$$

where \mathbf{n} is the vector of mole amounts of the stable phases. Note that according to the Gibbs phase rule, only s phases are stable (indicated with subscripts b) and $p - s$ phases remain metastable (subscript f) at every step of the minimization. The solution is subject to linear mass-balance constraints, i.e., the conservation equations for each oxide and a constraint that the mole amount of any stable phase cannot be negative:

$$\mathbf{B}^T \mathbf{n} = \mathbf{q} \tag{25}$$

Eqs. 24 and 25 define the linear programming problem that is solved in two alternating

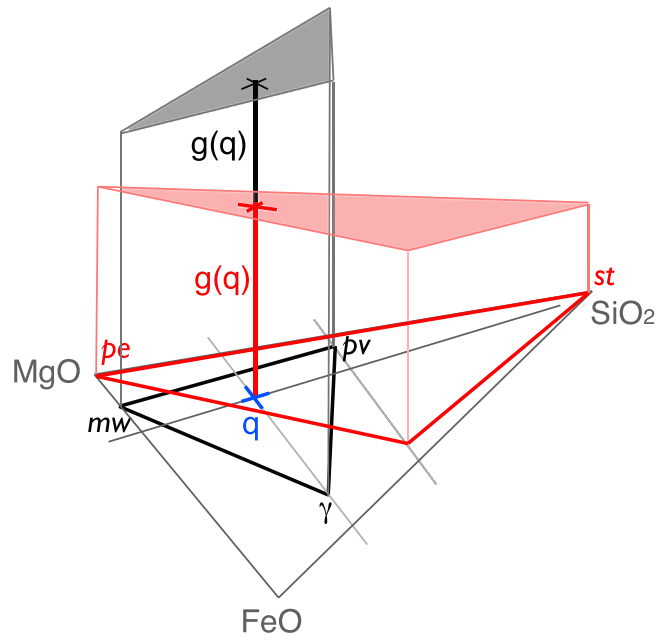


Figure 2: Illustration of the simplex minimization routine for the system MgO-FeO-SiO₂. Label q indicates the bulk composition in the base of the oxide system. Geometrically, the quantity to be minimized is the distance g between q and its projection on the plane that passes through the three metastable phases.

steps: (1) computation of phase proportions of the currently stable phases and of the Gibbs free energy of the system, and (2) phase switching whereby phases with higher Gibbs free energies are replaced by those with lower Gibbs free energies. The new stable phase is identified by the lowest Gibbs free energy with respect to the current energy hyperplane (Fig. 2). The vertical distance below the hyperplane, Δ , is defined as follows:

$$\Delta = \mathbf{g}_f - \mathbf{B}_f \mathbf{B}_b^{-1} \mathbf{g}_b. \quad (26)$$

The currently stable phase that will be replaced and excluded is found by respecting that all mole fractions of new stable phases must remain positive. This is accomplished by locating the smallest positive ratio, $\mathbf{n}_b/\mathbf{u}_i$, in the currently stable set of phases where $\mathbf{u}_i^T = -\mathbf{B}_f \mathbf{B}_b^{-1}$. After the phase switch, the calculation continues from Eq. 25 and it stops when the Gibbs free energy is at the minimum, i.e., when all elements of Δ are positive. As a consequence of separation of solid solutions into discrete pseudocompounds, the mole fractions of stable phases are processed and adjacent pseudocompounds belonging to the same solid solution are merged into one phase.

Table 2: Model of the solid solutions and their end-members. Each line gives the name of the end-member, its chemical formula, the name of the solid solutions it belongs to, an abbreviation that is used all-through the text and the ideal activity in the solid solution. The column “Activity” defines the activity of the end-member as a non-linear function of the mole fractions of individual end-members.

End-member	Formula	Solid solution/Abbreviation	Activity	#
Mg-perovskite	MgSiO ₃	Perovskite (<i>pv</i>)	$(a + \frac{3}{4}c)(a + b + \frac{3}{4}c)$	a
Fe-perovskite	FeSiO ₃		$b(a + b + \frac{3}{4}c)$	b
Al-perovskite	Al _{1/2} Mg _{3/4} Si _{3/4} O ₃		$\frac{16}{3\sqrt{3}}c^{1/2}(a + \frac{3}{4}c)^{3/4}(a + b + \frac{3}{4}c)^{3/4}$	c
Ca-perovskite	CaSiO ₃	Ca-Perovskite (<i>ca - pv</i>)	1	d
Periclase	MgO	Magnesiowuestite (<i>mw</i>)	e	e
Wuestite	FeO		f	f
Hp-clinoenstatite	Mg ₂ Si ₂ O ₆	Clinopyroxene (<i>cpx</i>)	$g(g + i)(g + h + i + l + \frac{m}{2})^2$	g
Hp-clinoferrrosilite	Fe ₂ Si ₂ O ₆		$h(h + l)(g + h + i + l + \frac{m}{2})^2$	h
Clinodiopside	CaMgSi ₂ O ₆		$(i + l + m)(g + i)(g + h + i + l + \frac{m}{2})^2$	i
Clinohedenbergite	CaFeSi ₂ O ₆		$(i + l + m)(h + l)(g + h + i + l + \frac{m}{2})^2$	l
Ca-Tschermak	CaAl ₂ SiO ₆		$4(i + l + m)m(\frac{m}{2}, \frac{g+h+i+l+m/2})^2$	m
Forsterite	Mg ₂ SiO ₄	Olivine (<i>ol, α</i>)	n^2	n
Fayalite	Fe ₂ SiO ₄		o^2	o
Mg-wadsleyite	Mg ₂ SiO ₄	Wadsleyite (<i>wads, β</i>)	p^2	p
Fe-wadsleyite	Fe ₂ SiO ₄		q^2	q
Mg-ite	Mg ₂ SiO ₄	Ringwoodite (<i>sp, γ</i>)	r^2	r
Fe-ringwoodite	Fe ₂ SiO ₄		s^2	s
Pyrope	Mg ₃ Al ₂ Si ₃ O ₁₂	Garnet (<i>gt</i>)	$(v + w)^3(v + z + j)^2$	v
Almandine	Fe ₃ Al ₂ Si ₃ O ₁₂		$(z + x)^3(v + z + j)^2$	z
Grossular	Ca ₃ Al ₂ Si ₃ O ₁₂		$j^3(v + z + j)^2$	j
Mg-majorite	Mg ₄ Si ₄ O ₁₂		$(v + w)^3w(w + x)$	w
Fe-majorite	Fe ₄ Si ₄ O ₁₂		$(z + x)^3x(w + x)$	x
Stishovite	SiO ₂	Stishovite (<i>st</i>)	1	y

Table 3: Database of the equation of state parameters and calorimetric data. The physical quantities are defined in the text. The letters in the first column indicate the mineral phases as in Table 2.

#	e.o.s. parameters										calorimetric data									
	V_0 $\frac{cm^3}{mol}$	K_0 GPa	$\frac{\partial K_0}{\partial T}$	K'_0	$\frac{\partial K_0}{\partial P}$	K''_0	$\frac{1}{K}$	a	b	c	d	ΔH_0 KJ	ΔS_0 $\frac{J}{K}$	a_1	a_2	a_3	a_4	a_5	a_6	a_7
	$K'_0 = K'_0 + K''_0$	$10^{-4}(T - 298.15)n(\frac{T}{298.15})$	$\frac{GPa}{K}$	$\alpha(T) = a * 10^5 + b * 10^9 T + c * 10^3 + \frac{d}{T^2}$	$[\alpha(T)] = \frac{1}{K}$	$C^P(T) = a_1 + a_2 T + \frac{a_3 * 10^6}{T^2} + a_4 * 10^{-6} T^2 + \frac{a_5 * 10^8}{T^3} + \frac{a_6}{\sqrt{T}} + \frac{a_7}{T}$														
a	24.45	262.5	-0.025	4.1	1.0	4.90	-2.31	-18.12	2.543	-1449.500	63.6	137.9	0.00156	-3.19	0.000	7.192	0	-14590		
b	25.59	272.6	-0.075	4.0	0.0	2.63	15.20	0.00	-0.040	-1096.780	91.1	142.2	0.00154	-1.18	0.000	2.733	0	-14556		
c	24.84	258.6	-0.039	4.0	0.0	3.37	9.14	-2.50	-0.370	-1501.300	65.8	139.6	-0.00486	-3.43	5.781	4.720	240	-17000		
d	27.45	232.0	-0.037	4.8	0.0	2.84	9.16	-2.60	-0.291	-1550.977	67.3	97.0	0.00811	2.21	1.845	3.550	1670	-31000		
e	11.25	160.8	-0.031	4.0	0.0	2.60	14.68	2.79	-0.428	-265.053	59.5	46.1	0.01148	0.00	0.000	0.000	0	0		
f	12.25	178.3	-0.029	4.2	0.4	3.64	8.35	0.85	-0.950	-601.490	27.0	45.5	0.00477	-2.16	0.000	1.744	0	2411		
g	30.45	111.0	-0.020	6.6	0.0	2.68	9.00	0.00	0.000	-1532.550	63.3	178.3	-0.01518	-6.41	5.491	6.000	-1730	-6.41		
h	32.07	97.2	-0.020	9.4	0.0	2.68	5.14	0.00	0.000	-1195.000	90.4	131.9	0.00066	-4.95	0.000	1.400	0	2320		
i	33.03	104.0	-0.026	6.2	0.0	1.76	22.11	4.53	-1.178	-1600.910	71.5	122.5	-0.00338	-4.07	3.260	4.725	230	-10770		
l	33.86	117.0	-0.015	4.3	0.0	2.71	5.67	-1.21	-0.315	-1419.410	85.1	122.5	0.00106	-4.18	1.459	4.275	300	-6875		
m	31.78	112.6	-0.025	4.2	0.0	3.62	4.76	8.74	-4.028	-1648.400	72.2	140.0	0.00134	-2.67	0.000	4.805	0	-13555		
n	43.67	128.1	-0.022	5.2	2.0	2.01	13.90	1.63	-0.338	-2174.140	95.6	165.8	0.01855	3.971	0.000	2.861	0	-5610		
o	46.28	126.9	-0.024	5.2	2.2	7.69	-2.78	-33.52	5.555	-1477.346	151.0	176.0	-0.00881	-3.89	2.471	0.000	0	0		
p	40.54	172.5	-0.029	4.3	3.0	2.32	9.04	-3.97	0.750	-2140.500	95.0	172.9	0.01129	-1.08	0.000	-2.187	0	13477		
q	43.14	171.3	-0.035	4.0	5.0	8.77	-2.61	-33.98	4.435	-1468.000	141.8	224.4	0.00892	15.59	0.000	-19.420	0	57576		
r	39.65	183.2	-0.041	4.3	6.0	1.22	11.04	2.50	-0.511	-2132.100	90.6	158.6	0.01220	-12.30	0.000	14.841	0	7971.9		
s	42.02	200.3	-0.145	4.0	8.0	8.90	2.80	-34.26	3.813	-1465.070	145.8	167.9	0.02812	-5.65	0.000	7.824	0	-3564.4		
v	28.29	173.0	-0.021	3.8	0.0	3.07	4.97	-3.03	-0.173	-1572.885	66.6	84.9	0.00818	-1.45	1.113	3.472	2290	-41662.5		
z	28.86	177.0	-0.018	4.0	0.0	2.58	3.20	-2.30	-0.142	-1658.580	84.1	92.6	0.00740	-2.48	0.338	3.665	1700	-29000		
j	31.32	168.0	-0.019	4.5	0.0	2.41	3.59	-1.94	-0.169	-1319.080	65.0	96.7	0.00631	-2.71	0.503	3.777	1522	-26337.5		
w	28.54	159.8	-0.020	4.9	0.0	1.88	5.34	0.00	0.000	-1513.000	59.0	127.5	0.00746	-11.06	0.000	19.760	0	0		
x	29.43	159.8	-0.026	4.9	0.0	1.88	5.34	0.00	0.000	-1163.850	88.2	112.6	0.01405	-0.62	0.000	5.755	0	0		
y	14.03	306.0	-0.019	2.8	0.0	2.28	1.12	-2.97	-0.096	-864.000	28.2	10.6	0.01158	4.41	-0.563	-1.150	3630	-67560		

2.5 Characteristics of the database

For building a thermodynamic database for mantle mineralogy a set of equation of state parameters and calorimetric data must be combined that jointly have predictive power for phase diagrams in the mineral systems considered (Table 3). Basing a global assessment on calorimetric data only (enthalpy and entropy of formation, as well as heat capacity) is a difficult task, and has proven illusive for the CFMAS system to this date. Alternatively, phase transitions themselves can be used to determine thermodynamically consistent datasets [e.g. *Fabrichnaya*, 1999; *Frost*, 2003].

In order to build up my database I have reviewed the extensive literature in the field [e.g. *Ita and Stixrude* 1992; *Saxena*, 1996; *Fabrichnaya*, 1999; *Matas*, 1999; *Stixrude and Lithgow-Bertelloni*, 2005 and references therein]. In particular *Fabrichnaya* [1999] shows meticulously the validity of the fitting for a relevant set of chemical subsystems. Data in the subsystems are assessed in order to optimize a set of constituent phase diagrams. Such a database becomes a predictive tool only when it is used in a larger system, for example a FMS database for the CFMAS system.

Due to stringent approach in the *Fabrichnaya* [1999] assessment and the compatibility with other thermodynamic datasets I have chosen this database as the core of my model and use the *Fabrichnaya* [1999] database for Mg- and Fe-*pv*, the *mw* solid solution, as well as the α -, β -, and γ -phases of the Mg_2SiO_4 solid solution (lines a, b, e, f, n-s in Tables 2 and 3). Below I compare this FMS database with more recent experimental results in the Mg_2SiO_4 based solid solution. For the purposes of this work, i.e. describing density and seismic velocities that is consistent in terms of buoyancy forces, temperature dependence of phase transitions and physical properties, it is important to include phases formed with the CaO and Al_2O_3 oxides, the CFMAS system for the mantle. I have therefore complemented the FMS system with data from *Matas* [1999] for Al-*pv*, the *gt* and *cp* solid solutions (lines c, g-m, v-x in Tables 2 and 3) and *Swamy and Dubrovinsky* [1997] for Ca-*pv*. In the mineralogical model Ca-*pv* is considered separate from the *pv* solid solution (Table 2), as there is a very low solubility of Ca in *pv* [*Hirose et al.*, 1999; *Tronnes and Frost*, 2002]. I also exclude the presence of Al in the Ca-*pv*, as my model is designed for magnesium-rich mantle compositions (Table 1) for which its solubility into Ca-*pv* has been found to be less than 2%mol [*Irifune*, 1994; *Kesson et al.*, 1998; *Wang and Takahashi*, 2000].

While akimotoite (ilmenite structured MgSiO_3 solid solution, *il*) is expected to be stable for cold temperatures at the base of the transition zone [*Wang et al.*, 2004] I have not been able to find or determine myself a reasonable set of thermodynamic parameters for *il*. While in the MgSiO_3 and $(\text{Mg,Fe})\text{SiO}_3$ systems its stability is well assessed [*Saxena*, 1996], in the presence of the other oxides many datasets yield an unexpected over-stabilization. As a consequence I have chosen to neglect the *il* phase in my database. The exclusion of *il* does not affect any of the geophysical discussion below.

The post-spinel transition, i.e. the breakdown of γ into the *pv* and *mw* solid solutions of the lower mantle, is of great geophysical significance as the Clapeyron slope of this

transition plays a central role in mantle convection. Depending on the Clapeyron slope, material exchange between the upper and lower mantle system can be hindered. There are many different models and experiments for the post-spinel transition in Mg_2SiO_4 , with a variety of Clapeyron slopes ranging from positive [Katsura *et al.*, 2003], close to zero and non-linear [Saxena, 1996] negative and small, [Katsura *et al.*, 2003; Fei *et al.*, 2004], to very negative [Ito and Takahashi, 1989; Ito and Katsura, 1989; Irifune *et al.*, 1998]. Furthermore, the pressure of the transition is not well determined, for reasons that include problems with the internal pressure standard [Fei *et al.*, 2004]. Almost all recent experiments predict a phase transition pressure that is too low for the post-spinel transition being consistent with the seismic discontinuity at 660 km depth [Fei *et al.*, 2004]. In order to circumvent this potential problem I have preferred a database that shows the transition at a pressure of about 23.8 GPa at 1900 K, consistent with the depth of the mantle discontinuity. Through the choice of thermodynamic data for the γ solid solution and the lower mantle assemblage the Clapeyron slope at geothermal average temperatures is on the order of ~ -1.2 MPa/K, consistent with recent experimental work [Katsura *et al.*, 2003; Fei *et al.*, 2004; Litasov *et al.*, 2005]. A comparison of the predicted P-X phase diagram of the Mg_2SiO_4 - Fe_2SiO_4 phase diagram from my model with recent experiments [Frost, 2003] shows excellent agreement (Fig. 3). For further comparison of phase diagrams with experimental work in the FMS system I refer to [Fabrichnaya, 1999].

In addition to changing phase relations chemical differences (heterogeneity) can affect physical properties. This is illustrated by changes in density and bulk modulus in response to the incorporation of Al_2O_3 and FeO into *pv* at pressures at the top of the lower mantle (Fig. 4). I find, in quantitative agreement with experimental studies, that the incorporation of Al_2O_3 has little effect on density ($< 1\%$ up to 15% Al_2O_3) while there is considerable softening in the compressibility, ~ 9 GPa for 5% Al_2O_3 (Fig. 4). In contrast, the incorporation of FeO causes the density to increase significantly: The unit cell volume increases with FeO content, but at the same time the specific weight increases more rapidly, causing a density increase by 0.2 g/cm³ (or ~ 4 -5%) per 10% FeO content (Fig. 4). The bulk modulus, however, is unaffected by the addition of FeO. Such changes are rather large compared to temperature effects for MgSiO_3 *pv* alone. To cause a density increase of 0.2 g/cm³ a temperature decrease of ~ 1500 K is required. In order to achieve a similar decrease in bulk modulus as caused by the addition of 5% of Al_2O_3 , an increase in temperature by 200-300 K is required.

The search for stable solid solution compounds by Gibbs-free energy minimization allows us to compute the Mg/Fe partitioning and its effect on the width and location of discontinuities in the mantle. In the transition zone I consider the balance of Fe^{2+} between the stable phases and look at the Fe content in the Mg_2SiO_4 phases (Fig. 5). In good agreement with experiments [Akaogi and Akimoto, 1979; Irifune and Isshiki, 1998; Frost, 2003] I find that iron partitioning into the Mg_2SiO_4 system increases by going from the α to the β to the γ phase (Fig. 5). For example, in the β stability field I find a Fe/(Fe+Mg) ratio of ~ 0.06 for pyrolite, slightly below the experiments for dry peridotite with a higher

bulk FeO content [Frost, 2003]. The Fe-Mg exchange is affected by a number of processes in the transition zone. At 15.5 GPa *cpx* is completely dissolved in *gt* and the relative amount of Fe in β decreases accordingly, as *gt* incorporates Fe more readily than *cpx*. At pressure above 21 GPa lower mantle phases start to appear and influence the Fe content in γ . Near the phase transitions (Figs. 5 and 6) large fluctuations in Fe content of the Mg_2SiO_4 polymorphs occur, reflecting the complexity of phase relations near transitions. In the lower mantle, *pv* and *mw* solid solutions compete in incorporating iron while Ca-*pv* is a repository of only a very small amount of iron, about 0.5 %wt [Irifune, 1994; Hirose *et al.*, 1999].

I now use the self-consistent Gibbs free energy minimization described above and estimate the stable phases for realistic bulk composition at P and T (Fig. 6). Some of the features of such a diagram are predetermined by the chemical model chosen for the mantle, prior to the minimization: the MgO+FeO/SiO₂ ratio in the bulk composition determines the ratio of the Mg_2SiO_4 (α and its high pressure polymorphs, β and γ) to MgSiO_3 (*cpx*+*gt*) based systems in the upper mantle, and that of *mw*/*pv* in the lower mantle. The percentage of CaO in the composition determines the maximum amount of Ca-*pv* present in the lower mantle, and the Al₂O₃ percentage sets the Al proportion in the *pv* solid solution.

Major features of the mantle mineralogy are not sensitive to chemistry, and occur in both the pyrolite and piclogite model. These include the pressure of phase transitions in the Mg_2SiO_4 system, and the breakdown of γ to *pv* and *mw*. However, in the MgSiO_3 -based part of the phase assemblage marked differences can be seen: at 1800 K the dissolution of *cpx* into *gt* is completed at lower pressure for pyrolite compared to piclogite. In the piclogite model the dissolution is complete at the same pressure as the occurrence of the β to γ transition, in agreement with previous results [Ita and Stixrude, 1992].

In both chemical models a small stability field of stishovite (*st*) appears around 20 GPa at moderate temperatures, where *gt* breaks down into *st* plus γ (Fig. 6); the proportion of *st* in piclogite is much bigger than in pyrolite due to the higher SiO₂ content. This is again consistent with other mantle mineralogical models [Ita and Stixrude, 1992] and the observation of traces of *st* in a pyrolitic composition near 20 GPa and 1900 K [Hirose, 2002]. For temperatures above 2000 K *st* is no longer stable. The stability of *st* may also partly be facilitated by the lack of the *il* phase in my database as discussed above: the transformation from *gt* to *il* could suppress the breakdown of *gt*.

2.6 Web interface

The thermodynamic model presented in the current section is accessible on the world wide web under www.earthmodels.org (currently still under <http://webmathematica.geophysik.uni-muenchen.de/gcubed/gcubed.jsp>). I believe that this can be a useful tool for studies of the Earth's interior and will serve as a teaching resource for mantle mineralogy in classes of geophysics and geochemistry to illustrate properties of the deep Earth. The interface has been built using webMathematica which performs part of the Mathematica program that

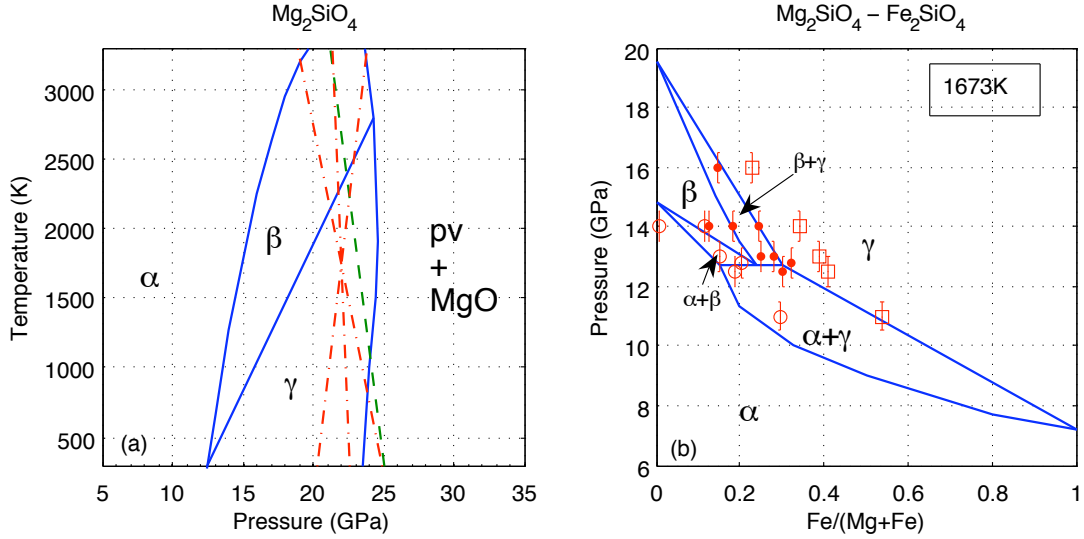


Figure 3: Phase transformation for the $(\text{Mg,Fe})_2\text{SiO}_4$ system. The panel (a) shows the pressure and temperature dependence of the phase transitions for Mg_2SiO_4 : Solid lines indicate my model, the dashed (green) line is from *Fei et al.* [2004] and the dotted-dashed lines (red) show three permissible Calpeyron slopes from *Katsura et al.* [2003]. The panel (b) shows phase transitions and coexistence areas as a function of pressure for the $(\text{Mg,Fe})_2\text{SiO}_4$ system at constant temperature (1673 K). Red symbols show the experiments of *Frost* [2003] for stable phases near the transition. Open circles stand for α , solid circles for the β phase and open squares for γ spinel. The vertical error indicates the pressure uncertainty from *Frost* [2003].

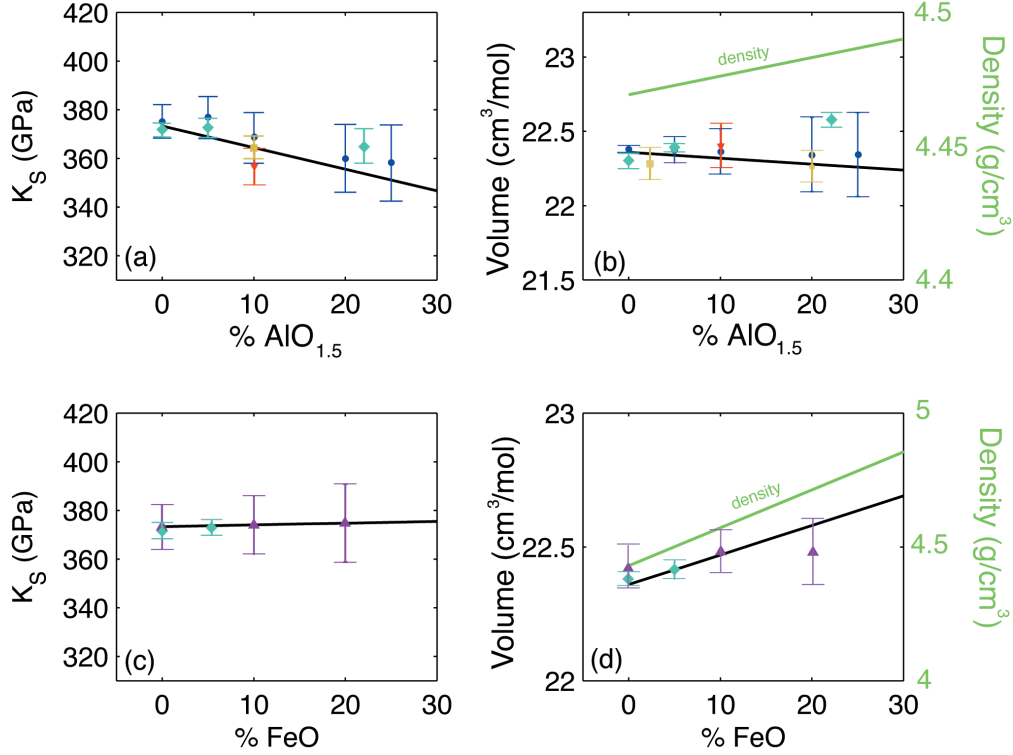


Figure 4: Chemical effects on the adiabatic bulk modulus (left column) and molar volume/density (right column) of pv at 298K and 28 GPa. The upper panels show my calculation (black solid line) for the binary solid solution $Mg-pv - Al-pv$, up to an Al_2O_3 content of 15%. The lower panels for the $Mg-pv$ and $Fe-pv$ binary solid solution. The molar volume is converted to density (green solid line in the right column). All results are compared with experiments that have been interpolated or extrapolated to 28 GPa and 298 K: circles (blue) [Walter *et al.*, 2004]; triangles down (red) [Daniel *et al.*, 2004]; squares (yellow) [Yagi *et al.*, 2004]; diamonds (turquoise) [Andraut *et al.*, 2001]; triangles up (violet) [Mao *et al.*, 1991]. Error-bars are taken from the experiments and appropriately propagated. Errors in Mao *et al.* [1991] were not reported and are added consistently with other experiments

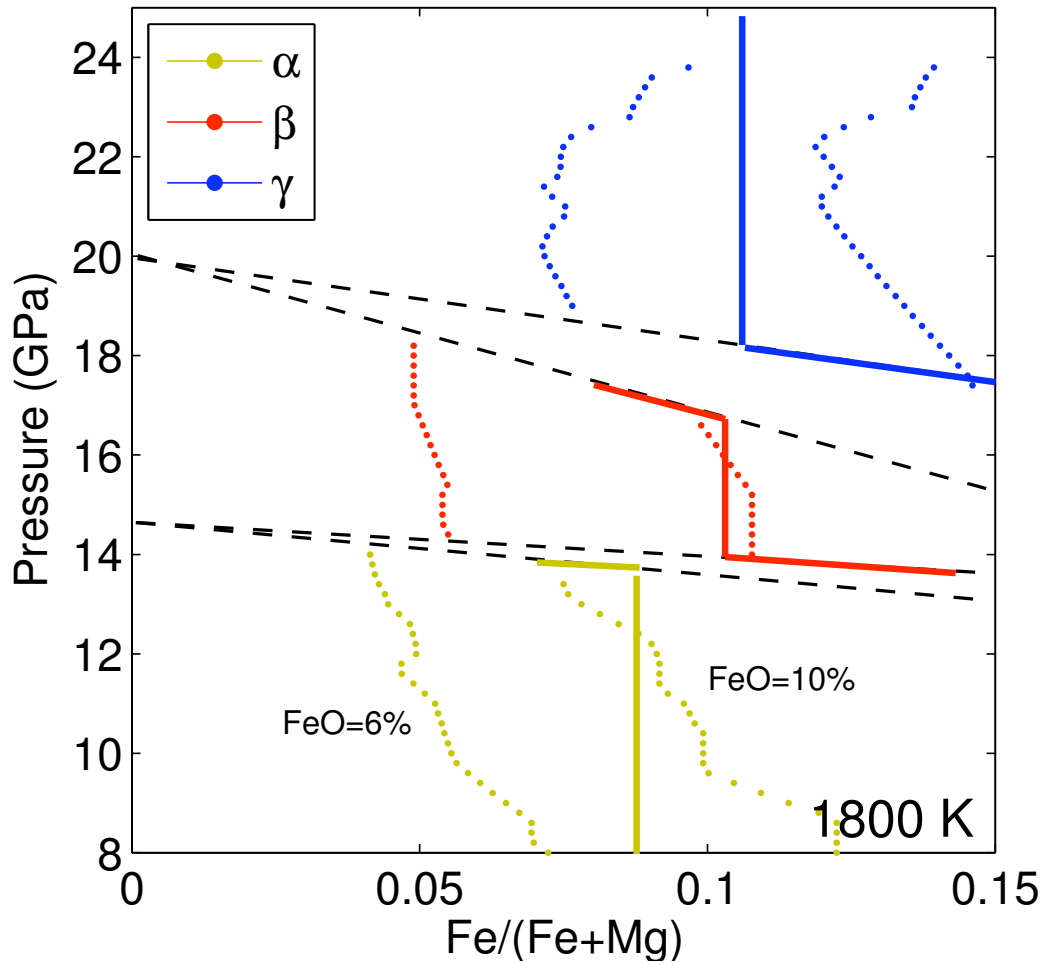


Figure 5: Iron partitioning in the $(\text{Mg,Fe})_2\text{SiO}_4$ system (α , β and γ) at transition zone pressures and 1800 K. Dotted curves show my model for two FeO contents (6% and 10%) in a pyrolite based bulk composition. The solid line is from experiments for dry peridotite (10% FeO) [Frost, 2003]. The calculation takes into account all the other stable phases of a pyrolite composition, i.e. *gt* and *cpx*. Dashed lines show the phase transition pressures of the phase transitions in the $(\text{Mg,Fe})_2\text{SiO}_4$ system as a function of Fe-content.

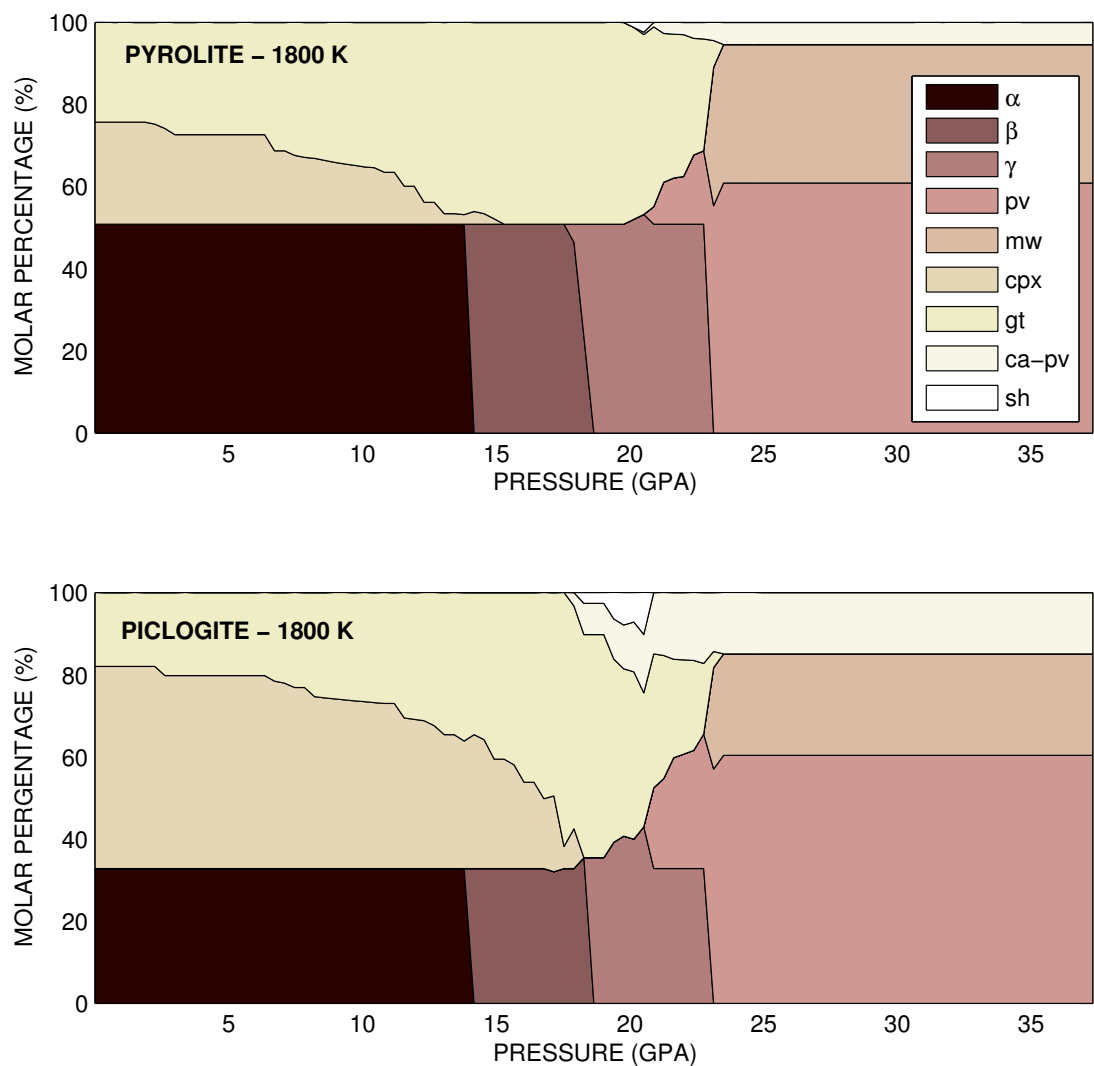


Figure 6: Stable phases and their proportions at a constant temperature of 1800 K. The upper panel shows the diagram for pyrolite bulk composition. The lower panel is computed at the same conditions as above but for piclogite composition. Abbreviations for mineral phases are introduced in Table 2. The diagram is not smoothed in order to illustrate numerical fluctuations in the minimization routine and the effect of discontinuities of the physical properties (as iron partitioning) on the phase abundances.

has been used for the calculations of this paper. The web interface allows the assessment of physical properties of deep Earth mineralogy as following. The calculator minimizes the Gibbs free energy for a given composition, depth (pressure) and temperature for a pyrolitic mantle model. The Gibbs free energy minimizer provides output in two blocks. First, global properties of the stable aggregate are given. These are pressure, density, the adiabatic bulk modulus, and the shear modulus. In the second part a list of stable phases is provided, with details on their chemical composition and mole proportion in the phase assemblage. This information is also illustrated in a pie chart.

2.7 Mantle structure

With the global mineral database it is possible to construct isentropic curves of temperature, by imposing the constraint:

$$S = -\left(\frac{\partial G}{\partial T}\right)_P = \text{const.} \quad (27)$$

I numerically compute curves of constant entropy in order to determine the adiabatic geotherm consistent with my mineral database (Fig. 7). At any phase transition the condition of constant entropy forces the temperature profile to change, compensating for the exothermic or endothermic effect of the transition. While the degree of adiabaticity in the Earth remains under debate [Bunge *et al.*, 2001] and it depends on considerations of the ratio between internal radioactive heating and bottom heating [Bunge, 2005], an adiabat provides a good starting point for a discussion of the thermal and physical state of the Earth’s mantle. To fully constrain a mantle geotherm an absolute temperature at 0 GPa (the surface), the footing temperature, has to be chosen. Alternatively, a fixed temperature at another pressure can be used. I have chosen a conventional footing temperature based on heat flow and sea-floor depth variations of 1500 K [Stein and Stein, 1992] (Fig. 7) and also provide alternative scenarios for ± 150 K (Fig. 7). The total ΔT from the core-mantle-boundary to the surface along the adiabats (excess temperature) depends on the footing temperature with hot adiabats showing a stronger increase than cold ones. I find ΔT to depend quite linearly on the footing temperature (Fig. 7), with the colder geotherm (footing temperature of 1350 K) undergoing a total temperature increase of ~ 730 K and the hotter geotherms (with a footing temperature of 1650 K) of ~ 910 K.

This implies that the excess temperature of an upwelling plumes increases as I go deeper into the mantle. From a dynamical point of view the petrologically inferred excess temperature in mantle plumes (on the order of 200 – 300 K [Schilling, 1991]) is much too low compared to the excess temperature in the mantle expected from geodynamics [e.g. Jeanloz and Morris, 1986]. While for this a number of explanations have been put forward, including a dense layer in D'' [Farnetani, 1997] or subadiabaticity in mantle due to internal heating [Bunge, 2005; Zhong, 2006] the adiabatic profiles through the mantle provide a

natural explanation by means of stronger cooling of hot upwellings relative to ambient mantle.

In order to assess the physical properties in the mantle the single phases that are stable under relevant pressure and temperature (Fig. 8) need to be considered. Major changes in specific volume (density), bulk modulus, and other thermodynamic parameters occur at phase transitions where minerals transform to more closely packed structures (Fig. 8). These changes - occurring discontinuously - are more pronounced than changes in response to temperature and pressure over a moderate pressure range. For example, in the MgSiO_3 solid solution the transition from gt to pv occurs with a volume decrease of $\sim 20\%$ (density increase of $\sim 20\%$). To obtain a comparable increase in density for pv alone the pressure must increase by more than 100 GPa. For the bulk modulus the $gt - pv$ transition goes along with an increase of $\sim 20\%$, comparable to an increase in pressure of ~ 10 GPa for pv .

Ca-pv has a significantly different molar volume (density difference of $\sim 4\%$) compared to the pv solid solution but their bulk moduli are comparable (Fig. 8). As in Fig. 6 I can see sensitivity of transition zone mineralogy and physical properties on temperature. st appears in the stable phase assemblage only up to ~ 2000 K, and for very high temperature β transforms directly to pv plus mw , without going through the γ stability field (Fig. 3). Compressibility curves for single phases converge at high pressure for the various temperatures, reflecting the fact that thermal expansion decreases significantly at high pressure.

Combining the single phase properties (Fig. 8) with the phase proportions (Fig. 6) one can obtain the properties of the phase assemblage (Eqs. 13-15). Taking the properties along an adiabat with footing temperature of 1500 K (Fig. 7) I plot one dimensional reference profiles of density, bulk modulus and bulk sound velocity through the mantle (Fig. 9). Density and bulk modulus (Fig. 9) are calculated from the same equations of state that are also used to compute the phase stabilities (Fig. 6). I find overall good agreement with seismic reference models for these parameters and the bulk sound velocity (Fig. 9).

Through the transition zone I find a number of small and relatively smooth increases in seismic properties. This is different from the seismological models that by construction locate - and hence predefine - discontinuities at 400 and 670 km for PREM [*Dziewonski and Anderson, 1981*] or 410 and 660 km for AK135 [*Kennett et al., 1995*]. However, there is good agreement in the width of the transitions both with seismological models and previous studies [*Bina and Wood, 1987; Frost, 2003*]. For example, the transformation of gt to pv takes place over a wide pressure region, smearing out the discontinuity at the top of the lower mantle to well below 660 km, in good agreement with experiments [*Hirose et al., 1999*]. Differences in the very upper mantle are due to the absence of low pressure phases in my model. The discrepancy of the mineralogical models with respect to PREM around 220km (~ 7 GPa) could also be affected by the layering in PREM - the 220 km discontinuity is not present in AK135. While a comparison between the density-depth relation constrained by seismology [*Dziewonski and Anderson, 1981; Masters and*

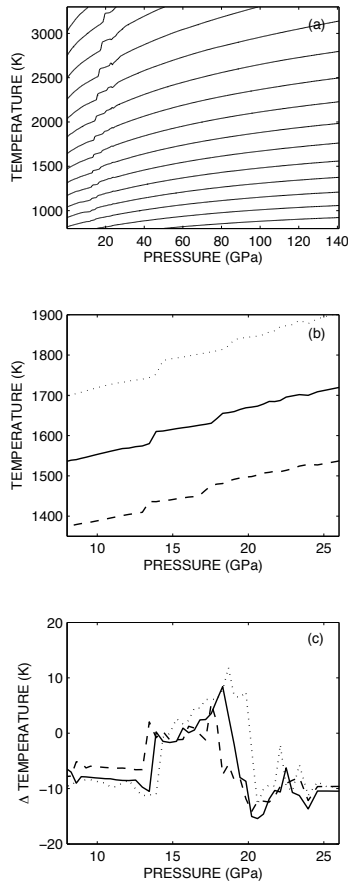


Figure 7: Adiabatic temperature profiles from the mantle mineralogical model. (a) shows lines of constant entropy as a function of pressure for pyrolitic composition. The adiabats are spaced at fixed difference of entropy, and cover a wide range of temperatures (800-3300 K). (b) is a blow-up of (a), focusing on the pressure range where the phase transitions occur and where jumps in temperature compensate for entropy changes due to exothermic and endothermic transitions. The three adiabats shown have a footing temperature of 1350 K (dashed), 1500 K (solid), and 1650 K (dotted). (c) shows the differences between pyrolite and piclogite models from the surface to the top of the lower mantle for three adiabats with the same footing temperatures as in panel (b). Differences are on the order of 10-15 K and are most pronounced in the transition zone.

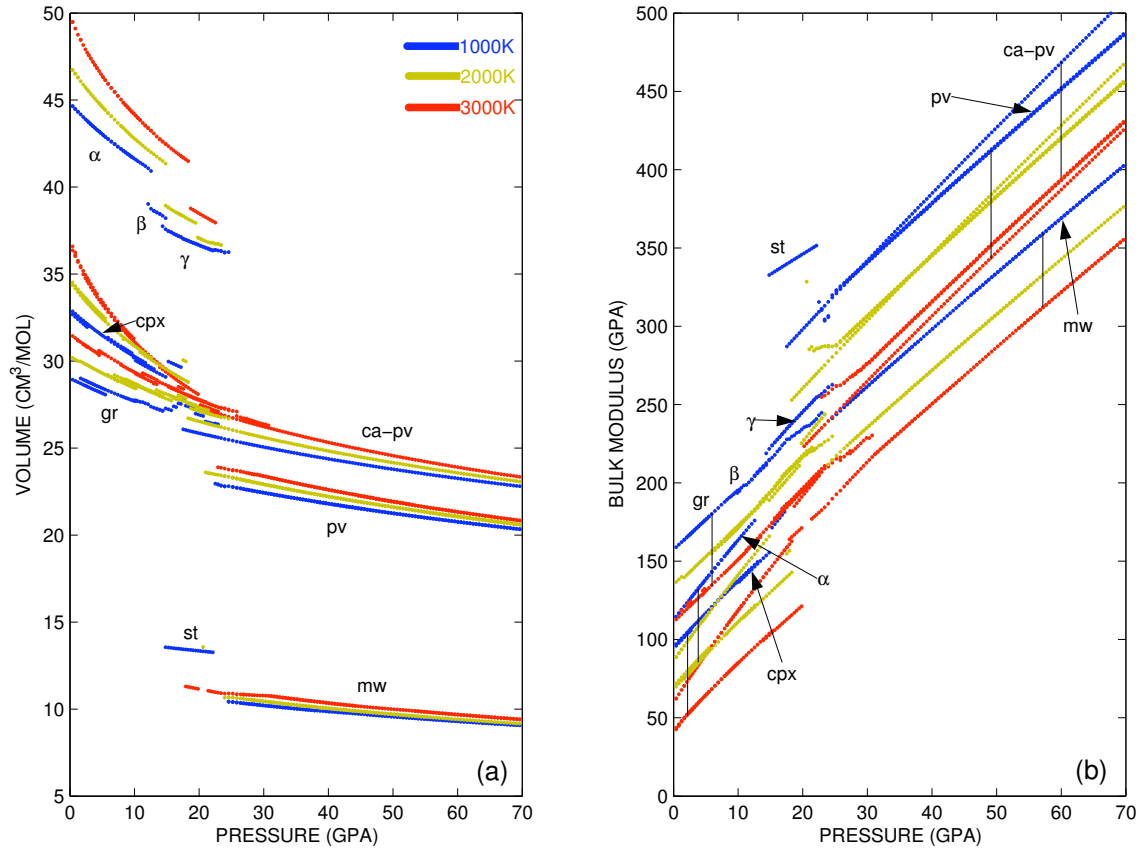


Figure 8: Physical properties of the stable phases in a pyrolitic mantle for isotherms of 1000 K (blue), 2000 K (yellow) and 3000 K (red) for pressures up to 70 GPa (mid-lower mantle). (a) Molar volume of the stable phases as a function of pressure. (b) Adiabatic bulk modulus of the stable phases. The stoichiometry of some of the phases has been rescaled for better comparison among different phases (e.g. pyrope *gr* volume is calculated on the stoichiometry $\text{Mg}_{3/4}\text{Al}_{1/2}\text{Si}_{3/4}\text{O}_3$), consistent with Table 2.

Gubbins, 2003] would be desirable, my model is not able to construct a meaningful profile, as uppermost mantle and crustal mineralogy is not considered here.

There is also good agreement between the shear moduli I calculated from the database of *Stixrude and Lithgow-Bertelloni* [2005] and seismological models, and as a consequence for the seismic wave velocities that depend on the shear modulus: the p- and s-wave velocity (Fig. 9).

The comparison with seismic models shown here has limitations for a number of issues: For example, deviations from an adiabatic profile (through internal heating, see section 4) would change the physical properties. Also, the conversion of temperature into seismic observables is non-linear, i.e. the average of the seismic velocity over a temperature range does not correspond to the seismic velocity for the temperature mean, and therefore 1-D profiles are intrinsically approximate. In order to quantify such effects a range of geodynamic models would need to be considered and the resulting T fields be evaluated in terms of seismic properties. Lastly it is worth noting that seismic reference models such as PREM and AK135 show differences among themselves that are often greater than the discrepancy between the mineralogical models and a particular reference model.

As mentioned above the phase transition near 23-25 GPa (the 670 km discontinuity in PREM, 660 km in AK135) plays a central role in the dynamics of the Earth's mantle. If the breakdown of γ to pv and mw has a negative Clapeyron slope as inferred in most experiments [*Ito and Takahashi*, 1989; *Ito and Katsura*, 1989; *Irifune et al.*, 1998; *Katsura et al.*, 2003; *Fei et al.*, 2004] and in my model for high temperatures, the buoyancy forces produced by the transition act as a barrier to vertical flow [*Christensen and Yuen*, 1985; *Tackley et al.*, 1993; *Bunge et al.*, 1997]. However, the set of phase transitions occurring at the top of the lower mantle are more complex than a separate consideration of the Mg_2SiO_4 and $MgSiO_3$ based systems would suggest [*Vacher et al.*, 1998; *Hirose*, 2002]: My thermodynamic model shows that st becomes stable at low temperatures (Figs. 6 and 7), other models and experiments observe the stability of il . In a dynamic mantle the additional negative buoyancy from dense st or il in a subducting slab will facilitate its sinking into the lower mantle, consistent with global observation in seismic tomography [*Becker and Boschi*, 2002].

Similarly, at high temperatures (~ 2300 K) γ does not break down into pv and mw directly but passes through the gt stability field, resulting in a transformation of γ into gt and mw (Fig. 10), in good agreement with experimental phase relations in dry pyrolyte [*Hirose*, 2002] (although my density changes are less pronounced than those in the experiment). This transition has a positive Clapeyron slope, and a hot upwelling would experience additional buoyancy at 660 km from the pv to gt transformation and readily penetrate the discontinuity, becoming part of the upper mantle circulation system before it is slowed down by the effects of the negative Clapeyron slope of the gt or pv plus mw to γ transition.

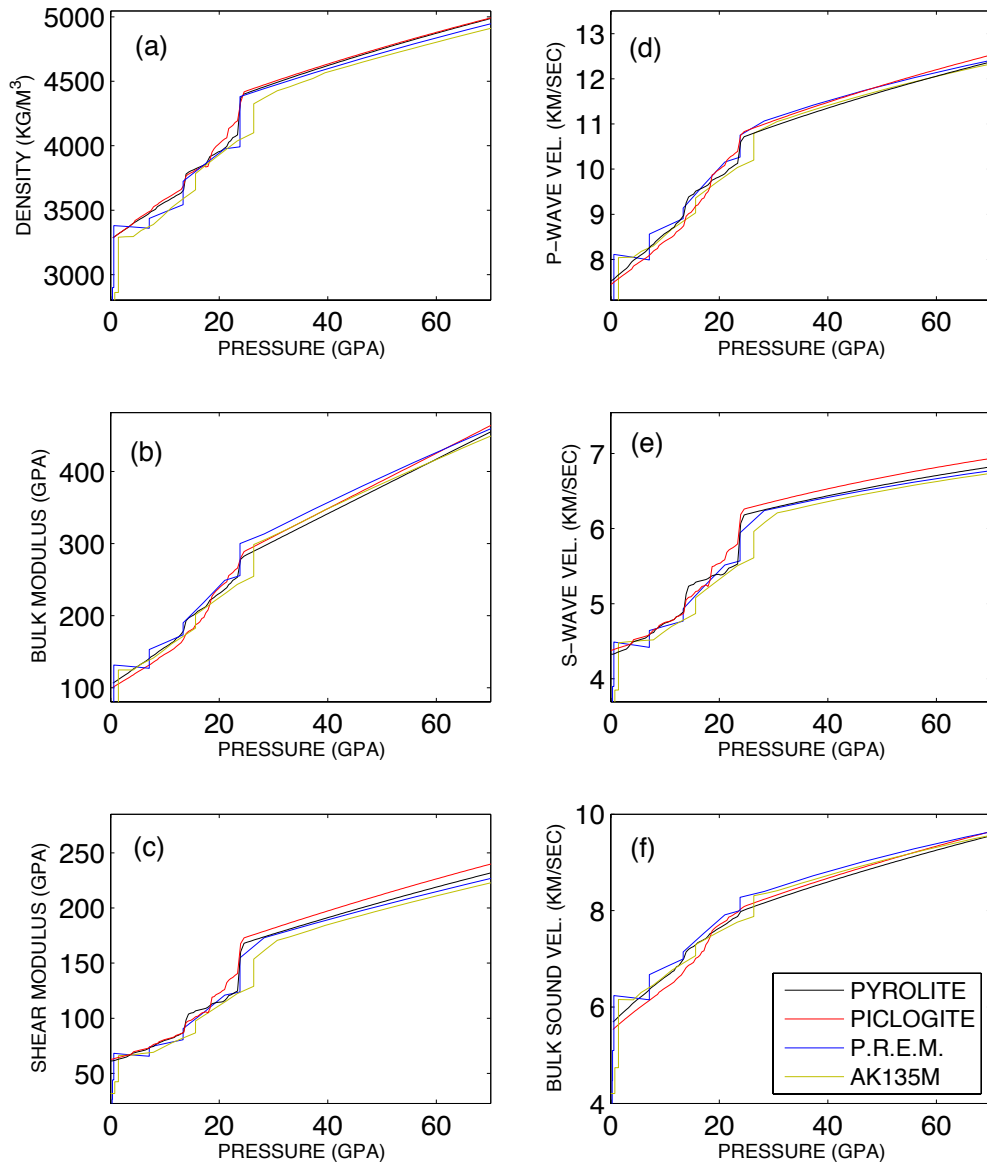


Figure 9: Comparison of physical properties from the mineralogical model for pyrolite and piclogite bulk compositions along an adiabat (footing temperature of 1500 K) with seismic reference models (PREM and AK135M). Panels (a)-(f) show the density, bulk and shear modulus, p-, s-wave and bulk sound velocities, respectively. The comparison is shown on a pressure scale, the natural variable in the Gibbs free energy minimization; the pressure values for the seismological models are based on the density structure of the seismological models themselves.

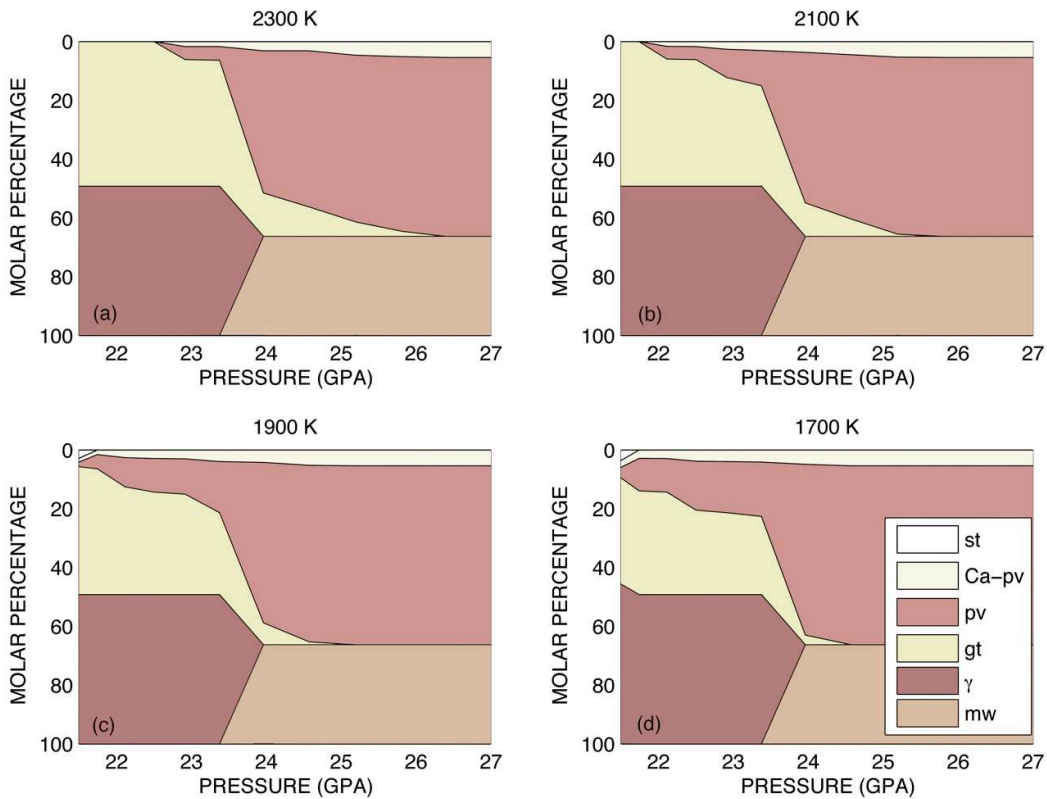


Figure 10: Molar percentage of the stable phases for a pyrolitic mantle at different temperatures (1700-2300K) over the pressure range of the transition zone. At low temperature (panels (c) and (d)) *pv*, *mw* and *Ca-pv* form over a narrow depth interval from *gt* and γ via the post-spinel transition (with negative Clapeyron slope). I note that my database does not include ~ 10 vol% of *il* (denser than *gt*) that is expected to be present at low temperatures [Hirose, 2002]. At high temperatures (panels (a) and (b)) *gt* is stable up to lower mantle pressures, transforming smoothly into *pv* (with positive Clapeyron slope). The pressure at which *gt* is completely transformed into *pv* corresponds at high temperature to about 720km. The post-spinel phase transition occurs at 23-24 GPa (650-670km).

2.8 Conclusions and limitations

A mineralogical model based on P-V-T equations of state and internally consistent thermodynamic data offers a viable route to explore mantle structure, complementing observations from seismology and geodynamic modeling. In particular, an understanding of underlying phase transitions is critical for the description of discontinuities in the Earth's mantle, and the resulting dynamic effects. The database presented here does not systematically re-evaluate thermodynamic parameters for mantle mineralogy; instead, it expands a previous assessment on FMS by *Fabrichnaya* [1999] to the CFMAS system, incorporating parameters that capture the crucial aspects of mantle mineralogy. I paid particular attention to a good description of density and its variations on compression, temperature and phase transitions, as well as elastic properties of the phase assemblage. These two sets of information are important to accurately describe buoyancy forces in a dynamic Earth and for predicting elastic structure.

Despite the progress on thermodynamics of mantle mineralogy reported here and elsewhere [*Stixrude and Lithgow-Bertelloni*, 2005; *Matas*, 1999] there are important petrological/mineralogical factors that have not been fully considered in such models.

Some of the physical parameters may not be known as well as the current state in mineral physics suggests. The P-V-T equation-of-state data used in thermodynamic models rely on powder X-ray diffraction refinements. Such measurements, however, yield slightly different compressibility data than single crystal work. For example for Mg-*pv* the isothermal K_0 from single crystal diffraction is 253 GPa [*Ross and Hazen*, 1990; *Vanpeteghem et al.*, 2006] while powder X-ray diffraction yields 263 GPa, as used in my database and elsewhere. Single crystal results for K_0 are further supported by direct determination of the elastic moduli by Brillouin spectroscopy [*Sinogeikin et al.*, 2004] and ultrasonic interferometry [*Li and Zhang*, 2005].

The current model does not consider ferric iron (Fe^{3+}), because a consistent thermodynamic model for Fe^{3+} incorporation in all mantle phases is not yet available. While the Mg_2SiO_4 polymorphs incorporate only negligible amounts of Fe^{3+} [*McCammon*, 2005], *gt*, *cpx*, and *pv* can include significant fractions of Fe^{3+} , in particular in the presence of Al^{3+} . This can be expected to affect phase relations and physical properties of the single phases considerably, in particular in the lower mantle where Fe in *pv* appears to be incorporated preferentially as ferric iron [*McCammon*, 1997; *McCammon et al.*, 1997].

The discovery of the post-perovskite (*ppv*) phase in the MgSiO_3 system at P and T coinciding with those of the D'' region [*Murakami et al.*, 2004; *Oganov and Ono*, 2004] potentially adds complexity to the mineralogy in the lowermost mantle. However, as for the ferric iron the database of experiments and computational work is still too limited to assess the stability of the *ppv* phase in the mantle. In particular, the addition of chemical complexity may change the phase transition and will open a multi-component phase loop with the *pv* and *ppv* coexisting over a potentially wide pressure region [*Akber-Knutson et al.*, 2005; *Tateno et al.*, 2005; *Murakami et al.*, 2005].

References

- [1] Akber-Knutson, S., G. Steinle-Neumann, and P.D. Asimow, Effect of Al on the sharpness of the MgSiO₃ perovskite to post-perovskite phase transition, *Geophys. Res. Lett.*, *32*, L14303, doi:10.1029/2005GL023192, 2005.
- [2] Akaogi, M. and S. Akimoto, High-pressure phase-equilibria in a garnet lherzolite with special reference to Mg²⁺-Fe²⁺ partitioning among constituent minerals, *Phys. Earth Planet. Interiors*, *19*, 31-51, 1979.
- [3] Albarede, F., Introduction to Geochemical Modeling, *Cambridge University Press*, 1995.
- [4] Allègre, C.J., J.P. Poirier, E. Humler and A.W. Hofmann, The chemical composition of the Earth, *Earth Planet. Sci. Lett.*, *134*, 515-526, 1995.
- [5] Anderson, D.L. and J.D. Bass, Transition region of the Earth's upper mantle, *Nature*, *320*, 321-328, 1986.
- [6] Anderson, G.M., Thermodynamics of natural systems, *Cambridge University Press*, 2005.
- [7] Andrault D., N. Bolfan-Casanova and N. Guignot, Equation of state of lower mantle (Al,Fe)-MgSiO₃ perovskite, *Earth Planet. Sci. Lett.*, *193*, 501-508, 2001.
- [8] Barry, T.I., A.T. Dinsdale, J.A. Gisby, B. Hallstedt, M. Hillert, B. Jansson, S. Jonsson, B. Sundman and J.R. Taylor, The compound energy model for ionic solutions with applications to solid oxides, *J. Phase Equil.*, *13*, 459-475, 1992.
- [9] Bass, J.D. and D.L. Anderson, Composition of the upper mantle - Geophysical tests of two petrological models. *Geophys. Res. Lett.*, *11*, 229-232, 1984.
- [10] Becker, T.W. and L. Boschi, A comparison of tomographic and geodynamic mantle models, *Geochem. Geophys. Geosyst.*, *3*, 1003, doi:10.1029/2001GC000168, 2002.
- [11] Bijwaard, H., W. Spakman and E.R. Engdahl, Closing the gap between regional and global travel time tomography, *J. Geophys. Res.*, *103*, 30,055-30,078, 1998.
- [12] Bina, C.R. and B.J. Wood, Olivine-spinel transitions - experimental and thermodynamic constraints and implications for the 400-km seismic discontinuity. *J. Geophys. Res.*, *92*, 4,853-4,866, 1987.
- [13] Birch, F., Elasticity and constitution of the Earth's interior. *J. Geophys. Res.*, *57*, 227-286, 1952.

- [14] Bouhifd, M.A., D. Andraut, G. Fiquet, and P. Richet, Thermal expansion of forsterite up to the melting point. *Geophys. Res. Lett.*, *23*, 1143-1146, 1996.
- [15] Bunge H.-P. and M.A. Richards, The origin of large scale structure in mantle convection: Effects of plate motions and viscosity stratification, *Geophys. Res. Lett.*, *23*, 2987-2990, 1996.
- [16] Bunge, H.-P., M.A. Richards and J.R. Baumgardner, A sensitivity study of three-dimensional spherical mantle convection at 10^8 Rayleigh number: Effects of depth-dependent viscosity, heating mode, and an endothermic phase change, *J. Geophys. Res.*, *102*, 11,991-12,007, 1997.
- [17] Bunge, H.-P., M.A. Richards, C. Lithgow-Bertelloni, J.R. Baumgardner, S. Grand and B. Romanowicz, Time scales and heterogeneous structure in geodynamic earth models, *Science*, *280*, 91-95, 1998.
- [18] Bunge, H.-P., Y. Ricard and J. Matas, Non-adiabaticity in mantle convection, *Geophys. Res. Lett.*, *28*, 879-882, 2001.
- [19] Bunge, H.-P., Low plume excess temperature and high core heat flux inferred from non-adiabatic geotherms in internally heated mantle circulation models, *Phys. Earth Planet. Interiors*, *153*, 3-10, 2005.
- [20] Cammarano F., S. Goes, P. Vacher and D. Giardini, Inferring upper mantle temperatures from seismic velocities, *Phys. Earth Planet. Interiors*, *138*, 197-222, 2003.
- [21] Christensen, U.R. and D.A. Yuen, Layered convection induced by phase-transitions, *J. Geophys. Res.*, *90*, 291-300, 1985.
- [22] Connolly, J.A.D. and D.M. Kerrick, An algorithm and computer-program for calculating composition phase-diagrams, *Calphad*, *11*, 1-55, 1987.
- [23] Connolly, J.A.D., Multivariable phase-diagrams - an algorithm based on generalized thermodynamics, *Americ. J. Science*, *290*, 666-718, 1990.
- [24] Connolly, J.A.D. and K. Petrini, An automated strategy for calculation of phase diagram sections and retrieval of rock properties as a function of physical conditions, *J. Metamorphic Geology*, *20*, 697-708, 2002. www.perplex.ethz.ch
- [25] Connolly, J.A.D., Computation of phase equilibria by linear programming: A tool for geodynamic modeling and its application to subduction zone decarbonation, *Earth Planet. Sci. Lett.*, *236*, 524-541, 2005.
- [26] Daniel, I., J. D. Bass, G. Fiquet, H. Cardon, J. Zhang and M. Hanfland, Effect of aluminium on the compressibility of silicate perovskite. *Geophys. Res. Lett.*, *31*, L15608, doi:10.1029/2004GL020213, 2004.

- [27] Davies, J.H. and H.-P. Bunge, Are splash plumes the origin of minor hotspots?, *Geology*, *34*, 349-352, 2006.
- [28] de Capitani, C. and T.H. Brown, The computation of chemical equilibrium in complex systems containing non-ideal solutions, *Geochim. Cosmochim. Acta*, *51*, 2639-2652, 1987.
- [29] Deschamps, F., R. Snieder and J. Trampert, Anomalies of temperature and iron in the uppermost mantle inferred from gravity data and tomographic models. *Phys. Earth. Planet. Inter.*, *129*, 245-264, 2002.
- [30] Downs, R.T., C.-S. Zha, T.S. Duffy and L.W. Finger, The equation of state of forsterite to 17.2 GPa and effects of pressure media. *Am. Min.*, *81*, 51-55, 1996.
- [31] Duffy, T.S. and D.L. Anderson, Seismic velocities in mantle minerals and the mineralogy of the upper mantle, *J. Geophys. Res.*, *94*, 1895-1912, 1989.
- [32] Dziewonski, A.M. and D.L. Anderson, Preliminary Reference Earth Model, *Phys. Earth Planet. Interiors*, *25*, 297-356, 1981.
- [33] Fabrichnaya, O.B., The phase relations in the FeO-MgO-Al₂O₃-SiO₂ system: assessment of thermodynamic properties and phase equilibria at pressures up to 30 GPa, *Calphad*, *23*, 19-67, 1999.
- [34] Farnetani, C.G, Excess temperature of mantle plumes: The role of chemical stratification across D'', *Geophys. Res. Lett.*, *24*, 1583-1586, 1997.
- [35] Fei, Y., J. Van Orman, J. Li, W. van Westrenen, C. Sanloup, W. Minarik, K. Hirose, T. Komabayashi, M. Walter and K. Funakoshi, Experimentally determined postspinel transformation boundary in Mg₂SiO₄ using MgO as an internal pressure standard and its geophysical implications, *J. Geophys. Res.*, B02305, doi:10.1029/2003JB002562, 2004.
- [36] Fiquet, G., D. Andraut, A. Dewaele, T. Charpin, M. Kunz and D. Hausermann, P-V-T equation of state of MgSiO₃ perovskite, *Phys. Earth Planet. Interiors*, *105*, 21-31, 1998.
- [37] Fiquet, G., A. Dewaele, D. Andraut, M. Kunz and T. Le Bihan, Thermoelastic properties and crystal structure of MgSiO₃ perovskite at lower mantle pressure and temperature conditions, *Geophys. Res. Lett.*, *27*, 21-24, 2000.
- [38] Frost, D.J. and F. Langenhorst, The effect of Al₂O₃ on Fe-Mg partitioning between magnesiowuestite and magnesium silicate perovskite. *Earth Planet. Science Letters*, *199*, 227-241, 2002.

- [39] Frost, D.J., The structure and sharpness of $(\text{Mg,Fe})_2\text{SiO}_4$ phase transformations in the transition zone, *Earth Planet. Sci. Lett.*, *216*, 313-328, 2003.
- [40] Funamori, N., T. Yagi, W. Utsumi, T. Kondo and T. Uchida, Thermoelastic properties of MgSiO_3 perovskite determined by in situ X-ray observations up to 30 GPa, *J. Geophys. Res.*, *101*, 8,257-8,269, 1996.
- [41] Glatzmaier, G.A., Numerical simulations of mantle convection: time-dependent, three-dimensional, compressible, spherical shell, *Geophys. Astrophys. Fluid Dyn.*, *43*, 223-264, 1988.
- [42] Grand, S.P., R. D. Van der Hilst and S. Widiyantoro, High resolution global tomography: A snapshot of convection in the Earth, *Geol. Soc. Am. Today*, *7*, 1-7, 1997.
- [43] Hazen, R.M., Effects of temperature and pressure on the crystal structure of forsterite. *Am. Min.*, *61*, 1280-1293, 1976.
- [44] Hillert, M., B. Jansson and B. Sundman, Application of the compound-energy model to oxide systems, *Zeitschr. Metallkunde*, *79*, 81-87, 1988.
- [45] Hirose, K., Y.W. Fei, Y.Z. Ma and H.-K. Mao, The fate of subducted basaltic crust in the Earth's lower mantle, *Nature*, *397*, 53-56, 1999.
- [46] Hirose, K., Phase transitions in pyrolitic mantle around 670-km depth: Implications for upwelling of plumes from the lower mantle, *J. Geophys. Res.*, *107*, B4, 2078, doi:10.1029/2001JB000597, 2002.
- [47] Igel, H., P. Mora and B. Rioulet, Anisotropic wave-propagation through finite-difference grids, *Geophysics*, *60*, 1203-1216, 1995.
- [48] Irifune, T., An experimental investigation of the pyroxene-garnet transformation in a pyrolite composition and its bearing on the constitution of the mantle, *Earth. Planet. Sci. Lett.*, *45*, 324-336, 1987.
- [49] Irifune, T., Absence of an aluminous phase in the upper part of the Earth's lower mantle, *Nature*, *370*, 131-133, 1994.
- [50] Irifune, T., N. Nishiyama, K. Kuroda, T. Inoue, M. Isshiki, W. Utsumi, K.-I. Funakoshi, S. Urakawa, T. Uchida, T. Katsura and O. Ohtaka, The postspinel phase boundary in Mg_2SiO_4 determined by in situ X-ray diffraction, *Science*, *279*, 1698-1700, 1998.
- [51] Irifune, T. and M. Isshiki, Iron partitioning in a pyrolite mantle and the nature of the 410-km seismic discontinuity, *Nature*, *392*, 702-705, 1998.

- [52] Ishii, M. and J. Tromp, Normal-mode and free-air gravity constraints on lateral variations in velocity and density of Earth's mantle, *Science*, *285*, 1231-1236, 1999.
- [53] Ita, J. and L. Stixrude, Petrology, elasticity and composition of the mantle transition zone, *J. Geophys. Res.*, *97*, 6849-6866, 1992.
- [54] Ito, E. and E. Takahashi, Postspinel transformations in the solid system Mg_2SiO_4 - Fe_2SiO_4 and some geophysical implications, *J. Geophys. Res.*, *94*, 10,637-10,646, 1989.
- [55] Ito, E. and T. Katsura, A temperature profile of the mantle transition zone, *Geophys. Res. Lett.*, *16*, 425-428, 1989.
- [56] Jackson, I. and S.M. Rigden, Analysis of P-V-T data: Constraints on the thermoelastic properties of high-pressure minerals, *Phys. Earth Planet. Interiors*, *96*, 85-112, 1996.
- [57] Jackson, I., J.D. Fitz Gerald, U.H. Faul and B.H. Tan, Grain-size-sensitive seismic wave attenuation in polycrystalline olivine, *J. Geophys. Res.*, *107*, 2360, doi:10.1029/2001JB001225, 2002.
- [58] Jeanloz, R. and S. Morris, Temperature distribution in the crust and mantle. *Annual Reviews of Earth and Planetary Sciences*, *14*, 377-415, 1986.
- [59] Jarvis, G.T. and D. McKenzie, Convection in a compressible fluid with infinite Prandtl number, *J. Fluid Mech.*, *96*, 515-83, 1980.
- [60] Katsura, T., M. J. Walter, H. Yamada, T. Shinmei, A. Kubo, S. Ono, M. Kanzaki, A. Yoneda, E. Ito and S. Urakawa, Post-spinel transition in Mg_2SiO_4 determined by high P-T in situ X-ray diffractometry, *Phys. Earth Planet. Inter.*, *136*, 11-24, 2003.
- [61] Khan, A., J.A.D. Connolly, J. MacLennan and K. Mosegaard, Joint inversion of seismic and gravity data for lunar composition and thermal state. *Geophys. J. Int.*, *168*, 243-258, 2007.
- [62] Khan, A., J.A.D. Connolly and N. Olsen, Constraining the composition and thermal state of the mantle beneath Europe from inversion of long-period electromagnetic sounding data. *J. Geophys. Res.*, *111*, B10102, doi:10.1029/2006JB004270, 2006.
- [63] Kennett, B.L.N., E.R. Engdahl and R. Buland, Constraints on seismic velocities in the Earth from travel times, *Geophys. J. Int.*, *122*, 108-124, 1995.
- [64] Kennett, B.L.N., On the density distribution within the Earth, *Geophys. J. Int.*, *132*, 374-382, 1998.
- [65] Kennett, B.L.N., S. Widiyantoro and R.D. van der Hilst, Joint seismic tomography for bulk sound and shear wave speed in the Earth's mantle, *J. Geophys. Res.*, *103*, 12,469-12,494, 1998.

- [66] Kesson, S.E., J.D. Fitz Gerald and J.M Shelley, Mineralogy and dynamics of a pyrolite lower mantle, *Nature*, 393, 252-255, 1998.
- [67] Komatitsch, D. and J. Tromp, Spectral-element simulations of global seismic wave propagation - I. Validation, *Geophys. J. Int.*, 149, 390-412, 2002.
- [68] Komatitsch, D. and J. Tromp, Spectral-element simulations of global seismic wave propagation - II. 3-D models, Oceans, Rotation, and Self-Gravitation, *Geophys. J. Int.*, 150, 303-318, 2002.
- [69] Kudoh, Y. and Y. Takeuchi, The crystal structure of forsterite Mg_2SiO_4 under high pressure up to 149kb. *Zeitschrift für Kristallographie*, 171, 291-302, 1985.
- [70] Labrosse, S., Hotspots, mantle plumes and core heat loss, *Earth Planet. Sci. Lett.*, 199, 147-156, 2002.
- [71] Li B.S. and J.Z. Zhang, Pressure and temperature dependence of elastic wave velocity of $MgSiO_3$ perovskite and the composition of the lower, *Phys. Earth Planet. Interiors*, 151, 143-154, 2005.
- [72] Litasov, K., E. Ohtani, A. Sano, A. Suzuki and K. Funakoshi, Influence of water on post-spinel transformation in a peridotite mantle: in situ X-ray diffraction study, *Geophys. Res. Abstracts*, 7, 1607-7962/gra/EGU05-A-00505, 2005.
- [73] Mao, H.K., R.J. Hemley, Y. Fei, J.F. Shu, L.C. Chen, A.P. Jephcoat, Y. Wu and W.A. Bassett, Effect of pressure, temperature, and composition on lattice parameters and density of (Fe,Mg)SiO₃-perovskites to 30 GPa, *J. Geophys. Res.*, 96, 8069-8079, 1991.
- [74] Masters G., G. Laske, H. Bolton and A. Dziewonski, The relative behavior of shear velocity, bulk sound speed, and compressional velocity in the mantle: Implications for chemical and thermal structure, in: S. Karato, A.M. Forte, R.C. Liebermann, G. Masters and L. Stixrude (eds.) *Earth's Deep Interior*, AGU Monograph 117, AGU, Washington D.C, 2000.
- [75] Masters, T.G. and D. Gubbins, On the resolution of density within the Earth. *Phys. Earth Planet. Interiors*, 140, 159-167, 2003.
- [76] Matas, J., Modélisation thermochimique des propriétés de solides a hautes pressions et hautes temperatures. Application géophysique. *PhD thesis, École Normale Supérieure*, Lyon, 1999.
- [77] Matas, J. and M.S.T Bukowinski, Anelasticity in the lower mantle: influence on the temperature dependence of seismic velocities. *Geophys. Res. Abstract*, 9, 1607-7962/gra/EGU2007-A-02039, 2007.

- [78] Mattern, E., J. Matas, Y. Ricard and J. Bass, Lower mantle composition and temperature from mineral physics and thermodynamic modeling, *Geophys J. Int.*, *160*, 973-990, 2005.
- [79] McCammon, C., M. Hutchison and J. Harris, Ferric iron content of mineral inclusions in diamonds from Sao Luiz: A view into the lower mantle, *Science*, *278*, 434-436, 1997.
- [80] McCammon, C.A., Perovskite as a possible sink for ferric iron in the lower mantle, *Nature*, *387*, 694-696, 1997.
- [81] McCammon, C., Mantle oxidation state and oxygen fugacity: Constraints on mantle chemistry, structure and dynamics. In R.D. van der Hilst, J. Bass, J. Matas, and J. Trampert., Eds. *Earth's Deep Mantle: Structure, Composition, and Evolution*, p. 221-242. American Geophysical Union, Washington D.C., 2005
- [82] McKenzie, D., J. Roberts and N.O. Weiss, Convection in the Earth's mantle: towards a numerical simulation, *J. Fluid Mech.*, *62*, 465-538, 1974.
- [83] McNamara, A.K. and S.J. Zhong, Thermochemical structures beneath Africa and the Pacific Ocean, *Nature*, *437*, 1136-1139, 2005.
- [84] Mégnin, C. and B. Romanowicz, The 3D shear velocity structure of the mantle from the inversion of body, surface and higher mode waveforms, *Geophys. J. Inter.*, *143*, 709-728, 2000.
- [85] Meng, Y., D.J. Weidner, G.D. Gwanmesia, R.C. Liebermann, M.T. Vaughan, Y. Wang, K. Leinenweber, R.E. Pacalo, A. Yeganeh-Haeri, and Y. Zhao, In situ high P-T X ray diffraction studies on three polymorphs (alpha , beta , gamma) of Mg₂SiO₄. *J. Geophys. Res.*, *98*, 22,199-22,207, 1993.
- [86] Miller, M.S., B.L.N. Kennett and V. Toy, Spatial and temporal evolution of the subducting Pacific plate structure along the western Pacific margin, *J. Geophys. Res.*, *111*, B02401, doi:10.129/2005JB003705, 2006.
- [87] Mittelstaedt, E. and P.J. Tackley, Plume heat flow is much lower than CMB heat flow, *Earth. Planet. Sci. Lett.*, *241*, 202-210, 2006.
- [88] Montelli, R., G. Nolet, F.A. Dahlen, G. Masters, E.R. Engdahl and S.-H. Hung, Finite-frequency tomography reveals a variety of plumes in the mantle, *Science*, *303*, 338-343, 2004.
- [89] Murakami, M., K. Hirose, K. Kawamura, N. Sata and Y. Ohishi, Post-perovskite phase transition in MgSiO₃, *Science*, *304*, 855-858, 2004.

- [90] Murakami, M., K. Hirose, N. Sata and Y. Ohishi, Post-perovskite phase transition and mineral chemistry in the pyrolitic lowermost mantle. *Geophys. Res. Lett.*, *32*, L03304, doi:10.1029/2004GL021956, 2005.
- [91] Oganov, A.R., J.P. Brodholt and G.D. Price, Comparative study of quasiharmonic lattice dynamics, molecular dynamics and Debye model applied to MgSiO₃ perovskite, *Phys. Earth Planet. Interiors*, *122*, 277-288, 2000.
- [92] Oganov, A.R. and S. Ono, Theoretical and experimental evidence for a post-perovskite phase of MgSiO₃ in Earth's D'' layer, *Nature*, *430*, 445-448, 2004.
- [93] Poirier, J.-P., Introduction to the Physics of the Earth's Interior, *Cambridge University Press*, 2000.
- [94] Powell, R., T. Holland and B. Worley, Calculating phase diagrams involving solid solutions via non-linear equations, with examples using THERMOCALC, *J. Metam. Geol.*, *16*, 577-588, 1998.
- [95] Reed, M.H., Calculation of simultaneous chemical equilibria in aqueous-mineral-gas systems and its application to modeling hydrothermal processes, *Rev. Econ. Geol.*, *10*, 109-124, 1998.
- [96] Resovsky, J. and J. Trampert, Reliable mantle density error bars: An application of the neighbourhood algorithm to normal mode and surface wave data, *Geophys. J. Int.*, *150*, 665-672, 2002.
- [97] Ricard, Y., E. Mattern and J. Matas, Synthetic Tomographic Images of Slabs from Mineral Physics, in *Earth's Deep Mantle: Structure, Composition, and Evolution*, edited by R.D. van der Hilst, J.D. Bass, J. Matas and J. Trampert, *Geophys. Monogr. Ser.*, AGU, Washington, D.C, pp. 285-302, 2005.
- [98] Ringwood, A.E., Composition and Petrology of the Earth's Mantle, *McGraw-Hill, New York*, 1975.
- [99] Ross, N.L. and R.M. Hazen, High-pressure crystal-chemistry of MgSiO₃ perovskite, *Phys. Chem. Minerals*, *17*, 228-237, 1990.
- [100] Samuel, H., C.G. Farnetani and D. Andraut, Heterogeneous lowermost mantle: compositional constraints and seismological observables, in *Earth's Deep Mantle: Structure, composition and evolution of Earth's mantle*, edited by R.D. van der Hilst, J.D. Bass, J. Matas and J. Trampert, *Geophys. Monogr. Ser.*, AGU, Washington, D.C., pp. 103-108, 2005.
- [101] Saxena, S.K., Earth mineralogical model: Gibbs free energy minimization computation in the system MgO-FeO-SiO₂, *Geochim. Cosmochim. Acta*, *60*, 2379-2395, 1996.

- [102] Saxena, S.K., L.S. Dubrovinsky, P. Lazor, Y. Cerenius, P. Haggkvist, M. Hanfland and J.Z. Hu, Stability of perovskite (MgSiO_3) in the Earth's mantle *Science*, *274*, 1357-1359, 1996.
- [103] Schilling, J.-G., Fluxes and excess temperatures of mantle plumes inferred from their interaction with migrating mid-ocean ridges, *Nature*, *352*, 397-403, 1991.
- [104] Schuberth, B., A.S. Piazzoni, H. Igel, H.-P. Bunge and G. Steinle-Neumann, Simulation of 3D global wave propagation through geodynamic models, *Eos Trans. AGU*, *86(52)*, Fall Meet. Suppl., Abstract NG43B-0570, 2005.
- [105] Sinogeikin, S.V., J.Z. Zhang and J.D. Bass, Elasticity of single crystal and polycrystalline MgSiO_3 perovskite by Brillouin spectroscopy, *Geophys. Res. Lett.*, *31*, L06620, doi:10.1029/2004GL019559, 2004.
- [106] Stein, C. and S. Stein, A model for the global variation in oceanic depth and heat flow with lithospheric age, *Nature*, *359*, 123-128, 1992.
- [107] Stixrude, L., R.J. Hemley, Y. Fei and H. K. Mao, Thermoelasticity of silicate perovskite and magnesiowustite and stratification of the Earth's mantle, *Science*, *257*, 1099-1101, 1992.
- [108] Stixrude, L. and C. Lithgow-Bertelloni, Thermodynamics of mantle minerals: 1. Physical properties, *Geophys J. Int.*, *162*, 610-632, 2005.
- [109] Sundman, B. and J. Aagren, A regular solution model for phases with several components and sublattices, suitable for computer applications, *J. Phys. Chem. Solids*, *42*, 297-301, 1981.
- [110] Swamy, V. and L.S. Dubrovinsky, Thermodynamic data for the phases in the CaSiO_3 system, *Geochim. Cosmochim. Acta*, *61*, 1181-1191, 1997.
- [111] Tackley, P.J., Strong heterogeneity caused by deep mantle layering, *Geochem. Geophys. Geosystems*, *3*, 4, 1024, doi:10.1029/2001GC000167, 2002.
- [112] Tackley, P.J., D.J. Stevenson, G.A. Glatzmaier and G. Schubert GLATZMAIER GA, Effects of an endothermic phase-transition at 670 km depth in a spherical model of convection in the Earth's mantle, *Nature*, *361*, 699-704, 1993.
- [113] Tackley, P.J., S. Xie, T. Nakagawa and J.W. Hernlund, Numerical and laboratory studies of mantle convection: Philosophy, accomplishments and thermo-chemical structure and evolution, in *Earth's Deep Mantle: Structure, Composition, and Evolution*, edited by R.D. van der Hilst, J.D. Bass, J. Matas and J. Trampert, *Geophys. Monogr. Ser.*, AGU, Washington, D.C, pp. 83-99, 2005.

- [114] Tateno, S., K. Hirose, N. Sata, N. and Y. Ohishi, Phase relations in $\text{Mg}_3\text{Al}_2\text{Si}_3\text{O}_{12}$ to 180 GPa: Effect of Al on post-perovskite phase transition, *Geophys. Res. Lett.*, *32*, doi:10.1029/2005GL023309, 2005.
- [115] Tronnes, R.G. and D.J. Frost, Peridotite melting and mineral-melt partitioning of major and minor elements at 22-24.5 GPa, *Earth Planet. Sci. Lett.*, *197*, 117-131, 2002.
- [116] Utsumi, W., N. Funamori, T. Yagi, E. Ito, T. Kikegawa and O. Shinomura, 1995, Thermal expansivity of MgSiO_3 perovskite up to 20 GPa, *Geophys. Res. Lett.*, *22*, 1,005-1,008, 1995.
- [117] Vacher P., A. Mocquet and C. Sotin, Comparison between tomographic structures and models of convection in the upper mantle. *Geophys. J. Int.*, *124*, 45-56, 1996.
- [118] Vacher, P., A. Mocquet and C. Sotin, Computation of seismic profiles from mineral physics: the importance of non-olivine components for explaining the 660 km depth discontinuity. *Phys. Earth Planet. Inter.*, *106*, 275298, 1998.
- [119] van der Hilst, R., S. Widiyantoro and E.R. Engdahl, Evidence for deep mantle circulation from global tomography, *Nature*, *386*, 578-584, 1997.
- [120] van der Voo, R., W. Spakman and H. Bijwaard, Mesozoic subducted slabs under Siberia, *Nature*, *397*, 246-249, 1999.
- [121] Vanpeteghem, C.B., J. Zhao, R.J. Angel, N.L. Ross and N. Bolfan-Casanova, Crystal structure and equation of state of MgSiO_3 perovskite, *Geophys. Res. Lett.*, *33*, doi:10.1029/2005GL024955, 2006.
- [122] Walter, M.J., A. Kubo, T. Yoshino, J. Brodholt, K. Koga and Y. Ohishi, Phase relations and equation-of-state of aluminous Mg-silicate perovskite and implications for Earth's lower mantle, *Earth Planet. Sci. Lett.*, *222*, 501-516, 2004.
- [123] Wang, W.Y. and E. Takahashi, Subsolidus and melting experiments of K-doped peridotite KLB-1 to 27 GPa: Its geophysical and geochemical implications, *J. Geophys. Res.*, *105*, 2855-2868, 2000.
- [124] Wang, Y., T. Uchida, J. Zhang, M.L. Rivers and S.R. Suttona, Thermal equation of state of MgSiO_3 and effects of the akimotoite-garnet transformation on seismic structure near the 660 km discontinuity. *Phys. Earth Planet. Interiors*, *143*, 57-80, 2004.
- [125] Wänke, H., G. Dreibus and E. Jagoutz, Mantle chemistry and accretion history of the Earth, in *Archean Geochemistry*, edited by A. Kröner, G.N. Hanson, and A.M. Goodwin, Springer-Verlag, Berlin, 1-24, 1984.

- [126] Webb, S. and I. Jackson, Anelasticity and microcreep in polycrystalline MgO at high temperature: an exploratory study. *Phys Chem Minerals*, 30, 157-166, 2003.
- [127] Will, G., W. Hoftbauer, E. Hinze and J. Lauterjung, The compressibility of forsterite up to 300 kbar measured with synchrotron radiation. *Physica*, 139 and 140B, 193-197, 1986.
- [128] Yagi, T., K. Okabe, N. Nishiyama, A. Kubo and T. Kikegawa, Complicated effects of aluminum on the compressibility of silicate perovskite, *Phys. Earth Planet. Interiors*, 143, 81-91, 2004.
- [129] Zhong, S., Constraints on thermochemical convection of the mantle from plume heat flux, plume excess temperature and upper mantle temperature, *J. Geophys. Res.*, 111, B04409, doi: 10.1029/2005JB003972, 2006.

3 Thermal and Elastic Structure in Multiphase Mantle Convection Models

During the last years, three important driving forces have separately contributed to progress in understanding the Earth's mantle: Geodynamic modeling, Mineral Physics and Seismology. In particular, seismic tomography has recently brought a wide range of spatial mantle heterogeneities scales into focus, and geodynamic models that simulate 3D spherical convection at high resolution explore an alternative route for the temperature state of the Earth's mantle. Despite this progress, many important features in mantle structure remain unexplained by geodynamics, as the chemical state and the mineralogical thermodynamics of the mantle are not sufficiently well understood and described in mantle convection models. In addition to mantle structure, the mantle phase transitions could interact with upwelling and downwelling thermal structures in a complex way that cannot be easily modeled by parameterized buoyancy forces, e.g. based only on the post-spinel transition in the Mg_2SiO_4 part of mantle mineralogy. Only Mineral Physics models that relate pressure, temperature and chemical conditions to density and elasticity account for the complexity of phase transitions and for the change of the physical properties. Recent experimental and theoretical advancements in Mineral Physics have made it possible to build self-consistent models of the (dry) phases of the Earth's mantle. The models are based exclusively on physical and thermodynamic measurements. Here I have used a new thermodynamic database for the mantle and have coupled the resulting density dynamically (through the buoyancy term) with mantle convection models. The database is built on a self-consistent Gibbs free energy minimisation of the system $\text{MgO-FeO-SiO}_2\text{-CaO-Al}_2\text{O}_3$ that is appropriate for standard chemical models of the Earth's mantle (e.g. pyrolite) for relevant high pressure and temperature phases. I have linked the database with a high-resolution 2-D convection code (2DTERRA), dynamically coupling the thermodynamic model (density) with the conservation equations of mantle flow. The coupled model is run for different parameterisations of viscosity, initial temperature conditions, and varying the internal vs. external heating. A common feature of all the models is that the convecting flow creates a characteristic discontinuity of temperature around 660 km depth in order to compensate for the entropy change due to the phase transitions. I discuss the importance and the possible consequences of such thermal regime on the excess temperature. Finally, my Mineral Physics model provides the conversion of the temperature field into seismic velocities so that the predictions of mantle convection can be tested with seismic observations in terms of lateral variations and radial profiles.

3.1 Introduction

Tomographic studies of the deep Earth have advanced to the point where they now provide considerable insight into the physical state of our planet [*Grand et al.*, 1997; *van der Hilst et al.*, 1997; *Bijwaard et al.*, 1998; *Masters et al.*, 2000; *Mégnin and Romanowicz*, 2000],

reaching a state where these models are useful in guiding tectonic interpretations of past plate motion and histories of subduction [*van der Voo et al.*, 1999; *Miller et al.*, 2006]. At the same time, seismic tomography shows substantial complexity throughout the mantle as brought out by simultaneous mapping of bulk sound and shear wave velocities [*Kennett et al.*, 1998], models of probabilistic mantle heterogeneity [*Resovsky and Trampert*, 2002], or studies of finite frequency effects [*Montelli et al.*, 2004]. In particular maps of bulk sound (V_{Φ}) and shear wave (V_S) velocities do not identify an unique picture of mantle heterogeneities: V_{Φ} variations diminish at lower depths compared to V_S variations and the two wave speeds anti-correlate in the lowermost mantle [*Masters et al.*, 2000]. Furthermore, studies based on seismic precursors have increased the precision in mapping the depth variation of seismic discontinuities that correspond to phase transitions, e.g. the 410 km and the 660 km depth discontinuities [*Shearer and Flanagan*, 1999; *Shearer*, 2000; *Deuss et al.*, 2006].

Seismology thus reveals indirect information on thermal and chemical conditions of the deep Earth that need to be interpreted in terms of material properties of mantle minerals and the dynamic state of the Earth's interior. For example, to this date we do not have a sample of MgSiO_3 perovskite (Mg-pv) from the mantle. The inference that Mg-pv is the major phase of the Earth's lower mantle comes from three sources: (1) a cosmo-/geochemical model of composition of the Earth [*McDonough and Sun*, 1995], (2) the study of phase transitions at high pressure and temperature [*Yagi et al.*, 1978] and (3) a comparison of its P-V-T equation-of-state with the compressibility of the lower mantle [*Stixrude et al.*, 1992].

Progress in mineral physics at high pressure has now advanced to a point where petrologic studies can be performed at lower mantle conditions [e.g. *Walter et al.*, 2004]. It is now possible to build a self-consistent mantle mineral models of (dry) phases in the Earth's mantle [*Fabrichnaya*, 1999; *Matas*, 1999; *Stixrude and Lithgow-Bertelloni*, 2005; *Piazzoni et al.*, 2007], based exclusively on phase relations, compressional and thermochemical measurements. Simultaneous advances in elastic measurements of minerals at high pressure using Brillouin spectroscopy [*Sinogeikin et al.*, 2004], ultrasonic measurements in the multi-anvil press [*Li and Zhang*, 2005] and diamond anvil cell [*Kantor et al.*, 2004], and ab-initio modeling [*Oganov et al.*, 2001] yield, for the first time, a comprehensive model of shear wave elastic properties at mantle conditions [*Stixrude and Lithgow-Bertelloni*, 2005; *Murakami et al.*, 2007]. These two developments provide important constraints for the interpretation of seismic measurements in terms of physical properties of constituting mineralogy.

Geodynamic models that simulate convection at high resolution provide an alternative route to explore the state of the mantle. Of particular relevance are studies of the mantle geotherm [*Bunge et al.*, 2001; *Matyska and Yuen*, 2000; *Sleep*, 2003], plume flux [*Labrosse*, 2002; *Bunge*, 2005; *Mittelstaedt and Tackley*, 2006; *Zhong*, 2006; *Schuberth et al.*, 2008] and the evolution of convection having different chemical components [*Tackley*,

2002; *Samuel et al.*, 2005; *Tackley et al.*, 2005]. However, convection models have traditionally applied a much simplified representation of mantle mineralogy. Some models restrict themselves to the Bousinesq approximation [*McKenzie et al.*, 1974; *Christensen and Yuen*, 1985; *Bunge and Richards*, 1996; *McNamara and Zhong*, 2005], in which all parameters are held constant and where density changes enter only through the buoyancy term of the Navier-Stokes equation, giving rise to gravitational forces. Other models have adopted a depth-dependent formalism through the use of the anelastic liquid approximation [*Jarvis and McKenzie*, 1980; *Glatzmaier*, 1988, *Bunge et al.*, 1997; *Schuberth et al.*, 2008]: The fluid under this assumption sustains compression or expansion due to changes in pressure as it sinks or rises, but thermal effects are ignored. In addition to mantle structure, the mantle phase transitions interact with upwelling and downwelling thermal structures in a complex way that cannot be easily modeled by parameterized buoyancy forces, e.g. based only on the post-spinel transition in the Mg_2SiO_4 part of mantle mineralogy. The phase transitions leading to the 410 km and 660 km discontinuities are highly simplified in geodynamic models: they are commonly modeled as two sharp boundaries where anomalous buoyancy forces reproduce the dynamic effects of the phase transitions [*Christensen and Yuen*, 1985; *Tackley et al.*, 1993; *Bunge et al.*, 1997]. Such sharp transitions do not adequately describe the complexity of the phase transitions [e.g. *Hirose*, 2002; *Frost*, 2003].

The mineralogical interpretation of tomography suffers from the tradeoff between temperature and composition. However this limitation can be overcome by evaluating the compositional effects of a mineralogical model directly within geodynamic models, that is by integration of mineral thermodynamics into convection modeling. I have compiled a thermodynamic model of mantle mineralogy in the five component CFMAS system ($\text{CaO-FeO-MgO-Al}_2\text{O}_3\text{-SiO}_2$), including mineral phases that occur close to typical chemical models of the mantle and reasonable mantle temperatures. In this system I have performed a system Gibbs free energy minimization, including pure end-member phases and a non-ideal formulation for solid solutions. Solid solutions were subdivided into discrete pseudocompounds and treated as stoichiometric phases during computation of chemical equilibrium by the simplex method. We have complemented the thermodynamic model with a model of shear wave properties [*Stixrude and Lithgow-Bertelloni*, 2005] to obtain a full description of aggregate elastic properties (density, bulk and shear moduli) that provide a useful basis for the consideration of seismic and geodynamic models of the Earth's mantle.

By using this thermodynamic database for the mantle we have coupled the resulting density dynamically (through the buoyancy term) with mantle convection models. We have linked the database with a high-resolution 2-D convection code (2DTERRA), dynamically coupling the thermodynamic model (density) with the conservation equations of mantle flow. The coupled model is run for different parameterisations of viscosity, initial temperature conditions, and varying internal vs. external heating. A common feature of all the models is that the convecting flow creates a characteristic discontinuity of temperature

around 660 km depth in order to compensate for the entropy change due to the phase transitions. I have studied the importance and the possible consequences of such a thermal regime on the excess temperature of plumes and on the transition zone thickness. The thermodynamic mantle mineralogy model provides the conversion of the temperature field into seismic velocities so that predictions from mantle convection can be compared to seismic observations in terms of radial profiles or lateral variations. This approach allows us to predict a number of seismic observables from the convection model, all of which agree remarkably well with observations from seismic tomography.

This section is arranged as follows. I briefly review my model of mantle mineralogy (see also section 2) and our mantle convection code, both of which have been described before [Piazzoni *et al.*, 2007; Yang and Baumgardner, 2000]. I then describe the thermal and elastic fields I obtain from our coupled mineralogy mantle convection model. The section is closed by comparing our geodynamic results to tomographic observations and present our general conclusions.

3.2 The model

3.2.1 Thermodynamically Self-Consistent Mantle Mineralogy Model

The availability of large amounts of high quality data in high pressure mineralogy has made it possible in recent years to build sophisticated mantle mineralogy models [Stixrude and Lithgow-Bertelloni, 2005; Khan *et al.*, 2007; Matas, 1999]. Thus every P,T,x (pressure, temperature, composition) condition of the mantle can in principle be related to a stable phase assemblage with associated physical properties such as density, bulk, and shear moduli. For this study we have selected a recent model based on Gibbs free energy minimization [Piazzoni *et al.*, 2007] in conjunction with a model of shear moduli [Stixrude and Lithgow-Bertelloni, 2005]. The physical properties of the stable assemblage are computed in a CFMAS (CaO-FeO-MgO-Al₂O₃-SiO₂) pyrolite bulk composition, resulting in a lower mantle phase assemblage of (Mg,Fe,Al) *pv* and magnesiowüstite (*mw*) solid solutions, plus calcium perovskite (Ca-*pv*). High-spin to low-spin transitions [e.g. Badro *et al.*, 2004] and the trivalent state of iron in *pv* [e.g. McCammon, 2005] are not included in this model. We represent the isothermal compression by a third order Birch-Murnaghan equation-of-state and fit the thermal expansion data by a polynomial [Saxena, 1996; Mattern *et al.*, 2005]. The density and elasticities of the system are computed using the Hill arithmetic mean of the Voigt and Reuss bounds. These and other model details are described more fully in [Piazzoni *et al.*, 2007].

3.2.2 Mantle Convection Model

Geodynamic models are often applied to an incompressible mantle utilizing the Boussinesq approximation [McKenzie *et al.*, 1974; Bunge *et al.*, 1996] in which physical parameters

	model	temperature (K)		radioactive heating	thermal conductivity	grid	viscosity		Rayleigh number
		CMB	TOP				LOWER MANTLE	UPPER MANTLE	
ISOVISCOUS	BOTTOM	3500	298	-	4 W/mK	1024:128	2*10 ²¹ Pa s	2*10 ²¹ Pa s	10 ⁸
	MIX	3500	298	10 ¹¹ W/kg	4 W/mK	1024:128	2*10 ²¹ Pa s	2*10 ²¹ Pa s	10 ⁸
	INTERNAL	-	298	10 ¹¹ W/kg	4 W/mK	1024:128	2*10 ²¹ Pa s	2*10 ²¹ Pa s	10 ⁸
LAYERED VISC.	BOTTOM	3500	298	-	4 W/mK	1024:128	6*10 ²² Pa s	2*10 ²¹ Pa s	10 ⁸
	MIX	3500	298	10 ¹¹ W/kg	4 W/mK	1024:128	6*10 ²² Pa s	2*10 ²¹ Pa s	10 ⁸
	INTERNAL	-	298	10 ¹¹ W/kg	4 W/mK	1024:128	6*10 ²² Pa s	2*10 ²¹ Pa s	10 ⁸

Figure 11: Parameters of the convection models (see text for details).

are assumed constant throughout the mantle and density changes enter the Navier-Stokes equation only through the buoyancy term to compute gravitational (driving) forces. Some models, however, account for the effects of compressibility. Commonly this is achieved by linearisation around a depth-dependent thermodynamic background state and applying the anelastic liquid approximation [Jarvis and McKenzie, 1980; Glatzmaier, 1988; Bunge *et al.*, 1997]. Here we go one step further and use densities from our mineralogy model directly to compute mantle buoyancy forces and enforce mass conservation in whole mantle convection model. This approach exploits the full thermodynamic information available from mineralogy since we compute density for every model grid point and every time step. In other words, we no longer linearize density variations around a background state, and this allows us to treat convection in a manner that is consistent with the underlying mineralogy.

Our 2-D Cartesian compressible mantle convection code is a modified version of the model described in [Yang and Baumgardner, 2000]. The code uses an efficient multigrid solver with matrix dependent transfer for the momentum balance, and has been benchmarked for numerical accuracy [Travis *et al.*, 1990]. We choose a long box of 8 : 1 aspect ratio (1024 : 128 cells in the x and y directions) to minimise the influence of artificial boundary conditions. The top and bottom boundaries are stress-free (free-slip). We perform our calculations at high numerical resolution and use a grid point spacing of ~ 22.5 km throughout the model mantle. This allows us to study highly vigorous mantle flow and to adopt earth-like values for mantle viscosity (2×10^{21} Pa s), thermal conductivity (4 W/m/K), and mantle depth (2890 km). Values for density and thermal expansivity are derived from our mineralogy model [Piazzoni *et al.*, 2007]. In order to isolate the different influences of the convection parameters we show the following mantle model cases:

- the mantle is purely heated from the bottom, that I refer to as "BOTTOM" ($T_{TOP} = 300K, T_{BOT} = 3500K$);
- the mantle is also homogeneously heated from within ($1 * 10^{-11} W/kg$), called "MIX";
- the mantle is purely heated from within ($1 * 10^{-11} W/kg$), called "INTERNAL".

All these models are run with constant viscosity ("ISOVISCOUS") and with the viscosity layered in an upper mantle and a lower mantle 30 times more viscous than the upper mantle ("LAYERED VISC."). My parameter choices all result in Rayleigh-Benard convection with the convective vigour described by a thermal Rayleigh number of 10^8 .

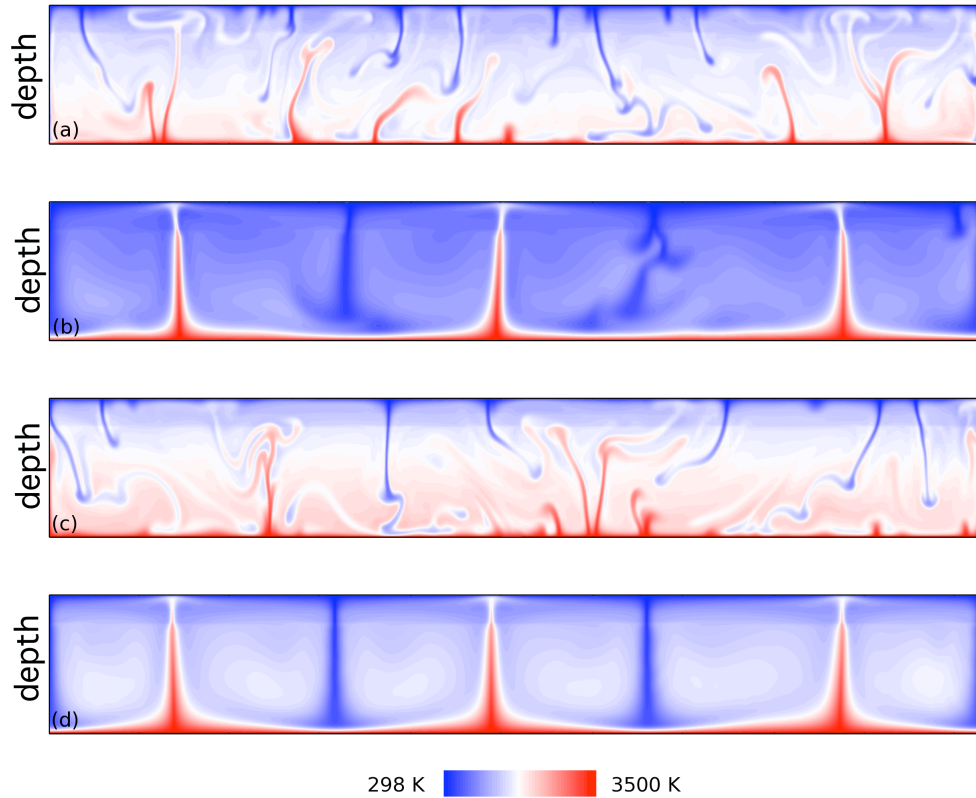


Figure 12: Contourplots of temperature for the convection models. The color indicates temperature (blue is 298 K, red is 3500K, the palette is linear). The panels show (from above to below) the "BOTTOM, ISOVISCIOUS", the "BOTTOM, LAYERED VISC.", the "MIX, ISOVISCIOUS" and the "MIX, LAYERED VISC." models.

3.3 Results

3.3.1 The thermal structure

Figure 12 shows time-snapshots of the convection models. The layered viscosity models show, as expected, horizontal flow in the upper mantle. All models result in Rayleigh-Benard convection with upwelling and downwelling structures through all the mantle. Layered viscosity stabilizes the flow into defined convection cells. The radial profiles of the mean temperature are shown in Figure 13. They strongly depend on the thermal boundary conditions, the amount of internal heating and the viscosity model. The cases "BOTTOM" yield a fully adiabatic mantle. In presence of internal heating the geotherm slightly deviates from adiabat [Bunge, 2005].

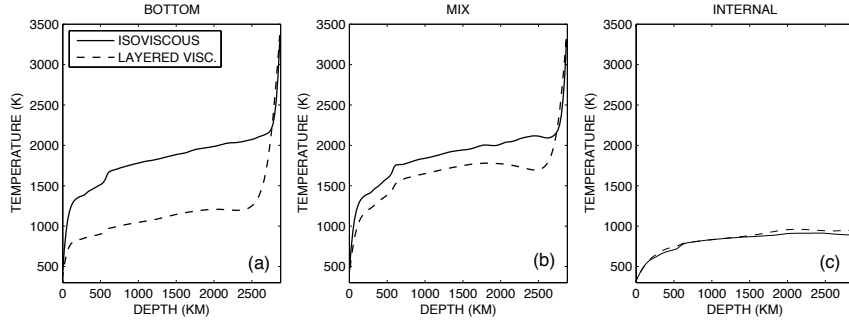


Figure 13: Radial average temperature for the "BOTTOM" (panel (a)), for the "MIX" (panel (b)) and "INTERNAL" (panel (c)) models. Solid lines show the isoviscous calculations, dashed ones indicate layered viscosity. Note that in correspondence with the "660km" there are sharp increases of temperature, created by the flow in order to compensate for the entropy change of the phase transitions (see text). Such discontinuities increase with temperature increasing; thus they are more pronounced on hotter profiles and barely visible for the "INTERNAL" cases.

I find that the models with layered viscosity result also in a different geotherm. In particular, the layered viscosity affects the transport of heat from the core into the mantle, with a smaller contribution of bottom heating to the thermal regime [*Schubert, 1979*]. This can be seen in Figure 13, where the "LAYERED VISC." cases are always colder than the corresponding "ISOVISCIOUS" cases. It can also be observed in Fig. 13b that in the presence of internal heating the differences are smaller. In Fig. 13c such a difference has disappeared and the average temperature profiles of the "ISOVISCIOUS" and "LAYERED VISC." cases overlap. In all the models the convective flow creates characteristic discontinuities of temperature that correspond to phase transitions (e.g. around 660 km depth) in order to keep the entropy constant. I have considered the latent heat release by equilibrium mineralogical transformations under the assumption of an adiabatic mantle i.e. there is in the model the assumption that the change of phases locally occurs without change of entropy (deviations from isentrope can occur elsewhere). Thus, metastable transformations and the latent heat release by metastable exothermic transformations (that can yield local superheating above the background adiabat) are not considered here. The temperature jump is a function of the entropy difference between the phases that increases with temperature. Therefore, hot geotherms have more pronounced jumps than colder ones. Consequently, around "660 km" there are two different thermal regimes (above and below the discontinuity). This affects the variation of physical properties across the seismic discontinuities: beside the dominant change of physical properties related to the phase transitions there is a variation of properties due to the temperature change. These models clearly indicate that purely internally heated models do not account for a realistic mean

temperature.

The temperature field in our geodynamic model with thermodynamically self-consistent mineralogy shows that the difference between mean and maximum mantle temperature increases systematically with depth (Figure 14). Put differently, the *excess temperature* of upwelling plumes decreases during ascent. This observation bears on the core-mantle heat flux, which has been considered to be similar to the surface heat flux from hotspots [Davies, 1988; Sleep, 1990]. Geodynamicists have long noted that the petrologically inferred excess temperature in mantle plumes (on the order of 200 – 300 K, [e.g. Schilling, 1991; Presnall and Gudfinsson, 2008]) is much lower than plausible estimates for the temperature increase across the CMB would suggest [Jeanloz and Morris, 1986].

A number of explanations for this have been advanced, including a dense basal layer in D'' [Farnetani, 1997] and a subadiabatic mantle geotherm due to internal mantle heat production [Bunge, 2005; Zhong, 2006; Stacey, 1995]. While these effects must be accounted for, our calculations show that low plume excess temperatures ought to be expected near the Earth’s surface where melt is extracted. Such low excess temperatures in plumes are simply a consequence of the fact that hot upwellings undergo much stronger adiabatic cooling relative to ambient mantle. For example, an isentrope tied to a footing temperature of 2000 K undergoes a temperature increase with depth nearly twice that of an adiabat footed at 1000 K (see Figure 15a,b). This conclusion is also supported by seismic tomography, which shows a strong increase in low velocity anomalies in the lowermost mantle [Dziewonski, 1984; Grand et al., 1997; Ritsema et al., 1999; Montelli et al., 2004; Romanowicz and Gung, 2002].

Buoyancy forces (f_B) are related to differences of density ($f_B = \rho\Delta\rho$) of material that has a different temperature than the surrounding mantle: again this is caused by different phase assemblages and direct effects of temperature on density. Fig. 14 shows the difference between the mean temperature profile and the maximum and minimum temperature for positive and negative buoyancy, respectively. The thermal buoyancy shown in Fig. 14 is for a time-snapshot but I find that average profiles do not vary with time. Density (Fig. 14a) and the correspondent buoyancies (Fig. 14b) are non-linear and can not be approximated with linearized functions. The phase stability and the consequent dynamics are temperature dependent and this is most pronounced for hot temperatures. At plume temperature the “660 km” discontinuity splits into two distinct phase transitions, the garnet to perovskite and the post-spinel, with opposite Clapeyron slope [Hirose, 2002], see also section 2. The buoyancies are discontinuous around phase transitions, since along different temperature profiles the phase transitions occur at different depths (Fig. 14b). Note that at depths of phase transitions density differences are large. By ascending in the mantle the upwelling structures first experience an acceleration induced by the negative buoyancy (caused by perovskite-to-garnet transition), followed by a resistance due to the post-spinel transition, and finally the negative buoyancy of the “410km”. As discussed above, I find this tradeoff between positive and negative buoyancies around “660km” very important for

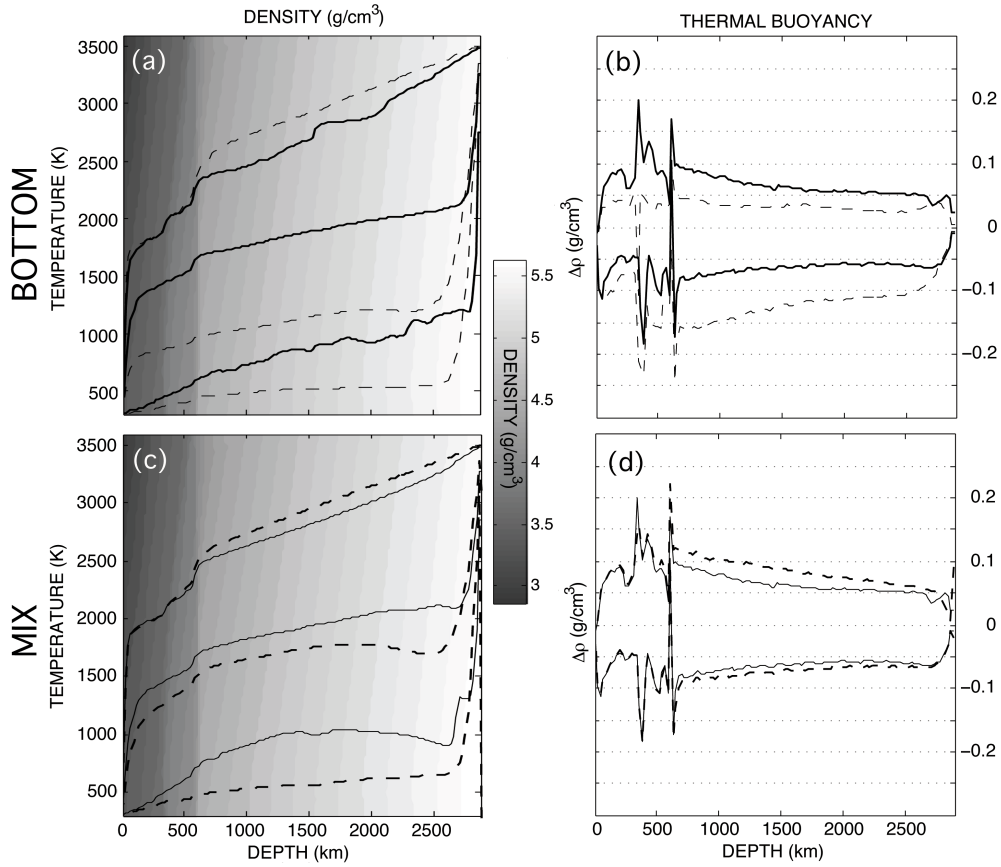


Figure 14: (a) Contourplot of density from my mineralogical model (section 2). The three overlapped lines represent the maximum, mean and minimum temperature at each depth from snapshots of the "BOTTOM, ISOVISCIOUS" model (solid line) and the "BOTTOM, LAYERED VISC." model (dashed line). (b) Lateral differences of density $\Delta\rho$ between the mean and the maximum and the minimum temperatures, respectively. Negative $\Delta\rho$ represent the rising buoyancy of plumes due to their excess temperature. Positive $\Delta\rho$ indicate the downward buoyancy of the cold material. The solid line is for "BOTTOM, ISOVISCIOUS", the dashed one for "BOTTOM, LAYERED VISC.". Panels (c) and (d) correspond to panels (a) and (b), respectively, for the "MIX" case.

the dynamics of this area.

Of particular importance is that at high temperature the positive Clapeyron slope garnet-to-perovskite transition differentiates from the post-spinel transition [Hirose, 2002] (see also section 2). I find that even if a layered circulation could temporarily begin, this transition would make the lower mantle upwellings entering the upper mantle circulation and create whole mantle convection. It can also be seen in Fig. 14b that $g\Delta\rho$, the heat flux carried by plumes is constant in the lower mantle. This is due to a combined effect of the thermal expansion (that decreases with pressure) and of the excess temperature of the plumes (that increases with pressure, since the adiabats are steeper at higher temperature). Furthermore, in all the models, the temperature jump at “660km” on plume temperature is twice to that on the average geotherm. This implies that upper mantle buoyancies of plumes are generally smaller than in the lower mantle (by factor of two). So, in my models, the estimate of heat flux at the surface corresponds to about one half of the heat flux that is present in the lower mantle. This effect might equilibrate the surface heat measurements with the energetic budget of the mantle [e.g. Hofmeister and Criss, 2005]. However, 2D convection models have geometrical limitations on quantitative heat flux predictions that do not stem from the temperature structure. Therefore, it is necessary to continue this investigation in 3-D convection models.

3.3.2 The elastic structure

The temperature field of the convection models can directly be converted into density, bulk sound and shear wave velocities by using the thermodynamic mineralogical model (section 2) in order to make comparisons with seismic observations. Figure 16 shows a comparison for shear wave velocity anomalies corresponding to the convection models of figure 12. For ease of comparison they are shown on a typical color scale for seismic models (e.g. SB10L18 [Masters et al., 2000]).

Note that V_S variations closely mimic the temperature of the model they are derived from, as, away from phase transformations, V_S depends on temperature quite linearly. Several large-scale structures are common to all the models, particularly for the cases with layered viscosity that show a more ordered convection flow. The high-velocity anomalies extend to the lowermost mantle. However, as it appears in Fig. 16c and 16d, the V_S anomalies with respect to the radial mean change throughout the lower mantle. Slow anomalies within subducting slabs (Fig. 16b) can be caused by the late post-spinel transition in cold material.

To explore the high temperature/high pressure behaviour of V_S and V_Φ more systematically I have computed the physical properties in the stable multiphase system for a wide range of mantle pressures and temperatures. Figure 17 shows the variation of V_S and V_Φ in P,T space. From the two panels of figure 17 it appears that the high pressure behaviour of V_S is different from the one of V_Φ . The sensitivity of V_S to temperature is constant

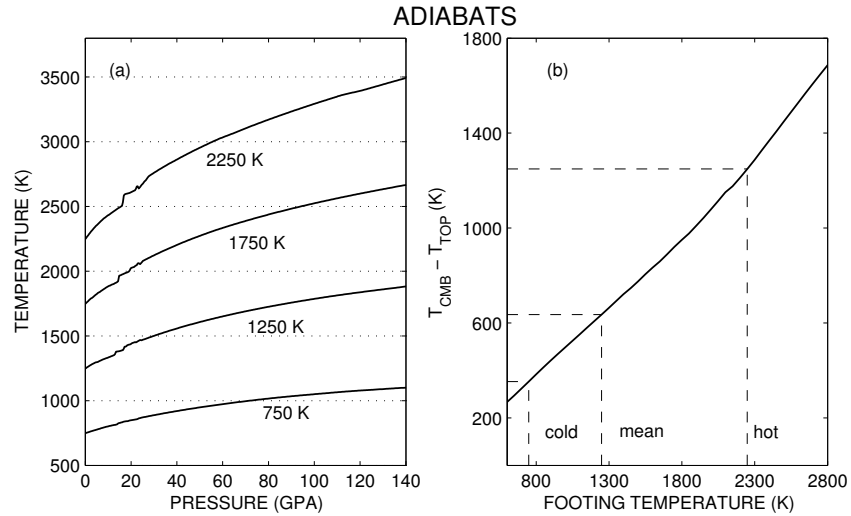


Figure 15: (a) Curves of constant entropy from the mineralogical model of [Piazzoni *et al.*, 2007] for footing (zero-pressure) temperatures of 750, 1250, 1750, 2250 K. The slope of the adiabat increases with footing temperature and generally decreases with depth. Temperature jumps corresponding to the discontinuities in entropy of the phase reactions are less pronounced in colder profiles. (b) Total adiabatic temperature variation from surface to CMB plotted against footing temperature. There is a sharp increase in adiabatic excess temperature with increasing footing temperature. Also shown are the footing temperatures corresponding to mean, minimum and maximum radial temperatures in the convection model (see text). Note that hot thermal upwellings (plumes) undergo strong adiabatic cooling relative to surrounding mantle, so that their excess temperature decreases systematically in the mantle from the bottom to the top.

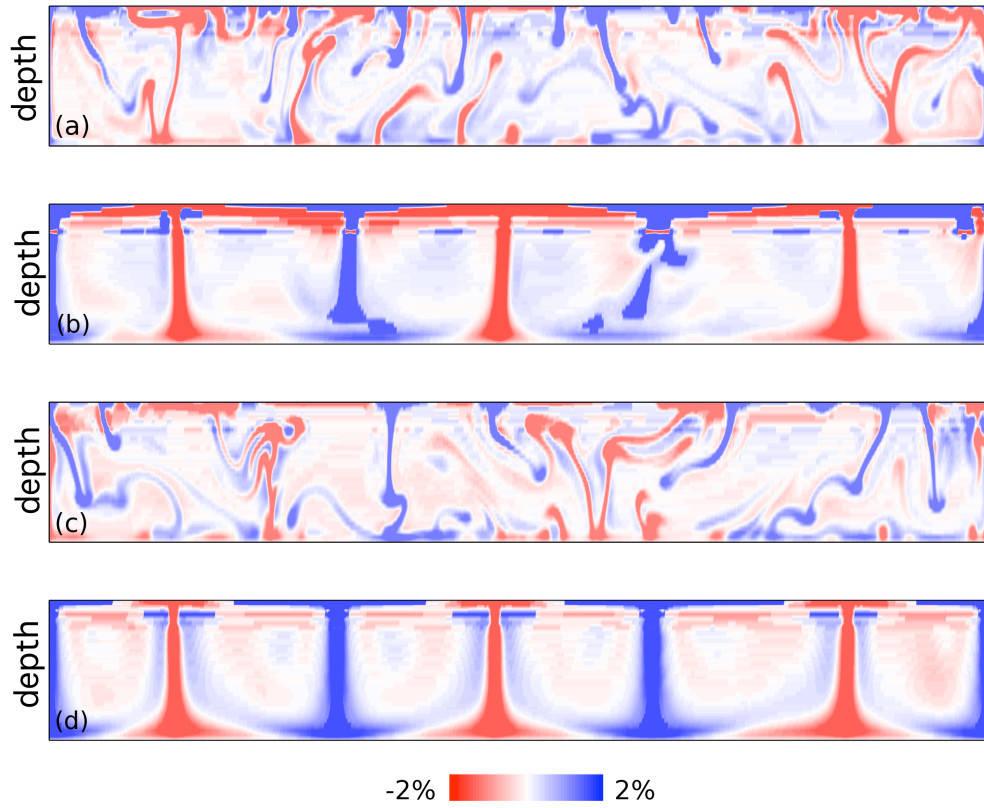


Figure 16: Contourplots of shear wave velocity (V_S) for the convection models presented above. The panels show (from above to below) the "BOTTOM, ISOVISCIOUS", the "BOTTOM, LAYERED VISC.", the "MIX, ISOVISCIOUS" and the "MIX, LAYERED VISC." models. The linear palette ranges from -2 % (red) to +2 % (blue).

with pressure and temperature and can be modeled linearly. For V_{Φ} , in contrast, the temperature-sensitivity in the lowermost mantle for high temperature changes. There, at high temperature $\partial V_{\Phi}/\partial T$ is close to zero. This behaviour is expected in mineral physics. In an isotropic material V_S and V_{Φ} are related to density (ρ), shear (G) and bulk modulus (K) through:

$$\begin{aligned} V_S &= \sqrt{G_S/\rho} \\ V_{\Phi} &= \sqrt{K_S/\rho}, \end{aligned}$$

where the subscript S indicates isentropic (adiabatic) conditions for finite frequency waves. When material is adiabatically compressed, the effect of the pressure change on volume is the sum of two contributions: (1) isothermal compression and (2) thermal expansion arising from the adiabatic temperature increase associated with the compression. While the effect of isothermal compression on volume decreases with increasing temperature, by contrast the thermal expansivity increases with increasing temperature. Adiabatic compression thus leads to two competing effects with opposite dependence on temperature. The thermal expansion contribution is greatest in the hottest regions of the mantle, while the isothermal compression contribution is smallest. It follows that while K_S and K_T behave similarly at low temperatures, they will behave differently at higher temperatures: while K_T will continue to decrease in the same way, K_S may lose sensitivity to temperature at high temperature.

This behaviour was anticipated by Anderson [*Anderson, 1967; Anderson, 1987*]. He has considered the temperature derivative of the bulk sound velocity:

$$\partial V_{\Phi}/\partial T = 1/(2\rho V_{\Phi})(\partial K_S/\partial T + \alpha K_S). \quad (28)$$

The ratio of the two terms on the right hand side defines the Anderson-Grüneisen parameter

$$\delta_S = -\frac{(\partial K_S/\partial T)_P}{\alpha K_S}. \quad (29)$$

As δ_S approaches 1, $\partial V_{\Phi}/\partial T$ becomes close to zero. In his considerations Anderson [*Anderson, 1967; Anderson, 1987*] divided $(\partial K_S/\partial T)_P$ into an extrinsic (volumetric or harmonic) temperature effect and an intrinsic (anharmonic) component related to changes in elasticity at constant volume:

$$(\partial K_S/\partial T)_P = \alpha K_S(\partial \log K_S/\partial \rho)_T - (\partial K_S/\partial T)_V. \quad (30)$$

A similar expression can be derived for the shear modulus.

Experiments at ambient conditions show that the intrinsic effect to the shear modulus is invariably negative and often larger than the volumetric component. Its effect on the

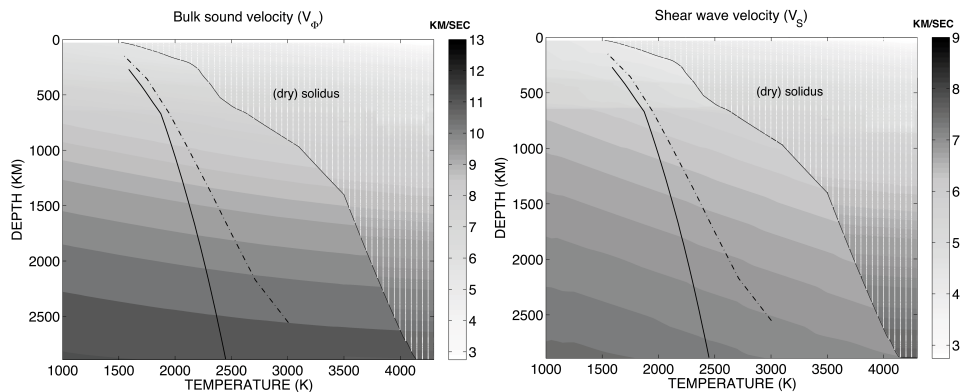


Figure 17: Contour plot (black=fast, white=slow) of bulk sound velocity (V_{Φ}) and shear wave velocity (V_S) over the mantle temperature and pressure range for a pyrolite bulk composition as provided by my mineralogy model (see text). V_{Φ} generally increases with depth and decreases with temperature, The solid and dot-dashed curves are Brown and Shankland [Brown and Shankland, 1981] and Stacey [Stacey, 1995] geotherms. I clip the figure at temperatures larger than the dry solidus [Zerr et al., 1998], where melting invalidates the considerations underlying the physical properties of the mineral assemblage.

bulk modulus, however, can be either negative or positive. The effect of the extrinsic part is expected to decrease rapidly at high pressure so that the extrinsic contribution should be small under lower mantle conditions. It is thus possible that bulk and shear modulus behavior diverge at high pressure due to the different sign of the intrinsic (anharmonic) components. This can be considered as a possible explanation for the missing slab signature in the lower mantle and also for the decreasing of V_S and V_{Φ} correlation in the lowermost mantle.

The possibility of large-scale mantle chemical heterogeneity has prompted a number of geodynamic studies with multiple chemical components [Nakagawa and Tackley, 2004; Farnetani, 1997]. Proper comparisons of temperature fields from geodynamic models with maps of elastic properties from seismic models, of course, ought to account for the material properties of the mantle mineralogy. Here, however, interpretations have lagged behind because there are substantial tradeoffs between thermal and chemical effects. Faced with this difficulty some investigators have instead sought to relate the elastic variations directly to the thermal and chemical state of convection [Cammarano et al., 2003; Deschamps and Trampert, 2003; Deschamps and Trampert, 2004; Farnetani and Samuel, 2005; Ricard et al., 2005; Mattern et al., 2005], but in doing so have reached competing conclusions on the need for chemical mantle heterogeneity and convective layering. Fig. 18 shows the radial root mean square (R.M.S.) of the shear wave velocities of my convection models versus a set of tomographic models for the lower mantle. My models show a good absolute fit and

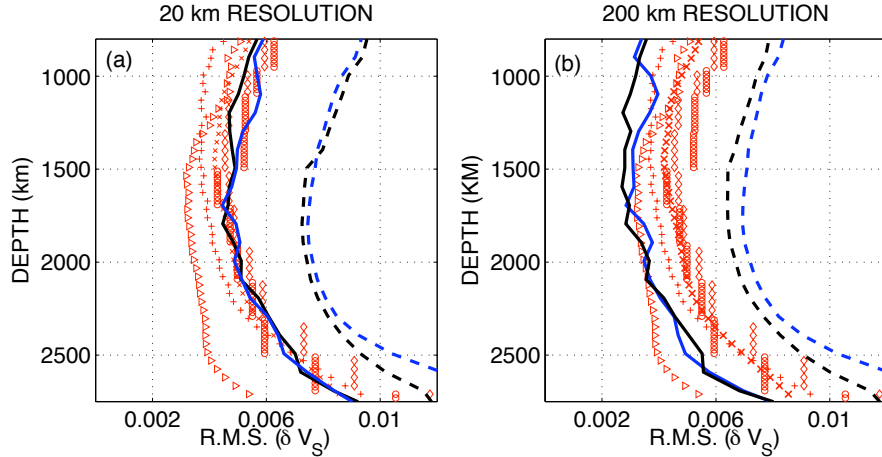


Figure 18: Root Mean Square (R.M.S.) of shear wave anomalies for the "BOTTOM" models (black lines) and for the "MIX" cases (blue lines). Solid lines indicate "ISOVISCOUS" models, dashed lines represent "LAYERED VISC." models. I have performed the root mean square calculation at full resolution of about 20 km (panel (a)) and also averaged over a scale of about 200 km (panel (b)). Red symbols show seismic tomography models: triangles for S20RTS [Ritsema *et al.*, 1999], crosses for PRI-S05 [Montelli *et al.*, 2006], diamonds for RMSL-S06 [Reif *et al.*, 2006], plus for TX2007 [Simmons *et al.*, 2007] and circles for SB10L18 [Masters *et al.*, 2000].

closely mimic the depth-dependence of the R.M.S with seismic tomography. In particular, the "ISOVISCOUS" models provide the best fit. To account for the spatial resolution of tomography [Nolet *et al.*, 2007], I have averaged the models on a scale of 200 km (right panel in Fig. 18). This makes the R.M.S. decreasing, bringing the "LAYERED VISC." case to a better fit. From this comparison there is no necessity of chemical heterogeneities [e.g. van der Hilst and Krason, 1999; Trampert *et al.*, 2004; van der Hilst, 2004] in order to account the observed V_S variations. Furthermore, it would be difficult to allow for much presence of chemical heterogeneities that would additionally increase the amount of V_S variations and consequently the R.M.S..

3.4 Conclusions

Mantle convection models that couple self-consistently with a thermodynamic database for mantle mineralogy can provide new insights into the thermal and elastic state of the Earth's mantle. Such simulations show that the *excess temperature* of upwelling structures decreases during ascent, since the differences between the maximum and average temperatures increase with depth (Fig. 14). Thus, hotspots surface heat flux observations cannot be related directly to those at the core-mantle-boundary without consideration of temper-

ature dependence of adiabatic profiles. Low excess temperatures in plumes at the surface are a consequence of the fact that hot upwellings undergo much stronger adiabatic cooling relative to ambient mantle.

Furthermore, high core-mantle-boundary temperatures and hence significant heating of the mantle from below appears necessary to obtain reasonable geotherms and physical properties that are consistent with seismic models. Purely internally heated models do not provide sufficient heat to the mantle in order to account for the observed seismic heterogeneities.

The coupling of the convection model with the mineralogical database provides the possibility to quantify complex effects that occur around "660km" on convection dynamics. There is a considerable temperature increase at "660km" to overcome the effect of latent heat of the phase transitions, i.e. to keep the entropy constant. Above and below "660km" there are two different thermal regimes that decrease the density change across the phase transition. For example, the isothermal density change (about 6% for pyrolite) is reduced of up to 15% with the 200-250 K jump that occurs on plume temperature. Dynamically due to the splitting of the "660km" at high temperature in a pv-gt and then the post-spinel transitions, the upwellings are accelerated in entering the upper mantle circulation. Both effects contribute to a decrease in resistance of the "660km" against plume penetration and contribute to the scenario of whole mantle convection.

By accounting for a realistic mineralogical description of physical properties the models with high temperature at the core-mantle-boundary show good depth-dependence of R.M.S. shear wave and bulk sound anomalies that compare well with seismic tomography (Fig. 18a) and good absolute R.M.S. anomalies if the resolution of our models is artificially decreased to that of tomography (200km - Fig. 18b). The mineralogical model accounts for a decrease in sensitivity of V_{Φ} to temperature in the lowermost mantle (Fig. 17a) that results in anomalies being less visible, consistent with seismic tomography.

References

- [1] Anderson, D.L., A seismic equation of state, *Geophys. J. Int.*, 13, 9-30, 1967.
- [2] Anderson, D.L., A seismic equation of state II. Shear properties and thermodynamics of the lower mantle, *Phys. Earth. Planet. Int.*, 45, 307-323, 1987.
- [3] Badro, J., J.P. Rueff, G. Vanko, G. Monaco, G. Fiquet and F. Guyot, Electronic transitions in perovskite: Possible nonconvecting layers in the lower mantle, *Science*, 305, 383-386, 2004.
- [4] Bijwaard, H., W. Spakman and E.R. Engdahl, Closing the gap between regional and global travel time tomography, *J. Geophys. Res.*, 103, 30,055-30,078, 1998.

- [5] Brown, J.M. and T.J. Shankland, Thermodynamic parameters in the Earth as determined from seismic profiles, *Geophys. J. Astron. Soc.*, *66*, 579-596, 1981.
- [6] Bunge H.-P. and M.A. Richards, The origin of large scale structure in mantle convection: Effects of plate motions and viscosity stratification, *Geophys. Res. Lett.*, *23*, 2987-2990, 1996.
- [7] Bunge, H.-P., M.A. Richards and J.R Baumgardner, The effect of depth dependent viscosity on the planform of mantle convection, *Nature*, *379*, 436-438, 1996.
- [8] Bunge, H.-P., M.A. Richards and J.R. Baumgardner, A sensitivity study of three-dimensional spherical mantle convection at 10^8 Rayleigh number: Effects of depth-dependent viscosity, heating mode, and an endothermic phase change, *J. Geophys. Res.*, *102*, 11,991-12,007, 1997.
- [9] Bunge, H.-P., Y. Ricard and J. Matas, Non-adiabaticity in mantle convection, *Geophys. Res. Lett.*, *28*, 879-882, 2001.
- [10] Bunge, H.-P., Low plume excess temperature and high core heat flux inferred from non-adiabatic geotherms in internally heated mantle circulation models, *Phys. Earth Planet. Interiors*, *153*, 3-10, 2005.
- [11] Cammarano, F., S. Goes, P. Vacher and D. Giardini, Inferring upper mantle temperatures from seismic velocities, *Phys. Earth Planet. Interiors*, *138*, 197-222, 2003.
- [12] Christensen, U.R. and D.A. Yuen, Layered convection induced by phase-transitions, *J. Geophys. Res.*, *90*, 291-300, 1985.
- [13] Davies, G.F., Ocean bathymetry and mantle convection, 1. Large-scale flow and hotspots, *J. Geophys. Res.*, *93*, 10,467-10,480, 1988.
- [14] Deschamps, F. and J. Trampert, Mantle tomography and its relation to temperature and composition, *Phys. Earth Planet. Int.*, *140*, 277-291, 2003.
- [15] Deschamps, F. and J. Trampert, Towards a lower mantle reference temperature and composition, *Earth Planet. Sci. Lett.*, *222*, 161-175, 2004.
- [16] Deuss, A., A.T. Simon, K.C Redfern and J.H. Woodhouse, The Nature of the 660-Kilometer Discontinuity in Earth's Mantle from Global Seismic Observations of PP Precursors, *Science*, *311*, 198-201, 2006.
- [17] Dziewonski, A.M. and D.L. Anderson, Preliminary Reference Earth Model, *Phys. Earth Planet. Interiors*, *25*, 297-356, 1981.
- [18] Dziewonski, A.M., Mapping the lower mantle: Determination of lateral heterogeneity in P-velocity up to degree and order 6, *J. Geophys. Res.*, *89*, 5,929-5,952, 1984.

- [19] Fabrichnaya, O.B., The phase relations in the FeO-MgO-Al₂O₃-SiO₂ system: assessment of thermodynamic properties and phase equilibria at pressures up to 30 GPa, *Calphad*, *23*, 19-67, 1999.
- [20] Farnetani, C.G, Excess temperature of mantle plumes: The role of chemical stratification across D'', *Geophys. Res. Lett.*, *24*, 1583-1586, 1997.
- [21] Farnetani, C.G. and H. Samuel, Beyond the thermal plume paradigm, *Geophys. Res. Lett.*, *32*, art. no. L07311, 2005.
- [22] Frost, D.J., The structure and sharpness of (Mg,Fe)₂SiO₄ phase transformations in the transition zone, *Earth Planet. Sci. Lett.*, *216*, 313-328, 2003.
- [23] Glatzmaier, G.A., Numerical simulations of mantle convection: time-dependent, three-dimensional, compressible, spherical shell, *Geophys. Astrophys. Fluid Dyn.*, *43*, 223-264, 1988.
- [24] Grand, S.P., R. D. Van der Hilst and S. Widiyantoro, Global seismic tomography: A snapshot of convection in the Earth, *Geol. Soc. Am. Today*, *7*, 1-7, 1997.
- [25] Hirose, K., Phase transitions in pyrolitic mantle around 670-km depth: Implications for upwelling of plumes from the lower mantle, *J. Geophys. Res.*, *107*, B4, 2078, doi:10.1029/2001JB000597, 2002.
- [26] Hofmeister, A.M. and R.E. Criss, Earth's heat flux revised and linked to chemistry, *Tectonophysics*, *395*, 159-177, 2005.
- [27] Jarvis, G.T. and D. McKenzie, Convection in a compressible fluid with infinite Prandtl number, *J. Fluid Mech.*, *96*, 515-83, 1980.
- [28] Jeanloz, R. and S. Morris, Temperature distribution in the crust and mantle. *Annual Reviews of Earth and Planetary Sciences*, *14*, 377-415, 1986.
- [29] Kantor, A.P., S. Jacobsen, I.Y. Kantor, L. Dubrovinsky, C.A. McCammon, H.J., Reichmann and I.N. Goncharenko, Pressure-Induced Magnetization in FeO: Evidence from Elasticity and Mossbauer Spectroscopy, *Phys. Rev. Lett.*, *93*, 215502, 2004.
- [30] Khan, A., J.A.D. Connolly, J. Maclennan and K. Mosegaard, Joint inversion of seismic and gravity data for lunar composition and thermal state. *Geophys. J. Int.*, *168*, 243-258, 2007.
- [31] Kennett, B.L.N., E.R. Engdahl and R. Buland, Constraints on seismic velocities in the Earth from travel times, *Geophys. J. Int.*, *122*, 108-124, 1995.

- [32] Kennett, B.L.N., S. Widiyantoro and R.D. van der Hilst, Joint seismic tomography for bulk sound and shear wave speed in the Earth's mantle, *J. Geophys. Res.*, *103*, 12,469-12,494, 1998.
- [33] Labrosse, S., Hotspots, mantle plumes and core heat loss, *Earth Planet. Sci. Lett.*, *199*, 147-156, 2002.
- [34] Li B.S. and J.Z. Zhang, Pressure and temperature dependence of elastic wave velocity of MgSiO₃ perovskite and the composition of the lower, *Phys. Earth Planet. Interiors*, *151*, 143-154, 2005.
- [35] Masters G., G. Laske, H. Bolton and A. Dziewonski, The relative behavior of shear velocity, bulk sound speed, and compressional velocity in the mantle: Implications for chemical and thermal structure, in: S. Karato, A.M. Forte, R.C. Liebermann, G. Masters and L. Stixrude (eds.) *Earth's Deep Interior*, AGU Monograph 117, AGU, Washington D.C, 2000.
- [36] Matas, J., Modélisation thermochimique des propriétés de solides a hautes pressions et hautes temperatures. Application géophysique. *PhD thesis, École Normale Supérieure*, Lyon, 1999.
- [37] Mattern, E., J. Matas, Y. Ricard and J. Bass, Lower mantle composition and temperature from mineral physics and thermodynamic modeling, *Geophys J. Int.*, *160*, 973-990, 2005.
- [38] Matyska, C. and D.A. Yuen, Profiles of the Bullen parameter from mantle convection modelling, *Earth Planet. Sci. Lett.*, *178*, 39-46, 2000.
- [39] McCammon, C., The Paradox of Mantle Redox, *Science*, *308*, 807-808, 2005.
- [40] McDonough, W.F and Sun, S.-S., Composition of the Earth, *Chemical Geology*, *120*, 223-253, 1995.
- [41] McKenzie, D., J. Roberts and N.O. Weiss, Convection in the Earth's mantle: towards a numerical simulation, *J. Fluid Mech.*, *62*, 465-538, 1974.
- [42] McNamara, A.K. and S. Zhong, Degree-One Mantle Convection: Dependence on Internal Heating and Temperature-Dependent Rheology, *Geophys. Res. Lett.*, *32*, art. no. L01301, 2005.
- [43] Mégnin, C. and B. Romanowicz, The 3D shear velocity structure of the mantle from the inversion of body, surface and higher mode waveforms, *Geophys. J. Inter.*, *143*, 709-728, 2000.

- [44] Miller, M.S., B.L.N. Kennett and V. Toy, Spatial and temporal evolution of the subducting Pacific plate structure along the western Pacific margin, *J. Geophys. Res.*, *111*, B02401, doi:10.129/2005JB003705, 2006.
- [45] Mittelstaedt, E. and P.J. Tackley, Plume heat flow is much lower than CMB heat flow, *Earth. Planet. Sci. Lett.*, *241*, 202-210, 2006.
- [46] Montelli, R., G. Nolet, G. Masters, F.A. Dahlen and S.-H. Hung, Global P and PP traveltime tomography: rays versus waves, *Geophys. J. Int.*, *158*, 637-654, 2004.
- [47] Montelli, R., G. Nolet, F.A. Dahlen and G. Masters, A catalogue of deep mantle plumes: New results from finite-frequency tomography, *Geochem. Geophys. Geosys.*, *7*, 1-69, 2006.
- [48] Murakami, M., S.V. Sinogeikin, J.D. Bass, N. Sata, Y. Ohishi and K. Hirose, Sound velocity of MgSiO₃ post-perovskite phase: A constraint on the D" discontinuity, *Earth. Planet. Sci. Lett.*, *259*, 18-23, 2007.
- [49] Nakagawa, T. and P.J. Tackley, Thermo-chemical structure in the mantle arising from a three-component convective system and implications for geochemistry, *Phys. Earth Planet. Int.*, *146*, 125-138, 2004.
- [50] Nolet, G., R. Allen and D. Zhao, Mantle plume tomography, *Chem. Geol.*, *241*, 248-263, 2007.
- [51] Oganov A.R., Brodholt J.P., Price G.D., The elastic constants of MgSiO₃ perovskite at pressures and temperatures of the Earth's mantle, *Nature*, *411*, 934-937, 2001.
- [52] Piazzoni, A.S., G. Steinle-Neumann, H.-P. Bunge and D. Dolejš, A mineralogical model for density and elasticity of the Earth's mantle, in press, *Geochem. Geophys. Geosyst*, 2007
- [53] Presnall, D.C. and G.H. Gudfinnsson, Origin of the oceanic lithosphere, *Journal of Petrology*, *49*, 615-632, 2008.
- [54] Reif, C., personal communication.
- [55] Resovsky, J. and J. Trampert, Reliable mantle density error bars: An application of the neighbourhood algorithm to normal mode and surface wave data, *Geophys. J. Int.*, *150*, 665-672, 2002.
- [56] Ricard, Y., E. Mattern and J. Matas, Synthetic Tomographic Images of Slabs from Mineral Physics, in *Earth's Deep Mantle: Structure, Composition, and Evolution*, edited by R.D. van der Hilst, J.D. Bass, J. Matas and J. Trampert, *Geophys. Monogr. Ser.*, AGU, Washington, D.C, pp. 285-302, 2005.

- [57] Ritsema, J., H.J. van Heijst and J.H. Woodhouse, Complex Shear Wave Velocity Structure Imaged Beneath Africa and Iceland, *Science*, *286*, 1,925-1,928, 1999.
- [58] Romanowicz, B. and Y.C. Gung, Superplumes from the core-mantle boundary to the lithosphere: implications for heat-flux, *Science*, *296*, 513-516, 2002.
- [59] Samuel, H., C.G. Farnetani and D. Andraut, Heterogeneous lowermost mantle: compositional constraints and seismological observables, in *Earth's Deep Mantle: Structure, composition and evolution of Earth's mantle*, edited by R.D. van der Hilst, J.D. Bass, J. Matas and J. Trampert, *Geophys. Monogr. Ser.*, AGU, Washington, D.C., pp. 103-108, 2005.
- [60] Saxena, S.K., Earth mineralogical model: Gibbs free energy minimization computation in the system MgO-FeO-SiO₂, *Geochim. Cosmochim. Acta*, *60*, 2379-2395, 1996.
- [61] Schilling, J.-G., Fluxes and excess temperatures of mantle plumes inferred from their interaction with migrating mid-ocean ridges, *Nature*, *352*, 397-403, 1991.
- [62] Schubert, G., Subsolidus convection in the mantles of terrestrial planets, *Ann. Rev. Earth Planet. Sci.*, *7*, 289-342, 1979.
- [63] Schuberth, B., H.-P. Bunge, G. Steinle-Neumann, C. Moder and J. Oeser, Thermal vs. Elastic Heterogeneity in High-Resolution Mantle Circulation Models with Pyrolite Composition: High Plume Excess Temperatures in the Lowmost Mantle, *Geochem. Geophys. Geosyst*, submitted, 2008.
- [64] Shearer, P.M. and M.P. Flanagan, Seismic velocity and density jumps across the 410- and 660-kilometer discontinuities, *Science*, *285*, 1545-1548, 1999.
- [65] Shearer, P.M., Upper mantle seismic discontinuities, in *Earth's Deep Interior: Mineral Physics and Tomography from the Atomic to the Global Scale*, *Geophysical Monogr. Ser.*, AGU, Washington, D.C, pp. 117, 115-131, 2000.
- [66] Sinogeikin, S.V., J.Z. Zhang and J.D. Bass, Elasticity of single crystal and polycrystalline MgSiO₃ perovskite by Brillouin spectroscopy, *Geophys. Res. Lett.*, *31*, L06620, doi:10.1029/2004GL019559, 2004.
- [67] Simmons, N.A., A.M. Forte and S.P. Grand, Thermochemical structure and dynamics of the African superplume, *Geophys. Res. Lett.*, *34*, art. no. L02301, 2004.
- [68] Sleep, N.H., Hotspots and mantle plumes - some phenomenology, *J. Geophys. Res.*, *95*, 6,715-6,736, 1990.
- [69] Sleep, N.H., Simple features of mantle-wide convection and the interpretation of lower-mantle tomograms, *Comptes Rendus Geoscience*, *335*, 9-22, 2003.

- [70] Stacey, F.D., Theory of thermal and elastic properties of the lower mantle and core, *Phys. Earth Planet. Int.*, 89, 219-245, 1995.
- [71] Stixrude, L., R.J. Hemley, Y. Fei and H. K. Mao, Thermoelasticity of silicate perovskite and magnesiowustite and stratification of the Earth's mantle, *Science*, 257, 1099-1101, 1992.
- [72] Stixrude, L. and C. Lithgow-Bertelloni, Thermodynamics of mantle minerals: 1. Physical properties, *Geophys J. Int.*, 162, 610-632, 2005.
- [73] Tackley, P.J., Strong heterogeneity caused by deep mantle layering, *Geochem. Geophys. Geosystems*, 3, 4, 1024, doi:10.1029/2001GC000167, 2002.
- [74] Tackley, P.J., D.J. Stevenson, G.A. Glatzmaier and G. Schubert GLATZMAIER GA, Effects of an endothermic phase-transition at 670 km depth in a spherical model of convection in the Earth's mantle, *Nature*, 361, 699-704, 1993.
- [75] Tackley, P.J., S. Xie, T. Nakagawa and J.W. Hernlund, Numerical and laboratory studies of mantle convection: Philosophy, accomplishments and thermo-chemical structure and evolution, in *Earth's Deep Mantle: Structure, Composition, and Evolution*, edited by R.D. van der Hilst, J.D. Bass, J. Matas and J. Trampert, *Geophys. Monogr. Ser.*, AGU, Washington, D.C, pp. 83-99, 2005.
- [76] Trampert, J, F. Deschamps, J. Resovsky and D. Yuen, Probabilistic Tomography Maps Chemical Heterogeneities Throughout the Lower Mantle, *Science*, 306, 853-856, 2004.
- [77] Travis, B.J., C. Anderson, J.R. Baumgardner, C.W. Gable, B.H. Hager, R.J. O'Connell, P. Olson, A. Raefsky and G. Schubert,, A benchmark comparison of numerical methods for infinite Prandtl number thermal convection in two-dimensional cartesian geometry, *Geophys. Astrophys. Fluid Dyn.*, 55, 137-160, 1990.
- [78] van der Hilst, R., S. Widiyantoro and E.R. Engdahl, Evidence for deep mantle circulation from global tomography, *Nature*, 386, 578-584, 1997.
- [79] van der Hilst, R.D and H. Kárason, Compositional Heterogeneity in the Bottom 1000 Kilometers of Earth's Mantle: Toward a Hybrid Convection Model, *Science*, 283, 1885-1888, 1999.
- [80] van der Hilst, R.D., Changing views on Earth's deep mantle, *Science*, 306, 817-818, 2004.
- [81] van der Voo, R., W. Spakman and H. Bijwaard, Mesozoic subducted slabs under Siberia, *Nature*, 397, 246-249, 1999.

- [82] Walter, M.J., A. Kubo, T. Yoshino, J. Brodholt, K. Koga and Y. Ohishi, Phase relations and equation-of-state of aluminous Mg-silicate perovskite and implications for Earth's lower mantle, *Earth Planet. Sci. Lett.*, *222*, 501-516, 2004.
- [83] Yagi, T., H.K. Mao and P.M. Bell, Structure and crystal-chemistry of perovskite-type MgSiO₃, *Phys. Chem. Min.*, *3*, 97-110, 1978.
- [84] Yang, W.-S. and J.R. Baumgardner, Matrix-dependent transfer multigrid method for strongly variable viscosity infinite Prandtl number thermal convection, *Geophys. Astrophys. Fluid Dyn.*, *92*, 151-195, 2000.
- [85] Zerr, A., A. Diegeler and R. Boehler, Solidus of Earth's Deep Mantle, *Science*, *281*, 243-246, 1998.
- [86] Zhong, S., Constraints on thermochemical convection of the mantle from plume heat flux, plume excess temperature and upper mantle temperature, *J. Geophys. Res.*, *111*, B04409, doi: 10.1029/2005JB003972, 2006.

4 Appendix: Transition zone thickness

The topographies of the "410 km" and "660 km" are believed to be anti-correlated as temperature deviations from the geotherm are expected to shift them in opposite directions. However, recent seismic studies based on SS precursors [e.g. *Schmerr et al.*, 2005] observe that the two seismic discontinuities are un-correlated or even positively correlated around hot-spots. Also, the most relevant depths variations are reported on the "660km" and not on the "410km" [*Gu and Dziewonski*, 2002], even if their Clapeyron slopes would suggest the opposite. In effect, the "410km" has about +2.9 MPa/K [*Steinberger*, 2007; *Bina and Helffrich*, 1994]. The "660km" has a less clear assesement (that varies among positive values [*Katsura et al.*, 2003], close to zero [*Saxena*, 1996] negative and small [*Katsura et al.*, 2003; *Fei et al.*, 2004] to very negative [*Ito and Takahashi*, 1989; *Ito and Katsura*, 1989; *Irifune et al.*, 1998]) but recent asesements converge on a value of about -1.2 MPa/K that is half of the one of "410km". However, topography variations depend both on transition zone dynamics, that are influenced by phase transformations, and on the location of phase transitions, that is temperature dependent. So, only combined mineralogical and dynamic models can account for this complexity. Promising potential stands in the comparison of geodynamic and seismological models. The comunication between the two is built upon the ability of interpreting seismic velocity variations in terms of temperature and, vice-versa, of making seismological predictions via convection models. However, seismological measurements can not be easily related to their physical origin, as temperature and chemical heterogeneities variations compete with similar effects on the variations of seismic wave velocities and are difficult to be distinguished (e.g. iron-enrichment or high temperature can yield indistinguishable thickening of the mantle transition zone [*Frost*, 2003; *Bina*

and Helffrich, 1994]). Furthermore, the relation between temperature and seismic wave velocities is complex, being non-linear [Stixrude and Lithgow-Bertelloni, 2005] (see section 2), strongly depth-dependent, (see section 3) and because the effect of temperature on the bulk sound velocity deviates from the one on shear wave speed at high pressure (see section 3).

I have computed topographies for the "410km" and "660km". The "410km" has been calculated mineralogically as the transformation of α olivine into the β phase, taking into account variations of iron concentration due to interactions with the garnet solid solution.

In order to be coherent with seismology, the "660km" is found by calculating the steepest gradient around 660 km depth of the shear impedance (i.e. the product of density and V_S). Both the "MIX" cases and the "BOTTOM, ISOVISCIOUS" (see section 3) predict a similar average thickness of about 250 km that is in good agreement with seismological studies [Lawrence and Shearer, 2006; Gu and Dziewonski, 2002; Saita et al., 2002]. The "BOTTOM, LAYERED VISC." case has an average thickness of 297 km, confirming (see section 3) that this model provides a poorer fit to the expected thermal regime. In our models, the difference between maximum and minimum thickness varies from 60 km to 150 km. If the resolution scaling is considered (see section 3), these variations are generally compatible with the typical peak-to-peak thickness variations in seismology (60-70 km [Shearer, 2000; Lawrence and Shearer, 2006]).

I have shown in section 3 that in the transition zone the phase transitions yield jumps of temperature that are maintained despite the convecting flux (see Fig. 14,15 and 16a). The total jump of temperature is a function of the entropy difference between the phases, increasing with temperature. Therefore, hot geotherms have more pronounced jumps than colder ones (Fig. 15a). This effect can explain that the depths of the "410km" and "660km" are more clearly anti-correlated around subduction areas than around hot-spots [Schmerr et al., 2005]. In my models, on slab-like geotherms, the adiabatic temperature is quite continuous (the jump is of the order of $\max \sim 10K$, see Fig. 15a). So, an expected thickening of the transition zone results from the combined divergence of the "410km" and the "660km" phase transitions (that have opposite Clapeyron slopes). However, on plume-like temperatures, the temperature jump can reach $\sim 200 - 250K$ (Fig. 15a). Such a decrease of temperature in the upper mantle compensates for the depth variations of the "410km". So, while the "660km" moves upward as expected by mineralogy, the depth variations of the "410km" are essentially reduced (Fig. 19,20). This can make the two discontinuities uncorrelated in regions with high temperature. A second interesting observation is that the most relevant changes of depths are observed on the "660km" and not on the "410km" [Gu and Dziewonski, 2002], even if their Clapeyron slopes would suggest the opposite. This discrepancy can be explained by taking into account the $\sim 200K$ reduction of excess temperature in the upper mantle, where the "410km" is located. Finally, such thermal regime makes cold and hot structures asymmetric around the geotherm in the upper mantle (i.e. the temperature difference between a plume and the geotherm is

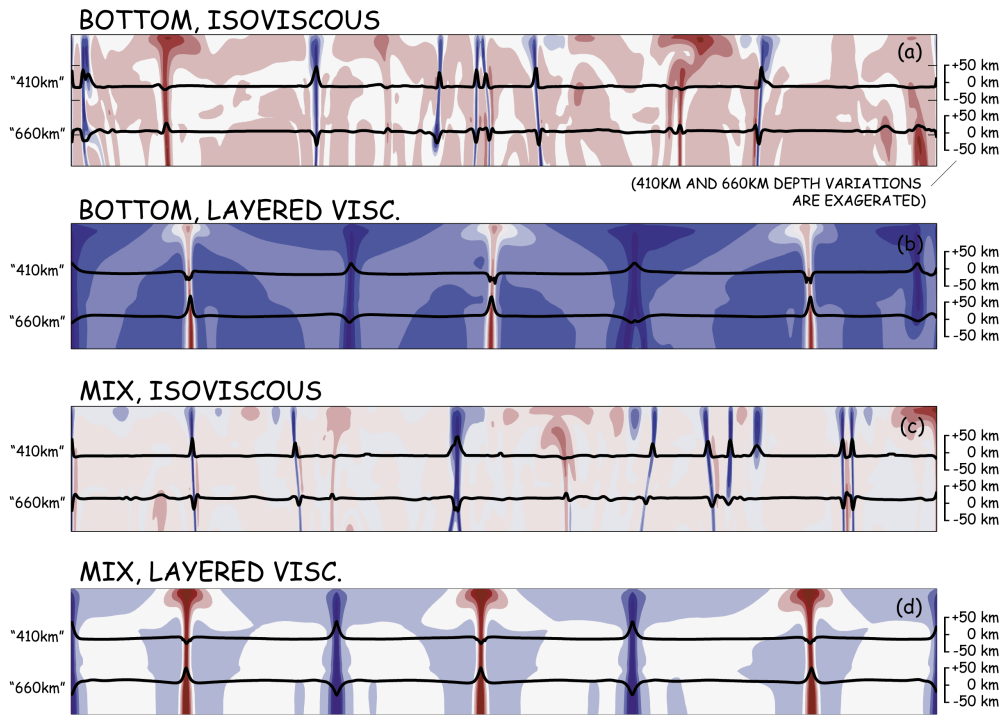


Figure 19: Depth variations of the 410 km and 660 km seismic discontinuities for the four convection models. In order to isolate temperature effects on transition zone thickness, the post-spinel transition has been modeled here with a constant Clapeyron slope of -2 MPa/K . Negative variations of the "410 km" appear less pronounced than positive variations for slab-like temperatures.

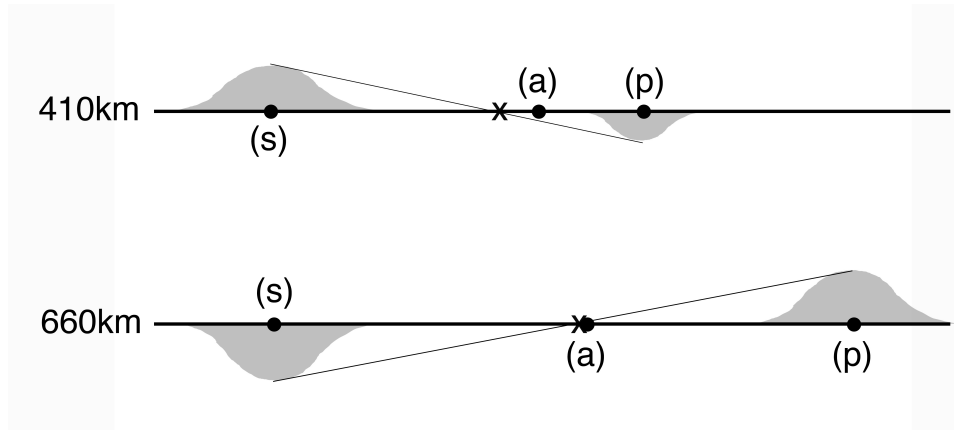


Figure 20: Sketch of temperature effects on the topography for the "410km and the "660km". The labels (s), (a) and (p) indicate slab, average and plume temperature, respectively. The symbols "X" point to the average thickness, that does not correspond necessary to the thickness of the average temperature (a). For this diagram, the relative differences of temperature between cold and hot structures are taken from the model "BOTTOM, ISO-VISCOUS". Due to a reduction of the excess temperature of plumes above the "660km", the "410km" varies less than the "660km" on plume-like temperature. A similar effect occurs at low temperature, where the temperature differences are generally smaller than on the "660km". So, the variations of the "410km" are reduced in respect to what is expected from mineralogy (see text).

smaller than the difference between a slab and the geotherm, see Fig. 20). So, above 660 km depth, the average thickness of the transition zone does not correspond anymore to the thickness of the average temperature, but it is expected to be greater.

References

- [1] Bina, C. R. and G. Helffrich, Phase transition Clapeyron slopes and transition zone seismic discontinuity topography, *J. Geophys. Res.*, *99*, 15,853-15,860, 1994.
- [2] Fei, Y., J. Van Orman, J. Li, W. van Westrenen, C. Sanloup, W. Minarik, K. Hirose, T. Komabayashi, M. Walter and K. Funakoshi, Experimentally determined postspinel transformation boundary in Mg_2SiO_4 using MgO as an internal pressure standard and its geophysical implications, *J. Geophys. Res.*, B02305, doi:10.1029/2003JB002562, 2004.
- [3] Frost, D.J., The structure and sharpness of $(\text{Mg,Fe})_2\text{SiO}_4$ phase transformations in the transition zone, *Earth Planet. Sci. Lett.*, *216*, 313-328, 2003.
- [4] Gu, Y.J. and A.M. Dziewonski, Global variability of transition zone thickness, *J. Geophys. Res.*, *107*, art. no. 2135, 2002.
- [5] Irifune, T., N. Nishiyama, K. Kuroda, T. Inoue, M. Isshiki, W. Utsumi, K.-I. Funakoshi, S. Urakawa, T. Uchida, T. Katsura and O. Ohtaka, The postspinel phase boundary in Mg_2SiO_4 determined by in situ X-ray diffraction, *Science*, *279*, 1698-1700, 1998.
- [6] Ito, E. and E. Takahashi, Postspinel transformations in the solid system Mg_2SiO_4 - Fe_2SiO_4 and some geophysical implications, *J. Geophys. Res.*, *94*, 10,637-10,646, 1989.
- [7] Ito, E. and T. Katsura, A temperature profile of the mantle transition zone, *Geophys. Res. Lett.*, *16*, 425-428, 1989.
- [8] Katsura, T., M. J. Walter, H. Yamada, T. Shinmei, A. Kubo, S. Ono, M. Kanzaki, A. Yoneda, E. Ito and S. Urakawa, Post-spinel transition in Mg_2SiO_4 determined by high P-T in situ X-ray diffractometry, *Phys. Earth Planet. Inter.*, *136*, 11-24, 2003.
- [9] Lawrence, J.F. and P.M. Shearer, A global study of transition zone thickness using receiver functions, *J. Geophys. Res.*, *111*, art. no. B06307, 2006.
- [10] Saita, T., D. Suetsugu, T. Ohtaki, H. Takenaka, K. Kanjo and I. Purwana, Transition zone thickness beneath Indonesia as inferred using the receiver function method for data from the JISNETS regional broadband seismic network, *Geophys. Res. Lett.*, *29*, doi: 10.1029/2001GL013629, 2002.

- [11] Saxena, S.K., Earth mineralogical model: Gibbs free energy minimization computation in the system MgO-FeO-SiO₂, *Geochim. Cosmochim. Acta*, 60, 2379-2395, 1996.
- [12] Schmerr, N., E. Garnero and L. Stixrude, Evidence for Positive Correlation of 400- and 670-km Discontinuity Topography Beneath the Central Pacific from SS Precursors, *Eos Trans. AGU*, Washington, D.C, 85 abstr. no. DI41A-1246, 2005.
- [13] Shearer, P.M., Upper mantle seismic discontinuities, in Earth's Deep Interior: Mineral Physics and Tomography from the Atomic to the Global Scale, *Geophysical Monogr. Ser.*, AGU, Washington, D.C, pp.117, 115-131, 2000.
- [14] Steinberger, B., Effect of latent heat release at phase boundaries on flow in the Earth's mantle, phase boundary topography and dynamic topography at the Earth's surface, *Phys. Earth Planet. Inter.*, 164, 2-20, 2007.
- [15] Stixrude, L. and C. Lithgow-Bertelloni, Thermodynamics of mantle minerals: 1. Physical properties, *Geophys J. Int.*, 162, 610-632, 2005.

Lebenslauf

Persönliche Daten

Name: Antonio Sebastiano Piazzoni
Aushrift: Theresienstr. 130, 80335, Muenchen
Geburstdatum: 17 Juni 1977
Geburstort: Lecco, Italia

Schul Ausbildung

1991-1996 Liceo Scientifico - Lecco - Italia

Hochschul Ausbildung

1997-2002 Laurea - Università degli Studi di Milano - Italia